VASODILATION AND ANTI-HYPERTENSIVE EFFECTS OF AN ORTHOGONAL STIMULUS-RESPONSE-OPTIMISED COMBINED FORMULATION OF EUPATORIN, SINENSETIN, AND 3'-HYDROXY-5,6,7,4'TETRAMETHOXYFLAVONE IN A RAT MODELS

YAM MUN FEI

DOCTOR OF PHILOSOPHY (CHINESE MEDICINE)

M.KANDIAH FACULTY OF MEDICINE AND HEALTH SCIENCES
UNIVERSITI TUNKU ABDUL RAHMAN
DECEMBER 2025

VASODILATION AND ANTI-HYPERTENSIVE EFFECTS OF AN ORTHOGONAL STIMULUS-RESPONSE-OPTIMISED COMBINED FORMULATION OF EUPATORIN, SINENSETIN, AND 3'-HYDROXY-5,6,7,4'TETRAMETHOXYFLAVONE IN A RAT MODELS

By

YAM MUN FEI

A thesis submitted to the Department of Chinese Medicine,
M. Kandiah Faculty of Medicine and Health Sciences,
Universiti Tunku Abdul Rahman,
in partial fulfillment of the requirements for the degree of
Doctor of Philosophy (Chinese Medicine)
December 2025

ABSTRACT

VASODILATION AND ANTI-HYPERTENSIVE EFFECTS OF AN ORTHOGONAL STIMULUS-RESPONSE-OPTIMISED COMBINED FORMULATION OF EUPATORIN, SINENSETIN, AND 3'-HYDROXY-5,6,7,4'TETRAMETHOXYFLAVONE IN A RAT MODELS

Yam Mun Fei

Modern medicine forms the backbone of current healthcare, providing a diverse array of synthetic and semi-synthetic compounds for both diagnosis and treatment. Designed to mimic or enhance the action of natural molecules, these compounds primarily target specific pathways within the body to alleviate symptoms or provide therapeutic benefits. Over the years, pharmaceutical development has been largely guided by the "single-compound, single-target" approach. While this paradigm has been effective in developing treatments that address distinct molecular pathways, it has limitations when dealing with the increasingly prevalent multifactorial diseases seen today. Complex conditions, such as metabolic syndrome, emerge from a blend of genetic, environmental, and lifestyle factors, which are challenging to manage with single-target therapies. These limitations call for a reevaluation of current therapeutic strategies and invite an exploration of alternative approaches.

As society's health landscape shifts, there is an increasing interest in exploring alternative therapeutic options that are believed to have better suited to the complexities of contemporary diseases. Botanical medicines, often incorporating multiple active compounds, offer a holistic approach that potentially addresses several pathways simultaneously. Traditional medicines, especially those compounds derived from plants, have a long history of empirical use for treating complex conditions in various approach. One such medicinal plant, *Orthosiphon stamineus* Benth. (Lamiaceae) (commonly known as Java tea), has been traditionally used in Southeast Asia for its diuretic, anti-inflammatory, and antihypertensive properties. This plant has gained attention as a potential adjunct in modern antihypertensive regimens, attributed to its rich phytochemical profile, which includes flavonoids like sinensetin, eupatorin, and 3'-hydroxy-5,6,7,4'-tetramethoxyflavone (TMF). These compounds, known for their vasodilatory effects, may provide a synergistic impact on blood pressure regulation, making *O. stamineus* a promising candidate for further research. According to the theory of Chinese Material Medica, *O. stamineus* shares similar characteristics with *Polyporus umbellatus* (Zhuling) and *Plantago asiatica* (Che Qian Zi), as all three promote urination and clear dampness, which is essential for hypertension associated with phlegm-dampness, where fluid retention contributes to hypertension. Additionally, its cooling nature helps to moderate excess heat or yang, making it suitable for hypertension patterns involving liver fire or liver yang rising. By clearing heat and supporting fluid metabolism, *O. stamineus* can aid in reducing blood pressure, particularly in cases where

dampness and heat are predominant.

Previous studies have revealed that the chloroform fraction of *O. stamineus* exhibits substantial vasodilatory effects on isolated rat aorta *in vitro*. These effects were notably greater than the combined vasodilatory effects of its main components—sinensetin, eupatorin, and TMF—when tested individually. Such findings suggest that a synergistic interaction occurs when these compounds are administered together, possibly enhancing the therapeutic efficacy of the plant extract. The present study aimed to elucidate the interactions among sinensetin, eupatorin, and TMF and to identify the optimal combination ratio that maximizes their vasodilatory effect. To achieve this, *in vitro* aortic ring assays from Sprague-Dawley (SD) rats were utilized for vasodilation study. Using an orthogonal stimulus–response compatibility approach, various ratios of the three compounds were systematically tested to identify the most efficacious combination. Once the optimal ratio was established, the antihypertensive effect and mechanism of action of the optimum ratio were investigated. In this study, aortic rings from spontaneously hypertensive rats (SHRs) and SD rats were used to examine the vasodilation mechanisms. The antihypertensive effect of optimum ratio was also assessed through repeated-dose administration in SHRs.

In the experiments, the combined formulation designated as G28 (comprising eupatorin, sinensetin, and TMF in the ratios of EC_{20}:EC_{15}:EC_5) exhibited a significant concentration-dependent vasodilatory response, with a maximum

response (R_{MAX}) of 119.05 ± 3.29% and an EC_{50} of 6.78 ± 0.70 µg/mL. Interestingly, the vasorelaxant effects of G28 were more pronounced in SHR aortic rings than in SD rat aortic rings, suggesting that the formulation has heightened potency under hypertensive conditions. This may indicate that the compounds within G28 are more effective in the pathological environment of hypertension, which could be due to altered receptor sensitivity or changes in signaling pathways associated with vascular reactivity in hypertensive states.

The mechanistic studies revealed that the vasorelaxant effects of G28 were partially endothelium-dependent, as removing the endothelium reduced the vasodilatory response in both SHR and SD aortic rings. Further investigations into the specific pathways involved indicated that G28's action was independent of the nitric oxide (NO)/soluble guanylate cyclase (sGC)/cyclic guanosine monophosphate (cGMP) pathway, as evidenced by its retained efficacy in the presence of inhibitors such as L-NAME, methylene blue, and ODQ. However, the presence of potassium channel blockers, including glibenclamide, $BaCl_2$, 4-AP, and TEA, significantly attenuated the vasorelaxant effect, implicating the involvement of potassium channels in the formulation's mechanism of action. In addition, G28 appeared to exert its effects through modulation of intracellular calcium (Ca^{2+}) dynamics. Specifically, G28 antagonized voltage-operated calcium channels (VOCC) and inositol triphosphate receptors (IP_3R), which are critical regulators of Ca^{2+} influx in vascular smooth muscle cells. By reducing intracellular Ca^{2+} concentrations, G28 further contributes to the relaxation of vascular smooth

muscle.

In vivo assessments of G28-treated groups (15 mg/kg, 30 mg/kg, and 60 mg/kg) demonstrated significant reductions in the blood pressure of SHRs in a time-dependent manner over 21 days of oral treatment. The initial systolic blood pressure (SBP) of G28-treated groups (15 mg/kg, 30 mg/kg, and 60 mg/kg) were documented at 210.94±5.31 mmHg, 213.23±5.31 mmHg, and 205.98±2.04 mmHg, respectively, and decreased substantially to 189.79±4.17 mmHg (P<0.05), 189.40±2.87 mmHg (P<0.05), and 180.75±1.67 mmHg (P<0.001), respectively, following the 21 days of oral treatment compared to the negative control. The initial diastolic blood pressure (DBP) levels of the G28-treated groups (15 mg/kg, 30 mg/kg, and 60 mg/kg) were 152.67±9.34 mmHg, 154.56±9.09 mmHg, and 139.46±4.64 mmHg, respectively, before treatment, and ended up at 133.83±4.68 mmHg, 138.25±3.12 mmHg, and 129.67±3.12 mmHg after 21 days of treatment. Similarly, the initial mean arterial blood pressure (MAP) values for G28-treated groups were 171.73±7.95 mmHg, 173.75±7.82 mmHg, and 160.33±4.11 mmHg, which decreased to 140.56±3.60 mmHg (P<0.01), 152.13±4.41 mmHg, and 146.56±2.13 mmHg (P<0.05), respectively, compared to the negative control.

In conclusion, this investigation delineates the vasodilatory potential of G28, a novel formulation comprising eupatorin, sinensetin, and TMF at specific ratios. G28 exhibits a remarkable capacity to activate NO/sGC/cGMP

signaling pathways while concurrently initiating the AC/cAMP/PKA signaling cascade by enhancing PGI_2 production in vascular endothelium. Additionally, G28 elicits hyperpolarizing currents by activating potassium channels (K_{Ca}, K_V, K_{ATP}, and K_{ir}). G28 also inhibits vasoconstriction, achieved through antagonism of VOCC and IP_3R. Although these mechanisms observed in SD rat aorta were consistent, some variations were noted in SHRs, underscoring the impact of altered vascular physiology in the hypertensive state. It is essential to recognize that ex vivo rat aortic ring assays, while informative, offer only a limited perspective on the intricate mechanisms underlying G28-induced vasodilation. Thus, further exploration using molecular and histochemical methodologies is necessary to unravel protein expression and delineate the precise mechanisms of G28-induced vasodilation. The *in vivo* antihypertensive results underscore G28's potential as a candidate for further research in developing novel therapeutic strategies for hypertension, given its complex modulation of vasodilation mechanisms and blood pressure regulatory pathways.

Keywords: Sinensetin; eupatorin; 3’-hydroxy-5,6,7,4’-tetramethoxyflavone; aortic ring; antihypertension; vascular tone; orthogonal stimulus-response

Subject Area： RM1-950 Therapeutics. Pharmacology

Subject Area： RM300-666 Drugs and their actions

Subject Area： RS1-441 Pharmacy and materia medica

Subject Area： RS153-441 Materia medica

ACKNOWLEDGEMENTS

This thesis is dedicated to the laboratory animals whose sacrifices made this research possible. Their invaluable contributions have enabled significant advancements in our understanding of cardiovascular health, paving the way for scientific progress and potential therapeutic breakthroughs. I honor their role with profound respect and gratitude.

The completion of this thesis would not have been possible without the unwavering support, guidance, and inspiration of countless individuals. First and foremost, I owe my deepest gratitude to my supervisor, Dr. Teh Lai Kuan, whose steadfast encouragement and mentorship have shaped my research journey over the past four years. Her boundless enthusiasm for science, relentless pursuit of excellence, and unwavering commitment to her students have been a constant source of motivation. Her approachability and willingness to guide me through challenges made this journey not only manageable but deeply rewarding.

To my beloved family—Mr. Yam Saik Kheong and Mdm. Teoh Chung Choo—I am forever indebted to your unconditional love and sacrifices. You have provided me with the strongest foundation, nurturing my growth with unwavering support even through life's toughest challenges. To Lee Fung, Yuan Yu, Fei Yang, Xiao Zhu, and Duo Duo, thank you for being my pillars

of strength, offering endless patience, encouragement, and belief in me even when the path seemed uncertain.

I am also immensely grateful to my co-advisor, Dr. Yap Yao Pin, for his invaluable academic guidance and mentorship. His passion for research and dedication to excellence have profoundly influenced my scholarly development. Beyond the lab, his thoughtful invitations and memorable trips brought light to some of the most demanding phases of my work, reminding me of the joy in discovery.

My sincere appreciation extends to my collaborators—Ms. Tew Wan Yin, Mr. Yan Chong Seng, and Dr. Tan Chun Shan—for fostering a dynamic and supportive research environment. Your camaraderie and shared dedication made this journey not just productive but truly meaningful.

I would also like to express my deepest gratitude to Prof. Xu Wei and Dr. Xu Wen from Fujian University of Traditional Chinese Medicine for their generous financial support and encouragement. Their contributions not only facilitated the practical aspects of my research but also strengthened an invaluable international collaboration, enriching my academic experience in countless ways. Finally, to all those who have contributed, directly or indirectly, to the completion of this thesis—thank you.

M. KANDIAL FACULTY OF MEDICINE AND HEALTH SCIENCES

UNIVERSITI TUNKU ABDUL RAHMAN

Date: 11-11-2025

SUBMISSION OF THESIS

It is hereby certified that **Yam Mun Fei** (ID No: **21UMD04373**) has completed this thesis entitled "*VASODILATION AND ANTI-HYPERTENSIVE EFFECTS OF AN ORTHOGONAL STIMULUS-RESPONSE-OPTIMISED COMBINED FORMULATION OF EUPATORIN, SINENSETIN, AND 3'-HYDROXY-5,6,7,4'TETRAMETHOXYFLAVONE IN A RAT MODELS*" under the supervision of Dr. Teh Lai Kuan (Supervisor) from the Department of Allied Health Sciences, Faculty of Science, and Dr Yap Yau Pin (Co-Supervisor) from the Department of Chinese Medicine, Faculty of M. Kandiah Faculty of Medicine and Health Sciences.

I understand that University will upload softcopy of my thesis in pdf format into UTAR Institutional Repository, which may be made accessible to UTAR community and public.

Yours truly,

_____

(*Yam Mun Fei*)

*Delete whichever not applicable

APPROVAL SHEET

This thesis entitled "**VASODILATION AND ANTI-HYPERTENSIVE EFFECTS OF AN ORTHOGONAL STIMULUS-RESPONSE-OPTIMISED COMBINED FORMULATION OF EUPATORIN, SINENSETIN, AND 3'-HYDROXY-5,6,7,4'TETRAMETHOXYFLAVONE IN A RAT MODELS**" was prepared by YAM MUN FEI and submitted as partial fulfillment of the requirements for the degree of Doctor of Philosophy (Chinese Medicine) at Universiti Tunku Abdul Rahman.

Approved by:

_____
(Asst. Prof. Dr. Teh Lai Kuan)
Date: 8/11/2025
Assistant Professor/Supervisor
Department of Allied Health Sciences
Faculty of Science
Universiti Tunku Abdul Rahman

_____
(Asst. Prof. Dr. Yap Yau Pin
Date: 8/11/2025
Assistant Professor/Co-supervisor
Department of Chinese Medicine
M. Kandiah Faculty of Medicine and Health Sciences
Universiti Tunku Abdul Rahman

DECLARATION

I hereby declare that the dissertation is based on my original work except for quotations and citations which have been duly acknowledged. I also declare that it has not been previously or concurrently submitted for any other degree at UTAR or other institutions.

(Yam Mun Fei)

11-11-2025

IST OF TABLES

LIST OF FIGURES

LIST OF ABBREVIATIONS

%	Percentage
~	Approximate
µL	Microliter
µM	Micromolar
ºC	Degree Celsius
2-APB	2-aminoethyl diphenylborinate
4-AP	4-aminopyrine
AA	Arachidonic acid
AC	Adenylyl cyclase
ACEIs	Angiotensin-converting enzyme inhibitors
ACh	Acetylcholine chloride
AKT	Protein Kinase B
ALT	Alanine aminotransferase
ARBs	Angiotensin receptor blockers
AST	Aspartate aminotransferase,
Aβ	Amyloid-beta
BaCl2	barium chloride
BKCa	Large-conductance K_{Ca} channels
CaCl2	Calcium chloride
cAMP	Cyclic adenosine monophosphate
CCBs	Calcium channel blockers
cGMP	Cyclic guanosine monophosphate

CMC	carboxymethyl cellulose
COX-2	Cyclooxygenase-2
CSE	Cystathionine gamma-lyase
DAG	Diacylglycerol
DCFH	Dichlorofluorescin
DNA	Deoxyribonucleic acid
DPPH	Diphenylpicrylhydrazy
EC_{50}	Half maximum concentration
EDHF	Endothelium-derived hyperpolarizing factor
EDRF	Endothelium-derived relaxing factor
EDRFs	Endothelium-derived relaxing factors
EGTA	Ethylene glycol tetraacetic acid
eNOS	Endothelial nitric oxide synthase
g	Gram
g/L	Gram per liter
GBAC	Gallbladder cancer adenocarcinoma
GCPRs	G-proteins coupled receptors
GDP	Guanosine diphosphate
GEFs	Guanine nucleotide exchange factors
GTP	Guanosine triphosphate
H_2S	Hydrogen sulfide
HCC	Hepatocellular carcinoma
Hep3B cells	Hepatocellular carcinoma G2 cell

HepG2 cell	Hepatocellular carcinoma G2 cell
HMGB1	High-mobility group box 1
HSL	Hormone-sensitive lipase
HUVEC	Human umbilical vein endothelial cell
IC_{50}	Half inhibition concentration
IC50	Half Maximal Inhibitory Concentration
IFNγ	Interferon-gamma
IκB	Inhibitor kappa B
IκB-α	Inhibitor kappa B-alpha
IKCa	intermediate-conductance KCa
IL-10	Interleukin-10
IL-1β	Interleukin-1 beta
IL-6	Interleukin-6
iNOS	Inducible Nitric Oxide Synthase
IP3	Inositol trisphosphate
KATP	ATP-sensitive K+ channels
KCa	calcium-activated K+ channels
KCl	Potassium chloride
KH2PO4	Potassium dihydrogen phosphate
Kir	Inwardly-rectifying K+ channels
Kv	Voltage-gated K+ channels
LC3B-II	Microtubule-associated proteins 1A/1B light chain 3B-II
LDH	Lactate dehydrogenase

L-NAME	Nω-Nitro-1-arginine methyl ester
LPS	Lipopolysaccharide
MAPK	Mitogen-activated protein kinase
MB	Methylene blue
mg	Milligram
mg/dL	Milligram per deciliter
mg/kg	Milligram per kilogram
mg/mL	Milligram per milliliter
MgSO4	magnesium sulphate
min	Minute
mL	Milliliter
MLCK	Myosin light chain kinase
mM	Millimolar
mm	Millimeter of mercury
mmHg	Millimeter of mercury
mmol/L	Millimole per liter
MPC5	Mouse Podocyte Clone-5
mRNA	Messenger ribonucleic acid
MTT	3-(4,5-dimethylthiazol-2-yl)-2,5-diphenyltetrazolium bromide
NaCl	sodium chloride
NaHCO3	sodium hydrogen carbonate
NaHCO3,	hydrogen carbonate
NF-κB	Nuclear factor-kappa B

NLRP3	Nod-like receptor pyrin domain-containing protein 3
nM	Nanomolar
NO	Nitric oxide
NO/sGC/cGMP	Nitric oxide/soluble guanylate cyclase/cyclic guanosine monophosphate
NRF2	Nuclear factor erythroid-2-related factor 2
ODQ	1H-[1,2, 4]oxadiazolo[4,3,-a]quinoxalin-1-one
p-AMPK	Expression of phosphorylated AMP-activated protein kinase
PARP	Poly(ADP-ribose) polymerase
PARP	Poly(ADP-ribose) polymerase
PE	phenylephrine hydrochloride
PFT-α	(pifithrin-α
PGH2	prostaglandin H2
PGI_2	Prostacyclin
PI3K	Phosphoinositide 3-Kinase
PIP2	phosphatidylinositol 4,5-bisphosphate
PKA	Protein kinase A
PKG	protein kinase G
PLA2	Phospholipase A2
PLC-beta	phospholipase C beta
PTEN	Phosphatase and Tensin Homolog

qRT-PCR	Quantitative reverse transcription polymerase chain reaction
RMAX	maximum relaxation
SD	Sprague-Dawley
SHRs	Spontaneously Hypertensive rats
SKCa	small-conductance KCa
SOD2	Superoxide dismutase 2
TCM	Traditional Chinese Medicine
TEA	tetraethylammonium
THLE2	T-antigen immortalized human liver epithelial cell line 2
TJ-GBC2	TongJi-GallBladder Cancer-2
TMF	3'-hydroxy-5,6,7,4'-tetramethoxyflavone
TNF-α	tumor necrosis factor alpha
TPA	Terephthalic acid
U/L	Units per liter
UPLC–MS/MS	Ultra-Performance Liquid Chromatography with Tandem Mass Spectrometry
VEGF	vascular endothelial growth factor
VOCC	voltage-gated calcium channels
SMCs	vascular smooth muscle cells

CHAPTER 1

INTRODUCTION

1.1 Background

Malaysian Clinical Practice Guidelines on hypertension of 2013 reveals that one-third of citizens aged 18 and above have hypertension in 2013. Above the age of 30, this figure rises to nearly 45%. Hypertension which is often referred to the "silent killer," challenges the global public health significantly contributes to atherosclerosis and coronary artery disease as well as to aortic aneurysm pathologies and congestive heart failure and strokes. The diseases congestive heart failure, stroke, diabetes, and renal and retinal diseases exist together in association with hypertension. Cardiovascular diseases remain the leading causes of death for those above 40 years old in Malaysia and hypertension, the direct precursor of the condition. Over the past decade, the prevalence of these diseases has shown a significant upward trend. Therefore, there is necessity to conduct further research and discover effective medications to manage hypertension to assist in significantly lowering the chances of cardiovascular diseases among our population. There are numerous antihypertensive drugs in the market, most of which have been proved efficient in the treatment of hypertension. Most synthetic antihypertensive drugs exert their effects by selectively targeting specific physiological mechanisms involved in blood pressure regulation, however research suggests that

combination of one or more target drug for hypertension therapy may offer greater efficacy compared to single-drug treatments (Xiong *et al.*, 2013a). This is also seen in clinical guidelines for hypertension treatment algorithm whereby a combination of agents are added to allow better control of patient's condition. Due to the complex nature of hypertension, which often coexists with a variety of related conditions, pharmacological research on antihypertensive drugs have been focused towards a more holistic and multi-targeting therapeutic agents approach in these recent years. Natural products and traditional medicines have gained significant attention worldwide as they meet these criteria, offering potential for more effective hypertension treatments (Xiong *et al.*, 2013b). The Malaysian government has actively promoted the development of local herbs through initiatives such as the NKEA 16 Entry Point Project, which identifies *Orthosiphon stamineus* as a medicinal plant with potential for effective hypertensive management. There are additional policies in place like *"Hala Tuju Kementerian Pertanian & Industri Asas Tani - Prioriti Dan Strategi 2019–2020"* emphasize the importance of local herbs, further supporting their research and development.

1.2 Problem Statement

The present study showed that the 3 isolates extracted from *Orthosiphon stamineus* which are eupatorin, sinensetin and 3'-hydroxy-5,6,7,4"-tetramethoxyflavone (TMF) exhibit significant vasodilatory effects which forms the scientific basis that *O. stamineus* extracts may be effective as an antihypertensive agent (Trimarco *et al.*, 2012). Although eupatorin,

sinensetin, and TMF all demonstrate vasodilatory properties, they appear to act through different distinct primary pathways. Eupatorin involves the soluble guanylyl cyclase/cyclic guanosine monophosphate (sGC/cGMP), inositol 1,4,5-trisphosphate receptor (IP_3R), and potassium and calcium channels, while sinensetin and TMF primarily act through the nitric oxide (NO)/sGC/cGMP pathway. Additionally, TMF also interacts with β-adrenergic and muscarinic receptors (Yam *et al.*, 2016a; Yam *et al.*, 2016b; Tan and Yam, 2018; Yam, Tan and Shibao, 2018). In a broader context, a concentration-vasodilation response curve using the chloroform extract of *O. stamineus* at 0.875 mg/mL demonstrated 60.59% relaxation. At this concentration, the extract contained 0.0407 mg/mL of eupatorin, 0.0261 mg/mL of sinensetin, and 0.00648 mg/mL of TMF. Notably, preliminary findings indicated that these compounds, when tested individually at the same concentrations, did not demonstrate any form relaxation which contrasted the results of using them in combination. Different compounds found in the chloroform extract do not show individual vasodilatory properties yet they work synergistically to create a notable vasodilatory response when measured together (Yam *et al.*, 2016a; Yam *et al.*, 2016b; Tan and Yam, 2018; Yam, Tan and Shibao, 2018). The simultaneous presence of eupatorin and sinensetin in addition to TMF within the chloroform fraction of *O. stamineus* appears to lead to potential synergistic interactions according to current observations. The precise biological processes involved in this combined action cannot be identified clearly. The mechanisms responsible for emerged vasodilatory effect need validation through additional studies investigating

compound-compound interactions within chloroform extract. Understanding these underlying effects will help establish new therapeutic treatments for hypertension management (Yam *et al.*, 2016a).

1.3 Hypothesis

The research hypothesizes that the combination of eupatorin, sinensetin, and TMF produces a synergistic effect, resulting in a collective vasodilatory activity.

1.4 Objective

1 To study the compound-compound interaction between eupatorin, sinensetin, and TMF resulting in vasodilatory activity using orthogonal stimulus-response model.

2 To elucidate the optimum ratio combination of eupatorin, sinensetin, and TMF using aortic ring model which produces the highest vasodilatory activity

3 To study the mechanism of vasodilation involved in the optimum ratio of eupatorin, sinensetin, and TMF via aortic ring model.

4 To study the anti-hypertensive effect of optimum ratio of eupatorin, sinensetin, and TMF using spontaneously hypertensive rats.

CHAPTER 2

LITERATURE REVIEW

2.1 Traditional Chinese Medicine

2.1.1 Syndromatic Differential Approach in Traditional Chinese Medicine

Within the context of Traditional Chinese Medicine (TCM) a syndrome, or pattern, occupies a central position within the theoretical construction of TCM and in clinical practice because it describes a patterned set of symptoms and signs presented by a patient at a particular point in the course of an illness. Instead of Western medicine where the treatment is usually aimed towards the disease or symptom presentation, TCM focuses on the detection and treatment of underlying deficiencies and excesses that are expressed as a constellation of symptoms and signs. Such a practice is largely representative of the holistic philosophy of TCM, which aim to address the source of disharmony and not only its superficial outcomes and symptoms.

TCM theory underlined that a syndrome involved a number of factors. This includes the demographics of the patient like gender, age, physical make up and the external factors like climate, weather and the lifestyle. It is the presence of both patient factor and external influences that helped to classify a syndrome and this is informed by the fundamental TCM theory, such as an

imbalance between Yin and Yang, a disturbance in the smooth flow of Qi (vital energy), the stagnation of blood or malfunction of a particular organ system. These principles assist practitioners to classify syndromes and formulate specific treatment plans, which fit with the distinct conditions of the patient.

2.1.2 Traditional Chinese Medicine in Hypertension Treatment

Hypertension is characterized by elevated systemic arterial blood pressure and is broadly classified into two categories: primary hypertension and secondary hypertension. Primary hypertension accounts for the majority of reported cases and serves as a major risk factor for cardiovascular and other systemic diseases. As opposed to that, secondary hypertension is due to identifiable underlying conditions; it is most times called symptomatic hypertension. Clinically, hypertension is diagnosed by repetitive high blood pressure readings, and patients may experience dizziness, headaches, chest discomfort, and fatigue. Long-term results in damage to vital organs: the brain, heart, and kidneys.

There are various combination factors causes the development of hypertension which includes genetics, age, occupation, environmental conditions, and lifestyle habits such as diet and physical activity. Blood pressure spikes can also be regarded as a response to emotional stress and straining physical activity. The most vulnerable people to the stated phenomenon are people of middle and advanced age, and in case it is

accompanied by complications related to the damage of the heart, brain, or kidneys, the prognosis can be not as positive.

In TCM, hypertension is classify under category of "dizziness" or "headache', reflecting its symptomatic presentation. TCM professionals are given special training to treat hypertension by focusing on the pathological processes, imbalances and disharmonies within the body, rather than focusing solely on the elevated blood pressure itself which is the biggest difference with Western medications which focuses on reducing the pressure and elevating of symptoms alone.

2.1.3 Etiology of Hypertension According to Traditional Chinese Medicine Principles

In TCM, hypertension is viewed as the result of different pathophysiological changes, which reflect different imbalances in the organism. Among these is the hyperactivity of Liver Yang which forms as a result of stagnant Liver Qi that has been transformed into fire and thus increasing Liver Yang and causing internal wind. The upper orifices are impacted by this unrest and the symptoms of this inconvenience are headaches, dizziness, irritability and bitter mouth, which is also a common symptom. The overall treatment plans usually target the pacification of the Liver and subordinated hyperactive Yang. This syndrome involves the use of Tianma Gouteng Decoction with modification.

Improper diet can weaken the spleen and stomach, this will have caused accumulation of dampness and phlegm and the syndrome is known as Phlegm-Dampness accumulation. The accumulation blocks the upward movement of clear Yang and the downward flow of turbid Yin, causing symptoms like dizziness, a heavy feeling in the head, and chest discomfort. The treatment strategy aims to dissolve phlegm and remove dampness, typically using modified prescriptions such as Banxia Baizhu Tianma Decoction.

Another common pattern, known as Kidney and Liver Yin deficiency is triggered by overexertion, excessive sexual activity and natural aging process depletes Kidney essence, resulting in hyperactivity of deficient Yang. Symptoms such as mild headaches, dizziness, tinnitus and soreness in the lower back are often manifested. Hence, the treatment principle according to TCM theory focuses on nourishing the Liver and Kidney, using with modified treatment approach, Dabuyuan Decoction.

Tongqiao Huoxue Decoction is a treatment approach that emphasizes on blood circulation and resolving stasis, often deployed to resolve hypertension that is related to blood stasis. This pattern of imbalance typically results from prolonged illness that damages the collaterals and leads to blood stasis within the vessels. Clinically, it often manifests as headaches with sharp, pricking sensations, stabbing chest pain, and numbness in the limbs, a purplish tongue and an irregular pulse.

Lastly, Yin and Yang deficiency occurs when Yin deficiency extends to involve Yang, resulting in deficiency of Yin and Yang in Liver and Kidney. This pattern is marked by symptoms such as dizziness, weight loss, fatigue, and frequent night time urination. The treatment principle is to regulate and nourish Yin and Yang, with herbal formulations like Jingui Shenqi Pill frequently prescribed.

2.2 Sinensetin

2.2.1 Chemical Profile of Sinensetin

Sinensetin is an achiral compound belonging to the 7-O-methylated flavonoid group, classified as a polymethoxylated flavonoid (Figure 2.1) (Feng *et al.*, 2023). The following provides a thorough description of sinensetin:

Molecular formula:	$C_{20}H_{20}O_7$
Molecular weight:	372.37 g/mol
Elemental composition:	Carbon: 64.51%, Hydrogen: 5.41%.Oxygen: 30.08%
IUPAC name:	2-(3,4-Dimethoxyphenyl)-5,6,7-trimethoxy-4H-chromen-4-one; **Synonyms**: 5,6,7,3′,4′-Pentamethoxyflavone, Pedalitin permethyl ether

Physical properties:	**Melting Point**: 174–176°C
	Boiling Point: 547.85 ± 50.0°C
	Solubility: 24.04 mg/L in water (25°C)
	Form: Powder (store at 2–8°C)
CAS registry number	2306-27-6

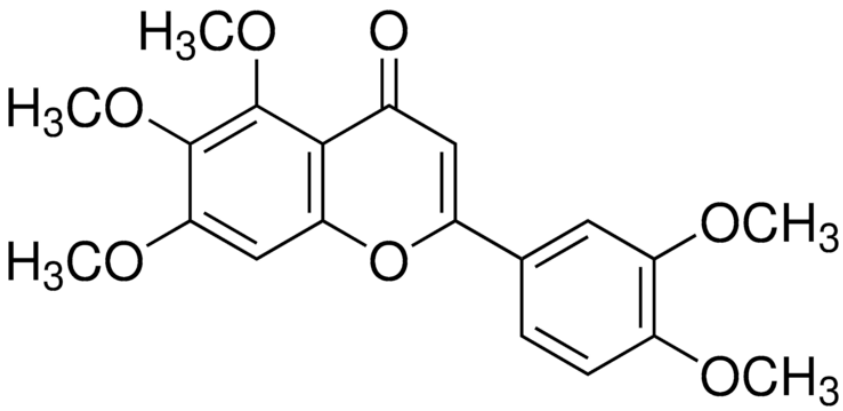

Figure 2.1: Chemical structure of sinensetin.

2.2.2 Bioactivity of Sinensetin

The efficacy of sinensetin as an antihypertensive agent has been extensively studied through both *in vitro* and *in vivo* experiments. Besides its vasorelaxant properties, sinensetin has been found to exhibit a range of beneficial pharmacological activities which includes anti-inflammatory, antioxidant, antibacterial, anti-obesity, anti-dementia, and anticancer effects. However, what makes it notably a promising candidate as a potential choice

of therapy in cancer management is its exhibition of minimal toxicity effects and still maintaining its high efficacy.

Numerous studies have highlighted that alongside with its other therapeutic effect, sinensetin has the ability to inhibit cancer growth. However, due to its finite natural availability, most researchers rely on commercially synthesized sinensetin to evaluate its pharmacological properties. Scientific data on sinensetin, for those obtained from natural sources or synthetic methods, are critically analyzed to provide valuable insights and provided a new possibility and perspective into its use for cancer prevention and treatment (Lee *et al.*, 2020).

2.2.2.1 Anti-cancer Properties of Sinensetin

Sinensetin has demonstrated significant anticancer activity, with several studies highlighting its potential in treating hepatocellular carcinoma (HCC) and gallbladder cancer. It is shown that as a bioactive molecule, sinensetin exhibits promising anticancer capabilities, while interferon-gamma (IFNγ) is well-known for its antiviral, anticancer, and immunoregulatory properties. According to the scientists Feng et al. (2023), sinensetin interacts with IFNγ by hydrophobic forces and static quenching and preserves the protein structures of IFNγ virtually unchanged. Molecular docking and dynamic simulation were employed for protein-ligand interaction and structural stability analysis.

Effect of sinensetin combined with IFNγ influences hepatocellular carcinoma HepG2 cell proliferation was reported using 3-(4,5-dimethylthiazol-2-yl)-2,5-diphenyltetrazolium bromide (MTT) assay. The experimental mixture of sinensetin with IFNγ resulted in substantial cell viability reduction to 65.46%. The study revealed that combining sinensetin with IFNγ enhanced anti-proliferative effects on HepG2 cells by increasing caspase-3 messenger ribonucleic acid (mRNA) expression level. Research reveals the ability of sinensetin to form complexes with proteins for cancer treatment applications (Feng *et al.*, 2023).

A previous study demonstrated that sinensetin caused programmed cell death through human hepatocarcinoma cells which occurred based on p53 genetic expression changes. Sinensetin activated autophagy in HepG2 cells (p53 wild-type) and apoptosis in Hep3B cells (p53-null).

THLE-2 (T-antigen immortalized human liver epithelial cell line 2), proliferation remained unaffected thus demonstrating the limited toxicity effect of sinensetin towards THLE-2. This selective toxicity to only the HCC cells highlights sinensetin's target-specific nature, making it a promising candidate for HCC treatment and prevention strategies (Kim *et al.*, 2020). Utilizing it as an agent for management of HCC would have the potential of deployment of a highly specific targeted treatment with minimal side effects towards normal cells and thus improved tolerability and efficacy of HCC treatment.

In this study, HepG2 cell was pre-treated with a combination of pifithrin-α (PFT-α, p53 inhibitor), and sinensetin. This therapy had led to increased levels of p62, cleaved poly(ADP-ribose) polymerase (PARP), and cleaved caspase-3 proteins and reduced the levels of phosphorylated AMP-activated protein kinase (p-AMPK), and microtubule-associated proteins 1A/1B light chain 3B-II (LC3B-II). It showed a significance over sinensetin treatment. Not blocking p53 translocation by PFT-α altered the cellular response of autophagy to apoptosis in HepG2 cell with sinensetin. This comes out strongly to be indicative of autophagy induction by the movement of p53 out of the cytosol and into the nucleus. To further verify the involvement of p53 in the p53-apoptosis of HepG2 cells, the p53-deficient Hep3B cells will be treated with sinensetin, leading to apoptotic cells with little autophagy markers revealed. The results reveal that sinensetin suppresses cell viability more evident in HepG2 compared to Hep3B cells due to the expression pattern of p53 in these two cell lines in the state of sinensetin-induced liver cancer cell death. The outcome of the molecular docking study revealed that sinensetin is able to bind to p53 core domain residues efficiently and further validated its cell death promoting potential (Kim *et al.*, 2020).

Research indicates that sinensetin displays anticancer properties against human gallbladder cancer adenocarcinoma cells that have become resistant to treatment. Sinensetin presents potential anti-tumor properties which induce cell mortality and blocks cell migration and invasion through the disruption of the phosphatase and tensin homolog/phosphoinositide 3-kinase/protein

kinase B (PTEN/PI3K/AKT) signaling pathway. The anti-cancer properties of sinensetin gain further significance because this signaling pathway controls cell proliferation along with growth and metabolism and apoptosis processes. The analysis indicated that Sinensetin produced a direct relationship between its concentration and its capability to restrict cell mobility and invasive actions of gallbladder cancer cells. Western blotting analysis confirmed how sinensetin affects the PTEN/PI3K/AKT signaling pathway within TongJi-gall bladder Cancer-2 (TJ-GBC2) cells. The use of sinensetin resulted in elevated PI3K and AKT enzyme levels but did not change the expression of PTEN or the modified of phosphorylated forms of PI3K and AKT (p-PI3K and p-AKT). When applied to cell cultures sinensetin diminishes the activity of PTEN/PI3K/AKT pathway with efficiency. Evidence from our studies indicates that sinensetin shows promise to serve as an anticancer therapeutic agent for gallbladder carcinoma (Huang *et al.*, 2020).

2.2.2.2 Sinensetin Inhibits Cisplatin-induced Pyroptosis and Attenuates Intestinal Injury

Scientists found that sinensetin specifically kills tumor cells effectively while it exhibits minimal impact on regular cell populations at different dose levels. The analysis through quantitative reverse transcription polymerase chain reaction (qRT-PCR) showed sinensetin reduced both interleukin-6 (IL-6) and tumor necrosis factor-alpha (TNF-α) mRNA levels thus confirming its anti-inflammatory properties. Prior exposure to sinensetin generated a substantial reduction in both lactate dehydrogenase (LDH) and

high-mobility group box 1 (HMGB1) proinflammatory factor release due to cisplatin treatment. Laboratory tests prove that sinensetin prevents tumor cell pyroptosis after cisplatin treatment by decreasing caspase-3 activation and blocking gasdermin E activity levels.

The compound sinensetin demonstrated ability to reduce the generation of reactive oxygen species and deoxyribonucleic acid damage which occurred after cisplatin exposure. Inflammatory lesions and intestinal damage caused by cisplatin received protection through sinensetin treatment which promoted lowered lytic cell death and decreased immune cell infiltration. Laboratory tests show the combined use of sinensetin with cisplatin maintained the treatment effectiveness of cisplatin while preventing a reduction in treatment power. Experimental results show that combined administration of sinensetin helps minimize unwanted side effects triggered by cisplatin without affecting its cancer-fighting properties (Li *et al.*, 2023b).

2.2.2.3 Sinensetin Ameliorates High Glucose-induced Diabetic Nephropathy

Research investigated how sinensetin affects autophagy together with cell survival performance in mouse podocyte clone-5 (MPC5) cells exposed to high glucose. The development of a diabetic nephropathy mice model occurred through streptozotocin (40 mg/kg) administration into the peritoneal space for five days followed by 60% high-fat diet feeding. The results found that intraperitoneal administration of sinensetin at 10, 20, and

40 mg/kg showed significant improvements in diabetic nephropathy mouse renal function and protection against high glucose damage of MPC5 cells. Under high glucose conditions the autophagy activity of MPC5 cells recovered after administration of sinensetin. Experimental data shows that sinensetin stimulates autophagic activity within renal tissues of diabetic nephropathy mice. Sinensetin functions as a protective therapeutic for diabetic nephropathy through its ability to restore autophagic activity and supports its potential development as a medical treatment (Kong *et al.*, 2023).

2.2.2.4 Anti-diabetic Effect of Sinensetin

A study by Mohamed et al. (2013) identified a fraction of compound rich in sinensetin and eupatorin from *Orthosiphon aristatus* can significantly reduce glucose levels. This fraction impedes the absorption of glucose in the jejunum without altering insulin levels in streptozotocin-induced diabetic rats. Since hyperglycaemia in type 2 diabetes mellitus is largely driven by elevated postprandial glucose levels resulting from starch hydrolysis by pancreatic α-amylase and subsequent glucose absorption mediated by intestinal α-glucosidase, the inhibition of these enzymes represents a promising strategy for managing postprandial hyperglycaemia in type 2 diabetes.

In a separate study, sinensetin demonstrated strong inhibition of α-glucosidase (89.0–32.0%) at concentrations dependent manner, with an IC_{50} value of 0.66 mg/mL. This inhibition efficacy of sinensetin is shown to be superior than acarbose and *O. aristatus* methanolic extract. Additionally,

sinensetin showed 85.8% inhibition of porcine α-amylase at 2.5 mg/mL, this further supporting its antidiabetic potential (Mohamed *et al.*, 2012).

2.2.2.5 Anti-inflammatory Activity of Sinensetin

Lipopolysaccharide (LPS) and TNF-α are primary stimuli that activate macrophages during inflammatory responses. In a study by Lin et al. (2023), sinensetin demonstrated protective effects against LPS-induced inflammatory injury in the lungs and liver. In LPS-challenged mice, sinensetin significantly reduced the liver-to-body weight ratio and improved lipid profiles, along with lowering serum levels of alanine aminotransferase (ALT) and aspartate aminotransferase (AST), which were otherwise elevated due to inflammation. Besides protection towards the liver, sinensetin acts in significantly reducing inflammatory infiltration and tissue damage in the liver as well as the lungs. The same study investigated the pathway involved in sinensetin mechanism and revealed that sinensetin targets sirtuin 1 which activates the nuclear factor erythroid-2-related factor 2/superoxide dismutase 2 (NRF2/SOD2) signaling pathway, promoting M2 macrophage polarization and inhibiting nod-like receptor pyrin domain-containing protein 3 (NLRP3) inflammation formation. This underscore the ability of sinensetin in modulating inflammatory responses by reducing the level of proinflammatory cytokines, including TNF-α and IL-6 while upregulating the anti-inflammatory cytokine interleukin 10 (IL-10) (Lin *et al.*, 2023).

In a different study, sinensetin's anti-inflammatory effects were assessed using LPS-stimulated RAW 264.7 macrophages. Activation of mitogen-activated protein kinase (MAPK) and nuclear factor-kappa B (NF-κB) pathways including the degradation of inhibitor kappa B (IκB) acts as a precursor of LPS-induced inflammation. Sinensetin inhibits NF-κB activation by stabilizing inhibitor kappa B-alpha (IκB-α), thereby suppressing excessive inflammation without affecting MAPK phosphorylation. Pre-treatment with sinensetin for an hour long resulted in sinensetin dose-dependently inhibited nitric oxide (NO) secretion and the protein expression of inducible nitric oxide synthase (iNOS) and cyclooxygenase-2 (COX-2). At 50 μM, sinensetin attenuated the mRNA levels of proinflammatory cytokines interleukin-1 beta (IL-1β), IL-6, and TNF-α (Shi *et al.*, 2024).

The research indicates that sinensetin controls IκB-α protein activity to reduce the expression of inflammation-linked genes (iNOS, COX-2, IL-1β, IL-6, and TNF-α) in LPS-induced inflammatory macrophages. The observed research data demonstrates that sinensetin shows strong potential as an anti-inflammatory therapeutic agent (Shi *et al.*, 2024).

2.2.2.6 Antioxidant Activity of Sinensetin

Strong antioxidant properties of sinensetin serve as a protective mechanism for organism cells during oxidative stress situations. Its antioxidant function permits radical free scavenging activities that protect against oxidative harm because such damage plays a vital role in disease

formation, including cancer, neurological conditions and cardiovascular diseases. The direct protective effects of sinensetin against cells stem is come from its ability to scavenging free radicals thus minimizing the development of radical-related illness. Researchers investigated the inhibitory impact of 15-lipoxygenase on low-density lipoprotein oxidation because this enzyme contributes to atherosclerotic plaque formation. Sinensetin functions as an agent that reduces atherosclerotic plaque production which leads to direct benefits that protect the heart. Experimental evidence reveals that sinensetin reduces soybean 15-lipoxygenase sensitivity to air damage yet fails to protect sulfhydryl groups below 160 μM. Additionally, sinensetin's free radical scavenging ability was evaluated using dichlorofluorescin (DCFH) and diphenylpicrylhydrazyl (DPPH) assays, where it demonstrated low free radical scavenging effect (Lyckander and Malterud, 1996).

2.2.2.7 Anti-obesity Activity of Sinensetin

An imbalance between adipogenesis often leads to obesity. Phytochemicals that encourage adipocyte lipolysis is an effective therapeutic agent to curb obesity. A study by Kang et al. (2015) found that sinensetin enhances adipogenesis in both 3T3-L1 and preadipocytes. Besides that, sinensetin also caused lipolysis in mature adipocytes. This study evaluated glycerol levels in culture supernatants as an indication of lipolytic capacity of sinensetin in mature adipocytes 3T3-L1. Sinensetin significantly increases lipolytic activity in adipocytes at 24 hours and 48 hours after treatment. The result showed that sinensetin enhanced the phosphorylation of protein kinase

A (PKA) and activation of hormone-sensitive lipase (HSL). HSL hydrolytic activity rises and HSL relocates to lipid droplets as a result of this process. Treatment with Sinensetin induces a fast increase of cyclic adenosine monophosphate (cAMP) levels which intensifies with rising concentrations of the drug. Independent laboratory tests indicate that sinensetin raises cAMP levels within cells which subsequently results in lipolysis throughout adipocytes (Kang, Shin and Kim, 2015).

2.2.2.8 Vasorelaxant Effect of Sinensetin

Researcher evaluated sinensetin vasodilatory effects through the phenylephrine (PE) precontraction aortic ring assay. Results indicated that sinensetin successfully produced vasodilation effects in PE precontraction aortic ring assays both with and without endothelium. The vasodilation mechanism functions through at least four pathways including NO/sGC/cGMP and cyclooxygenase pathway and potassium channels and calcium channels and muscarinic and beta-adrenergic receptors. Research evidence shows that sinensetin elicits vasorelaxation results independently from endothelial function yet additional systems require examination (Yam, Tan and Shibao, 2018).

2.2.2.9 Anti-microbial Effect of Sinensetin

The parasite inhibition study showed a direct connection between sinensetin dosage with *Trypanosoma brucei* resistance levels. The tested compounds demonstrated their potency in the following order: pentamidine

followed by nobiletin then reagent-grade nobiletin before reagent-grade sinensetin and lastly sinensetin. Researchers used Resazurin assay to evaluate the toxicity of these compounds against human embryonic kidney cells. While sinensetin and nobiletin exhibited anti-trypanosomal activity, their IC_{50} values and selectivity indexes were inferior to modern anti-trypanosomal drugs. In another study, sinensetin was evaluated for its ability to inhibit quorum sensing, biofilm formation, and the type three secretion system in an *in vitro* model. Sinensetin showed high selectivity and minimal toxicity to normal cells, highlighting its potential as an antimicrobial agent (Vikram *et al.*, 2010).

2.2.2.10 Anti-angiogenesis Activity of Sinensetin

A present research studied the anti-angiogenic potential of 7 polymethoxylated flavonoids (Lam *et al.*, 2012), Lam and colleague found that sinensetin was the most effective with a high therapeutic index and low toxicity. Sinensetin also inhibits angiogenesis in human umbilical vein endothelial cell (HUVEC) cultures by inducing early cell cycle arrest at the G0/G1 phase. The study also revealed sinensetin suppresses the vascular endothelial growth factor (VEGF)-stimulated HUVECs growth in concentration-dependent manners. Moreover, sinensetin inhibits intersegmental vessels (ISV) and dorsal longitudinal anastomotic vessels (DLAV) formation in Tg(fli1a:EGFP)^y1 transgenic zebrafish. These finding further support sinensetin's anti-angiogenic properties, which is associated

with the downregulation of angiogenesis-related genes, including *flt1*, *kdrl*, and *hras* (Lam *et al.*, 2012).

2.2.2.11 Toxic Effects of Sinensetin on Zebrafish Embryos

Research has shown that using zebrafish embryos established sinensetin as a less fatal compound among other tested. The zebrafish embryo assay monitored heartbeat activity of the embryos following compound exposure to check their survival rate. Among all the compounds tested sinensetin presented the most potent anti-angiogenic properties yet it maintained the lowest mortality rate. The survival rate of embryos exposed to 100 μM sinensetin reached 40% after 48 hours post-treatment. Researchers determined nobiletin to be the most harmful compound because it killed all embryos at its lowest concentration within 48 h post-treatment period. The toxicity of hesperetin rested in the middle range due to its killing effect on 80% of embryos exposed to maximum concentrations after 48 hours of treatment. All compounds exhibited developmental problems in zebrafish embryos which resulted in differences ranging from incomplete pigmentation to diminished trunk size and reduced embryo survival rates. Steps forward can be pursued as scientists assess sinensetin due to its minimal toxic nature when compared to alternative compounds (Lam *et al.*, 2012).

2.3 Eupatorin

2.3.1 Chemical Profile of Eupatorin

Molecular formula:	$C_{18}H_{16}O_7$
Molecular weight:	344.3 g/mol
Elemental composition:	Carbon: 62.79%, Hydrogen: 4.68%.Oxygen: 32.53%
IUPAC name:	5,3′-Dihydroxy-4′,6,7-trimethoxyflavone
Physical properties:	**Melting Point**: 587.0 ± 50.0 °C **Boiling Point**: 573.7 ± 50.0°C **Solubility**: 45.5mg/L in water (25°C) Density: 1.4 ± 0.1 g/cm³
CAS registry number:	855-96-9

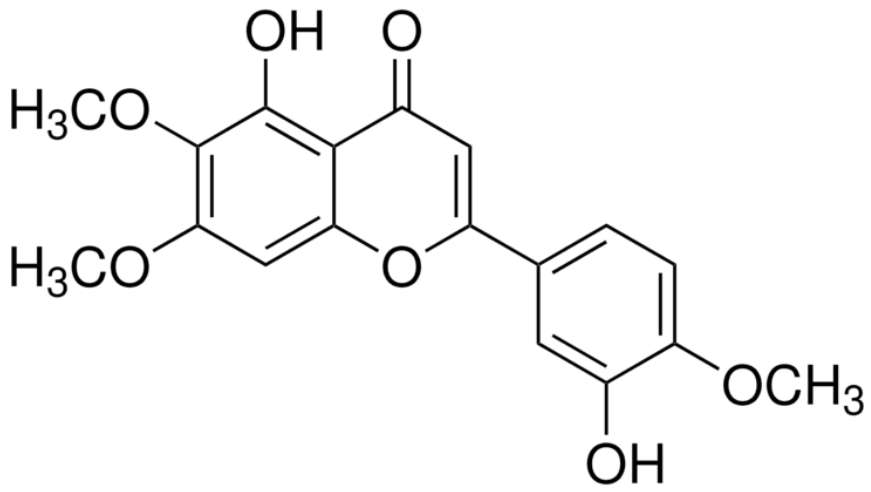

Figure 2.2: Chemical structure of eupatorin.

Eupatorin belongs to the category of 6-hydroxyluteolin trimethoxyflavone derivatives. Three methyl groups occupy the phenolic positions 4', 6', and 7 in the molecular arrangement (Figure 2.2). The stability of the molecule develops from hydrogen bonds inside the molecule and between different molecule parts through hydroxyl hydrogen atoms bonding to carbonyl oxygen atoms (Rizou *et al.*, 2023).

2.3.2 Anti-proliferative, Cytotoxic, and Antiangiogenic Effects of Eupatorin

Laboratory research establishes eupatorin along with its separated compounds demonstrate antiproliferative and antiangiogenic activities. The quantity of eupatorin present in the extract was determined through Ultra-Performance Liquid Chromatography with Tandem Mass Spectrometry (UPLC–MS/MS) analysis and showed a concentration of 0.53 ± 0.08 mg/g dry weight. This measurement was then compared to pure eupatorin standard compound. Scientific analysis confirmed that pure eupatorin extract possessed micromolar IC_{50} inhibitory concentrations that showed significant mitotic control activity against cancerous cells. Study results revealed eupatorin presented selective toxicity which proved more efficient against multiple cancer cell types than regular human cells (Dolečková *et al.*, 2012).

In the study, researcher determined eupatorin cytotoxicity in MCF-7 and MDA-MB-231 cells of human breast adenocarcinoma utilizing MTT. The cell proliferation inhibitory activities were dependent on the period of time

(24, 48 and 72 hours) and concentration range (0.16-20 μg/mL). The two cellular lines obtained IC_{50} values that were more than 20 ug/mL with the duration of the treatment being 24 hours. At 72 hours IC_{50} values of exposing eupatorin to MCF-7 cells showed 5 μg/mL succeeding 3 μg/mL and MDA-MB-231 cells showed 2 μg/mL. The eupatorin cytotoxicity was also extremely low considering the measurement of the effects of this compound on the MCF-10a non-cancerous cells where it required an IC_{50} of 30ug/mL to be toxic after 72 hours (Razak *et al.*, 2019).

2.3.3 Anti-inflammatory Effects of Eupatorin

The anti-inflammatory effect of eupatorin has been verified by its ability to suppress terephthalic acid (TPA)-induced inflammatory edema in mouse ear tissues. The study found eupatorin to be the most bioactive compound in a dichloromethane extract which exhibited strong antimicrobial and anti-inflammatory activities. The anti-inflammatory action is exerted related to the cyclooxygenase-1 (COX-1) inhibition and the concurrent suppression of the pro-inflammatory mediators, such as iNOS, COX-2, and TNF-α, which culminates in the down-regulation of the production of NO. *In vivo* studies revealed eupatorin's ability in inhibiting paw edema induced by carrageenan and TPA-induced ear edema in mice models (González-Cortazar *et al.*, 2022).

In the TPA test, eupatorin was found to be the most active compound showcasing anti-inflammatory effects by inhibition of enzyme COX-1. In one

of these studies, an increase in the study of biological activities of diterpenes and flavones found that eupatorin can inhibit iNOS, COX-2, and TNF-α. Besides, it can also produce NO (González-Cortazar *et al.*, 2022).

2.3.4 Vasorelaxation Effects of Eupatorin

Vasorelaxation, the relaxation or widening of blood vessels, plays a critical role in maintaining cardiovascular health. Thoracic aorta rings of rats that have been isolated were used to carry out research involving the investigations into the vasorelaxant properties of eupatorine. The experimental process began by carefully cleaning the aortic rings without damaging their endothelium, which is the element that controls the tone of the vascularity. Phenylephrine was used to contract the aortic rings before assessing eupatorin-impaired vasorelaxation in the condition to mimic vascular tension (Yam *et al.*, 2016b). Phenylephrine was used to put the aortic rings into tension before assessing eupatorin-impaired vasorelaxation in the condition to mimic vascular tension (Yam *et al.*, 2016b).

2.3.5 Anti-proliferative and Anti-angiogenic Effects of Eupatorin

Chloroform extract from the *O. stamineus* leaves was subject to intensive studies to elucidate the anti-proliferative action of this extract, which was due to eupatorin. The chloroform extract of pure quality was highly active on cancer cells since the resulting extract attained IC_{50} levels in the micromolar range that demonstrated a high cytotoxic potential. Pure eupatorin still had similar antiproliferative activity as the entire extract, which

demonstrates its essential participation in the therapeutic benefits of this herb. The extract and purified form of eupatorin caused G2/M phase cell cycle arrest leading to disrupted mitosis and tumor cell proliferation inhibition.

The anti-tumour effect of eupatorin includes causing mitotic catastrophe which develops from errors occurring during mitosis. The anti-tumour effects of eupatorin lead to standard apoptotic markers of deoxyribonucleic acid (DNA) fragmentation and caspase activation which demonstrate its capability to destroy cancer cells. The anti-tumor properties of eupatorin operated through selectivity which allowed cancer cells to suffer damage without causing significant harm to normal healthy tissues.

Angiogenesis, the process of new blood vessel formation, is critical for tumor growth and metastasis. Eupatorin demonstrates action against HUVEC movement and displays destructive effects on their tubular formation which is essential for angiogenesis development. Eupatorin blocks vascular development which results in tumors losing their access to vital nutrients and oxygen and subsequently causes cancer cell death.

Eupatorin is a promising anticancer effect since it acts as antiproliferative and antiangiogenic agents. This mode of action enables sinensetin to inhibit the proliferation of tumor cells and the induction of cell death provides it with improved anti-neoplastic property. Its selective cytotoxicity on cancer cells

along its angiogenesis inhibitory property makes it an attractive agent to be subjected to further preclinical and clinical studies (Dolečková *et al.*, 2012).

2.3.6 Eupatorin as an Anti-amyloid Agent in Alzheimer's Disease

The deposition of amyloid-beta (Aβ) peptides in the brain is critical factor of Alzheimer's disease. Recent therapeutic studies showed that eupatorin disrupts amyloidogenesis process, particularly slow down the aggregation of Aβ42 (a highly neurotoxic isoform) concentration-dependent manner. These results implies the critical role of eupatorin in reducing the formation of amyloid plaque (Rizou *et al.*, 2023).

2.3.7 Effects of Eupatorin on Centrosome Abnormalities

Previous scientific investigations uncovered the ability of eupatorin in preserving genomic integrity by interfering with cell divisions and chromosomal stability. Experimental evidence indicates eupatorin interfere with spindle microtubule organisation and delays M-phase in cell cycle. These intercession disrupt its mitotic checkpoint, hence leading to chromosomal instability.

The antiangiogenic and anti-proliferative properties of eupatorin enable it to function as dual-action anticancer agent. Angiogenesis is an important process that facilitates tumourigenesis and metastasis. The inhibitory action of eupatorin on HUVEC migration and disruption of tubular structure formation highlights its potential in suppressing angiogenic processes. Tumor

survival along with expansion becomes impossible when eupatorin blocks blood vessel growth thus depriving cancer cells of vital nutrients and oxygen thus promoting cell death. The compound eupatorin stands as a promising anticancer agent because it can block cancer cell proliferation as well as stop new blood vessel formation. Both inhibitory functions give this agent the ability to restrict tumors from growing and killing cancer cells to become an efficient anti-neoplastic medication. Future preclinical research and clinical evaluation will benefit from eupatorin because this agent selectively destroys cancer cells and restricts angiogenesis development. The pharmaceutical value of eupatorin as both a complementary therapeutic agent or standalone cancer treatment highlights its vital position in search for effective natural cancer solutions (Lam *et al.*, 2012).

2.4 3’-hydroxy-5,6,7,4’-tetramethoxyflavone

2.4.1 Chemical profile of 3’-hydroxy-5,6,7,4’-tetramethoxyflavone

Molecular formula:	$C_{19}H_{18}O_7$
Molecular weight:	358.3 g/mol
Elemental composition:	Carbon: 65.86%, Hydrogen: 4.91% .Oxygen: 29.24%
IUPAC name:	5,3′-Dihydroxy-4′,6,7-trimethoxyflavone
Physical properties:	**Melting Point**: 173-176 °C **Boiling Point**: 573.7 ± 50.0°C **Solubility**: 34.62 mg/L in water (25°C)

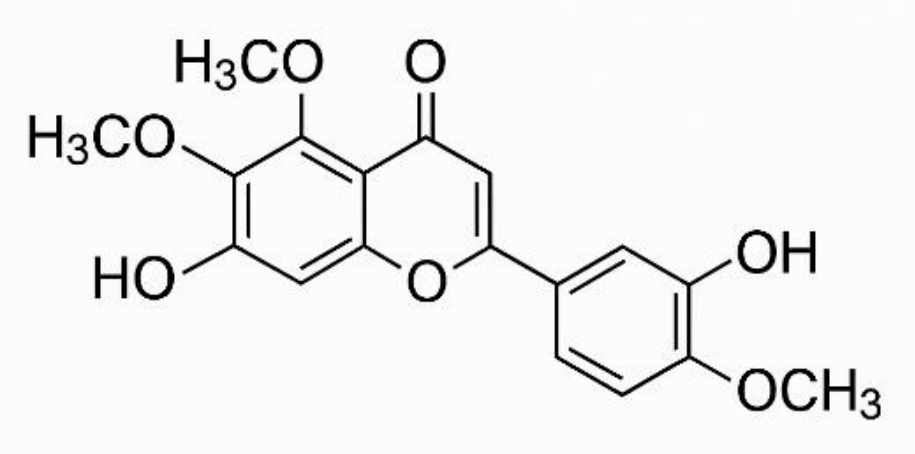

Figure 2.3: Chemical structure of 3'-hydroxy-5,6,7,4'-tetramethoxyflavone.

2.4.2 Vasorelaxation Effect of 3'-hydroxy-5,6,7,4'-tetramethoxyflavone

The *in vitro* examination of rat aorta models validated 3'-hydroxy-5,6,7,4'-tetramethoxyflavone (Figure 2.3) as a substance with substantial vasodilatory potential (Tan and Yam, 2018). Several distinct mechanisms which depend on NO/cGMP signaling, voltage-dependent potassium (K_V) channels, and calcium channels produce these results. The study conducted by Tan and Yam (2018) indicates that 3'-hydroxy-5,6,7,4'-tetramethoxyflavone achieves its vasorelaxation effect through two main calcium channel regulatory mechanisms which include blocking voltage-operated calcium channel (VOCC) and decreasing the amount of released intracellular calcium (Tan and Yam, 2018).

2.4.3 Anti-diabetic Effects of 3'-hydroxy-5,6,7,4'-tetramethoxyflavone

The compound 3'-hydroxy-5,6,7,4'-tetramethoxyflavone demonstrates effectiveness in blocking the enzyme activity of α-glucosidase and α-amylase which control carbohydrate digestion. α-amylase breaks down

starch into short-chain dextrins which are later processed into glucose by α-glucosidase. The binding interactions of TMF with these enzymes reduce their degradation capabilities of carbohydrates so blood sugar absorption slows down which helps control post-meal blood sugar spikes thus demonstrating potential therapeutic value for diabetes management (Mohamed *et al.*, 2012).

2.4.4 Anti-microbial Activity of 3'-hydroxy-5,6,7,4'-tetramethoxyflavone

Research demonstrates that TMF displays strong antimicrobial properties against prevalent bacterial and fungal strains. The compound destroys microbial cell walls and disrupts membranes to produce leakage that results in cellular destruction. The compound shows effective enzyme inhibition of critical bacterial and fungal microorganisms that are essential in growth and reproduction and thus restricts the growth of such microorganism (Cushnie and Lamb, 2005; Hossain *et al.*, 2012). The flavone compound TMF had excellent antibacterial activity in laboratory tests against different bacterial strains, especially reaching an 85.7% inhibition of *Staphylococcus aureus*. Additional experimental research confirmed antibacterial properties against *Bacillus subtilis* and *Salmonella typhi* alongside its broad-spectrum antibacterial action (Cushnie and Lamb, 2005). TMF demonstrates anti-*Candida albicans* properties which make it a promising agent for dealing with fungal infections conditions (Hossain *et al.*, 2012). TMF may also be utilized in combination with existing antibiotics to enhance their efficacy, particularly against drug-resistant strains. Nevertheless, further investigation is required

to fully elucidate its therapeutic potential, including its applicability in both topical and systemic treatments for infections, as well as its effectiveness against a broader spectrum of resistant pathogens.

2.4.5 Cytotoxicity potential of 3'-hydroxy-5,6,7,4'-tetramethoxyflavone in different cell types

A cytotoxicity study of polymethoxyflavones starting from 3,5,7,4'-tetramethoxyflavone through TMF and 5-hydroxy-3,7,3',4'-tetramethoxyflavone tested their activity against HCT-15 human colorectal cancer cells. Among the studied compounds TMF showed the strongest cytotoxic properties which targeted cancer cells through an apoptosis mechanism that depended on the compound concentration.

The characteristic apoptotic cell death morphology was detected by examining fragmented nuclei together with chromatin condensation after the exposure tests. Treated cells displayed DNA fragmentation as an apoptosis marker although the results indicated stronger effects occurred from TMF treatment than its related compounds 3,5,7,4'-tetramethoxyflavone and 5-hydroxy-3,7,3',4'-tetramethoxyflavone. The study shows that TMF works as an anticancer agent because it breaks down genetic material within tumor cells (Hossain *et al.*, 2012).

2.5 Current Therapeutic for Hypertension

The global market contains several antihypertensive drugs along with angiotensin-converting enzyme inhibitors (ACEIs) and angiotensin receptor blockers (ARBs) and beta-blockers and calcium channel blockers (CCBs) and diuretics (Ahmad *et al.,* 2023). Decisions about drug therapy are often based on overall vascular risk rather than just blood pressure levels (Al-Makki *et al.,* 2022). Angiotensin-converting enzyme inhibitors, ARBs, diuretics, and CCBs are first-line monotherapy options for patients with newly diagnosed asymptomatic uncomplicated hypertension (Collaboration, 2021). During the management of uncontrolled hypertension, increasing the dosage of monotherapy drugs remains the standard practice (Guerrero-García and Rubio-Guerra, 2018), which may cause long term exposure of adverse effects of drugs on the patients. Furthermore, some researches demonstrates that treatment that contains combination of two or more drugs has been more superior in providing higher flexibility in the management of hypertension and also protecting the cardiovascular system than using a single drug (Mancia *et al.,* 2019). This effectiveness is enhanced by the availability of diverse groups of antihypertensive drugs within these dual combinations. Hypertension sometimes requires alternative medicines, such as vasodilators which assists in reducing hypertension rate and provide adequate control of blood pressure. Vasodilators generally dilate blood vessels, lower blood pressure, and perfuse more organs so that they may function normally (Tarkin and Kaski, 2016). Hence, this calls for the urgent need for discovering newer effective drugs with no contraindications, such as vasodilators. At the same

time, since combination of drugs with multiple mechanism of action proves to be superior in management of hypertension, utilizing a drug that is able to adopt multiple pathways in reducing blood pressure might be more efficacious that a traditionally single pathway agent.

2.6 Vascular Tone

The response of vascular system to vascular tone and how vasomotor system responds to it is via vasodilation and vasoconstriction (Brozovich *et al.*, 2016). These responses are simply controlled by the expression of receptors on vascular smooth muscle and vascular endothelial cells, as well as the interaction of their signaling pathways (Sandoo *et al.*, 2010; Triggle *et al.*, 2012; Brozovich *et al.*, 2016; Tarkin and Kaski, 2016). The process of widening of blood vessels, also known as vasodilation, decreases blood pressure and increases blood flow because relaxation of smooth muscle cells that line the walls of the arteries and vein takes place. A certain class of substances known as vasodilators may be present, like endothelium-derived relaxing factor (EDRF) and endothelium-derived hyperpolarizing factor (EDHF) that act in one pathway, triggering a series of pathways that end up relaxing smooth muscle around blood vessels.

2.6.1 Endothelium-derived Relaxing Factors

The vascular endothelium forms an important part of a vascular system interface between the circulatory fluid and close tissues, modulating vascular tone by synthesizing prostaglandins, nitric oxide and other

vasodilatory substances (Sandoo *et al.*, 2010). Endothelial dysfunction is a pivotal determinant in categorizing the severity of hypertension. Current research showing that inhibition of NO which produce by endothelial nitric oxide synthase (eNOS) may elevated the blood pressure in human. This finding provides significant evidence that endothelial dysfunction is the underlying cause for the onset of hypertension (Kang, 2014). The endothelial dysfunction not only consists of the deficiency of endothelium-dependent vasodilation but also features the induction of endothelial inflammatory responses (Sun *et al.*, 2020).

Endothelium-derived relaxing factors, NO, prostacyclin (PGI_2), and EDHFs, serve as the principal mediators of endothelium-dependent vasodilation (Kang, 2014). Among these, NO is the most prominent EDRF and is involved in mediating vasodilation through multiple mechanisms. NO is responsible in regulation of vascular tone by activating the sGC that can be found predominantly in the vascular smooth muscle (Chen, Pittman and Popel, 2008). Most NO synthesis takes place in the endothelium and is catalysed by eNOS, which activates its calmodulin-binding domain when cytosolic Ca^{2+} levels rise (Förstermann and Sessa, 2012). L-arginine is then converted by eNOS into NO when activated. This is one of the major pathway of NO through which vasodilation occurs, operating by subsequent activation of cGMP-dependent pathways downstream of soluble guanylyl cyclase, which in turn activates the protein kinase G (PKG) that decreases intracellular calcium levels responsible for its vasodilatory effect.

Prostacyclin is one of the most extensively studied EDRFs, alongside NO. In endothelial cells, PGI_2 is synthesized from arachidonic acid (AA), a polyunsaturated fatty acid predominantly located within the phospholipid bilayer of cell membranes (Mitchell *et al.*, 2008). Phospholipase A_2 (PLA_2) or diacylglycerol (DAG) lipase releases the AA into the cytosol by hydrolysing the available phospholipid. COX, through peroxidase activity, subsequently transforms the free mobile AA into prostaglandin G_2 (PGG_2) and subsequently into prostaglandin H_2 (PGH_2). Conversion of PGH_2 into PGI_2 will then be catalysed by prostacyclin synthase. PGI_2 is a prostanoid that acts through prostacyclin receptors (IP) present on the membranes of vascular smooth muscle cells (VSMCs). The consequent binding of PGI_2 to the IP receptor then stimulates membrane-bound phospholipases D, which converts adenosine triphosphate (ATP) to cyclic adenosine monophosphate (cAMP) and activating PKA to inhibit myosin light chain kinase (MLCK) activity leading to relaxation of vascular muscle (Majed and Khalil, 2012).

2.6.2 G-protein Coupled Receptors

Vascular tonality regulation functions through G-proteins coupled receptors (GCPRs) expressed within endothelial cells and vascular smooth muscle cells (Li *et al.*, 2023b). Extracellular agonists binding to GCPRs activate their functional state which permits cells to receive signals from outside the cell environment. The activated GPCRs create structural changes in these proteins so these proteins can serve transiently as guanine nucleotide exchange factors (GEFs). G-proteins become activated when GPCRs

transform their bound guanosine diphosphate (GDP) to guanosine triphosphate (GTP) (Ushio-Fukai, 2009; Kamato *et al.*, 2015; Syrovatkina *et al.*, 2016).

Muscarinic receptors play an equally important role in vasodilation regulation, along with EDRFs. There are five muscarinic receptor subtypes (M_1–M_5), and with the most potent induction produced by the M_3 subtype. M3 receptors are present in both endothelial cells and vascular smooth muscle cells; however, their vasorelaxant effect is primarily mediated through the endothelium (Gericke *et al.*, 2014). To support the above statement, studies were conducted with stripping of endothelium from the rat's mesenteric vascular beds. This methodology led to lower expression of the M_3 receptor. It is then observed that the vasorelaxant effect of acetylcholine is markedly attenuated by removal of the endothelium because M_3 receptors are G-protein-coupled receptors mainly located in vascular endothelial rather than vascular smooth muscle cells (Tangsucharit *et al.*, 2016). When an agonist or ligand binds to the M_3 receptors, phospholipase C beta (PLC-beta) is involved in a signaling cascade that eventually produces DAG and inositol trisphosphate (IP_3). Inositol trisphosphate binds with the IP_3R receptor, causing further Ca^{2+} ion efflux from the endoplasmic reticulum into the cytosol, resulting in more calcium-calmodulin complex formation (Ahumada-Castro *et al.*, 2021). On the contrary, DAG binds and activates PKC, which in turn binds calmodulin, thus facilitating the calcium-calmodulin complex formation. The elevated calcium-calmodulin complex in turn activates endothelial nitric oxide

synthase (eNOS) and cystathionine gamma-lyase (CSE), resulting in the production of NO and H_2S (Gheibi *et al.*, 2018), respectively. This ultimately results in vasodilation.

Besides muscarinic receptors, there are β_2-adrenergic receptors (also G-protein-linked receptors) that occur mainly in vascular smooth muscle cells and have a central role in causing vasorelaxation. When these receptors are activated, a signal cascade is triggered, which includes AC, which transforms ATP into cyclic adenosine monophosphate (cAMP). This causes an increase in cAMP levels which then stimulates PKA which in turn suppresses the MLCK, thus the relaxation of vascular smooth muscle.

2.6.3 Channel-linked Receptors

The recent studies have shifted the focus on the GPCR and EDRF into the channel-linked receptor which is also referred to as the ligand-gated ion channels. These receptors play a central role in controlling the vascular tone, the activities of these receptors directly depend on the membrane potential of VSMCs. They are the channels of regulated transport of ions through the cellular membrane that affects contractility and vascular responsiveness. In turn, depolarization and hyperpolarization processes of such ion channels play the critical role in controlling the contractile properties of VSMCs of the vascular system (Jackson, 2000; Gao *et al.*, 2013). Among the various ion channels potassium and calcium channels represent key elements which control vascular tone regulation (Beghi *et al.*, 2022).

2.6.4 Calcium Channels

Voltage-operated calcium channels (VOCCs) act as important receptors which regulate vascular tone together with membrane potential stability. A change in membrane potential occurs when intracellular calcium level rises to create calcium-calmodulin complexes which increase signaling pathway transcription for vasorelaxation (Beghi *et al.*, 2022). The targeted MLCK activation process by calmodulin complexes creates adenosine monophosphate (AMP) production which leads to vascular smooth muscle cell contraction. As a result, when the membrane potential is depolarized, calcium ions enter the cytosol through L-type calcium channels and cause vasoconstriction (Gao *et al.*, 2013; Kuo and Ehrlich, 2015).

Furthermore, membrane potential depolarization is influenced not only by VOCCs but also by the release of calcium ions from the sarcoplasmic reticulum (SR). Activation of the phospholipase C (PLC) pathway triggers the efflux of calcium ions from the SR into the cytosol (Zsolnay, Fill and Gillespie, 2018). Phospholipase C activates phosphatidylinositol 4,5-bisphosphate (PIP_2), causing decomposition to IP_3, which binds to the IP_3R receptor, thereby elevating cytosolic levels of Ca^{2+}. In this instance, the binding of IP_3 to the IP_3R receptor differs slightly from the others, such as in G-protein-linked receptor stimulation signaling pathways taking place in the endothelial cell. When there is an increase in cytosolic Ca^{2+} within the vascular smooth muscle cells, the elevated Ca^{2+} will bind to calmodulin, activating MLCK (Falzone and MacKinnon, 2023). Consequently, MLCK

induces contraction of VSMCs, leading to vasoconstriction, by phosphorylating the myosin light chains (MLC) (Martinsen, Dessy and Morel, 2014).

2.6.5 Potassium Channels

Potassium channels represent the most abundant class of ion channels and are ubiquitously expressed across nearly all living organisms. Their primary roles in VSMCs are to modulate vascular tone and regulate membrane potential. Occasionally enhancing the channel performance may function as a compensatory mechanism to sustain elevated vascular tone. There are four different types of vascular potassium channels that have been studied extensively in identifying their respective function in controlling vascular tone, with an emphasis on their vasodilation characteristics. These consist of voltage-gated K^+ channels (K_v), ATP-sensitive K^+ channels (K_{ATP}), calcium-activated K^+ channels (K_{Ca}), and inwardly-rectifying K^+ channels (K_{ir}) (Nelson and Quayle, 1995; Jackson, 2017). Membrane hyperpolarization is caused by the efflux of K^+ ions as a result of K_{Ca}, K_{ATP}, and K_V activation. Following this hyperpolarisation, calcium channels are inhibited or blocked, which lowers the amount of Ca^{2+} influx and ultimately causes vasodilation (Sobey, 2001). Out of the 4 different potassium channels, only one that differs from the others - K_{ir}, and when K_{ir} is activated, K^+ enters the cytosol and causes a repolarisation effect. Moreover, there are three subtypes of K_{Ca} that can be distinguished: small-conductance K_{Ca} (SK_{Ca}), intermediate-conductance K_{Ca} (IK_{Ca}), and large-conductance K_{Ca} channels (BK_{Ca}). Large-

conductance K_{Ca} channels is the most well-known K^+ channel among the various K^+ channel types found in VSMCs, and it is widely expressed in the membrane of these cells (Félétou, 2009). When the intracellular Ca^{2+} level rises, they become functionally activated. They produce a hyperpolarising current that causes Ca^{2+} channels to shut down, aiding in the efflux of K^+ ions from the cytosol. Vasodilation results from the inhibition of MLCK activity caused by the decrease in cytosolic Ca^{2+}. BK_{Ca} can be indirectly activated by PKA and PKG in addition to being directly activated by Ca^{2+} (Haddy, Vanhoutte and Feletou, 2006) IK_{Ca} and SK_{Ca}, in contrast to BK_{Ca}, are expressed more frequently in vascular endothelium and respond differently to voltage changes (Félétou, 2009). They are, nevertheless, extremely responsive to variations in cytosolic Ca^{2+} and calmodulin concentrations that regulate the closure of calcium channels in cell membranes and SR stores. It has been suggested that SK_{Ca} and IK_{Ca} affect nearby VSMCs and contribute to the production of EDHF signals (Haddy, Vanhoutte and Feletou, 2006).

2.7 Transition from Conventional Pharmaceuticals to Combination and Herbal Therapies

The conventional pharmaceutical approach works with the principle of "one drug, one target, one disease". This theory served as the foundation that supported conventional pharmaceutical drugs development, aiming to produce therapeutic compound that target specific pathological mechanism involved in disease development (Li *et al.*, 2022; Jung and Cheon, 2024). While conventional therapeutic agents are highly effective in treating acute

condition, they demonstrate limited efficacy in treating multifactorial diseases like cancer, hypertension and diabetes. Together with the emergence of drug resistance and associated adverse effects, these limitations has caused the scientific community to re-evaluate and refine current therapeutic approaches (Wang *et al.*, 2023).

Combination therapeutic approaches have recently garnered great amount of attention. The use of multiple pharmacologically active agents resolves the limitations face by conventional approaches. The synergistic interactions between pharmacologically active components in combination regimens markedly increase therapeutic efficacy in addressing multifactorial conditions, simultaneously reduce the chance of drug resistance development and avoid adverse effects. Emerging scientific evidence establishes combination therapies is always superior to monotherapies, and the clinical effectiveness of combination therapy has proven to be more effective in a variety of conditions (Wang *et al.*, 2023; Zhang *et al.*, 2024b). Combination therapies is always superior to monotherapies, and the clinical effectiveness of combination therapy has proven to be more effective in a variety of conditions.

The recent discoveries in the field of molecular biology and systems pharmacology have contributed to the change of the old-fashioned monotherapies to the concept of combinatorial or multi-herb therapies. Scientific studies suggests that therapeutic approaches targeting single molecular pathway often fail to achieve sustained therapeutic effects because

of the complex interplay between signaling molecular pathways involved in disease mechanisms. In contrast, combination therapies rely on the multi-target properties of the therapeutic involving a greater control and conservation of the therapeutic responses. The ability of multi-target interventions by modulating diseases processes at various biological levels has expand the scope for more effective and personalized regimens (Li *et al.*, 2022; Wang *et al.*, 2023; Jung and Cheon, 2024; Zhang *et al.*, 2024b).

Most of the herbal medicine possesses spectrum of biologically active phytochemicals which could concurrently acting with multiple signaling pathways. This conceptual compatibility is complementary with the tenets of combination therapies where herbal medicines take advantage of their intrinsic multi-target behavior to induce therapeutic responses comparable to those of traditional forms of therapy. Furthermore, some interactions between the compounds that constitute the mixture might lead to synergy, which will increase effectiveness and reduce adverse events. The future of such benefits has led to the increased attention to the topic of herbal medicines as a supplementary or alternative to conventional pharmaceuticals. However, the combination therapy, whether it is the use of synthetic medicine or herbal preparations is a very promising field that is yet unexplored in contemporary medicine (Li *et al.*, 2022; Wang *et al.*, 2023; Jung and Cheon, 2024; Zhang *et al.*, 2024b).

2.8 Herbal medicine and Synergistic Effects

Herbal medicine has been practised over thousands year in many countries Asian countries, including China, Japan, Korea, Indonesia, Malaysia, and Thailand. Such traditional medicine is highly based on herbal medicine to prevent and cure a broad spectrum of illnesses (Koon *et al.*, 2011). Herbal therapeutic approaches have evolved over centuries and have shifted into multi-herb preparations This development is indicative of an increased awareness of the fact that multi-herb system offer greater therapeutic benefits compared to single-herb or isolated compound. The historical notion of the effectiveness of concomitant herbs mixture is based on the idea that complex herbal preparations allow the simultaneous action on several physiological pathways, which improves the effects of the therapeutic effects.

Multi herb regimens also aimed to obtain balanced and synergistic interactions, interactions between various active constituents that are complementary in each other, and hence enhance overall effectiveness and reduce possible side effects (Li *et al.*, 2022). On the other hand, single-herb preparations are usually subjected to scientific doubt because bioactive constituents are in low concentrations, and there is a possibility that purported action of one herb would be due to placebo effect but not due to active pharmacological action (Koon *et al.*, 2011).

Bioactive constituents are usually found in low levels and therefore tend to be sceptical by scientific standards connected to single-herb preparation. This

creates the question that the perceived action of a single herb can be due to placebo instead of actual pharmacological action due to its active compounds (Ekor, 2014). This synergism may modulate different molecular targets, improve bioavailability, or alleviate unwanted effects associated with specific constituents. These findings collectively highlight the necessity of shifting conventional single component to herbal medicine, particularly polyherbal approaches that harness natural synergies.

Despite all the advances, comprehensive scientific investigation remain crucial to validate the synergistic effects and therapeutic efficacy of complex herbal formulations (Ekor, 2014). While preclinical data are promising, standardized preparation methods, quality assurance, and verifiable bioactivity are critical to translate all validated therapeutics benefits into reliable clinical therapies. These solid scientific validations will not only increase the credibility of herbal medicine, also enable its translation into modern evidence-based healthcare systems (Ekor, 2014).

2.9 Concept of Synergism

It is possible to define synergy as one of the phenomena when the effect of interaction between two or more agents is greater than the result of the sum of separate effects of these agents. In pharmacology, synergistic interactions are more of a consequence in the evaluation of combination therapy and complex herbal preparations. The reason is that they can substantially improve treatment efficacy and hence allow the reduction of

dosage levels of each agent and minimise side effects without at the same time inhibiting several biological pathways (Spinella, 2002). The intrinsic nature of synergy is therefore central in the optimisation of the treatment regimens and this is particularly apparent in situations where mono-agent treatments are often ineffective in multifactorial conditions.

Pharmacological research has two main synergies; pharmacodynamic and pharmacokinetic synergy. Pharmacodynamic synergy is a type of synergy which two or more agents interact on the same biological target or pathway, leading to enhanced therapeutic effects through positive interactions For example, two compounds activate the same receptor which cause an enhanced biological activity that is greater than that when the agents are used individually. Pharmacodynamic synergy is particularly important in the modulation of complex disease network where multiple signalling pathways are converged.

In contrast, pharmacokinetic synergy involves interaction within the drug absorption, distribution, metabolism, and elimination processes. The agent may influence the pharmacokinetic profile of another agent through such interactions. This will enhance the bioavailability of agent, prolong its half-life, or facilitate its distribution to target tissues (Tang, Wennerberg and Aittokallio, 2015), which this may end up improving the therapeutic outcomes of the involved agents. For example, pharmacokinetic synergy can be occurring, where one compound inhibits the metabolism of another

compound, which increase the compound concentration in plasma that will prolonging the therapeutic effects. There is a must for critical distinction between synergistic and additive effects. In a synergistic effect, the combination of two or more agents produce outcomes which greater than the simple addition of their individual effects. This reflect a true interaction that enhances efficacy beyond what is expected (Chou, 2006). In contrast, an additive effect refers the outcome of combined agents is simply equal to the sum of the individual effects, whereby there is no interaction between the agents. The arithmetic addition of outcomes is a widespread misconception regarding the definition of additive effects, because they are independent actions that lack the true interactive amplification of outcomes (Zhou *et al.*, 2016).

Despite the growing recognition of synergy as a critical component in therapeutic design, the accurate determination and validation of synergistic effects remain challenging. Traditional methods for detecting synergy is not always precise and reproducible especially when dealing with complex multi-component preparations such as herbal medicines. Therefore, a more effective and practical model are required to accurately evaluate the synergistic interactions in both animal and human studies (Chou and Talalay, 1984; Chou, 2006; Chou, 2010; Zhou *et al.*, 2016). To allow better characterize of pharmacodynamic and pharmacokinetic contributions in therapeutic effects, computational simulations, improved experimental designs, and advanced statistical methods are developed to meet the needs.

Identification and quantification of synergy does not only promote drug development but also support the scientific rationale of application of multi-component herbal therapies. Herbal formulations often contain numerous bioactive compounds that is usually involved in extensive pharmacological interactions. Therefore, the mechanism and consequences of synergy is essential to be understand to maximize the therapeutic benefits as well as minimizing the risk of herbal formulations. Thus, the development of our approaches to the study of synergy will be one of the vital steps toward the combination of modern and traditional medicine.

2.9.1 Loewe Additivity and Bliss Independence

In pharmacology study, the interactions between combinations of drugs are quantified to differentiate whether they are additive, synergistic, or antagonistic interactions. Among the widely used models for evaluating such interactions are the loewe additivity, and bliss independence models.

The loewe additivity model follows that two agents with similar mechanism of action can be evaluated based on their combined effect in comparison to single agent effect. It is useful in predicting additive interactions and is easy to be applied in systems where individual components share comparable pharmacodynamics. However, the model is only applicable to compounds with similar modes of action and in order to get accurate predictions, the

detailed dose-response data is required (Tang, Wennerberg and Aittokallio, 2015).

The Bliss Independence model, on the contrary, is based on the hypothesis that the action of all individual drugs is independent of each other. This model has a benefit to consider combinations of compounds that address different biological entities or pathways. It can be used to establish interactions that are not only additive, and include synergistic and antagonistic interactions. However, it also demands specific details about the effects that individual drugs have and can be ineffective in the cases of high interactive effects (Chou and Talalay, 1984; Chou, 2006; Chou, 2010). Integrating these models gives researchers the supplementary approaches to researching drug interactions. The pharmacological properties and mechanism of action of the agents involved should be considered in the selection of mode between loewe additivity and bliss independence (Adam *et al.*, 2009; Zhou *et al.*, 2016).

2.9.2 Comparison of Current Models for Assessing Drug Synergy

Understanding the interaction between multiple compounds is fundamental in pharmacological research, especially aiming to improve the therapeutic efficacy through synergistic combinations. Few evaluation models have been developed to quantify these interactions. Among the established models, combination index model and the isobole method are widely adopted (Chou, 2006).

Combination index (CI) model established by Chou and Talalay, is one of the most robust and commonly used methods to quantitatively assess drug interactions. It classifies interactions as synergistic (CI<1), additive (CI=1), or antagonistic (CI>1). This model is especially valued for its practical experimental utility and flexibility. These features enable analysis regardless of the number of compounds in the combination. Additionally, the software, *CalcuSyn* and *CompuSyn*, were developed to streamline the model implementation. However, valid result need accurate dose-response data for both the individual components and their combinations (Chou, 2006).

Unlike CI model, isobole method provides a graphical illustration of the pharmacodynamic interaction between the components. It involves plotting the doses of two agents that produce the same effect, with interactions classified based on their position relative to a reference line (the "iso-effect" line). This method is well established and remains one of the most accessible experimental techniques for determining synergistic, additive, or antagonistic effects. This makes it especially attractive due to its simplicity and clarity. However, similarly to the CI model, it also requires the availability of reliable dose take into account information and the model is often limited to 2 drug combinations (Berenbaum, 1989).

The CI and isobole techniques are convenient and educative in determination of pharmacological synergy. Whereas the CI model can be used to provide more flexibility in the multi- component mix formation, the isobologram

method allows a graphical analysis of the intuitive interactions between two drugs. Proper methodology used should be based on study design, availability of sufficient agent used, and the existence of valid dose response data (Cheung and Terry, 1980; Chou and Talalay, 1984).

2.9.3 Orthogonal Stimulus-response Model

The orthogonal stimulus-response model presents a systematic, but versatile, approach to study the multifaceted interactions, which are often evident in multi-component systems, in particular, to the phenomenon of herbal medicine. This framework combines the main concepts such as orthogonal experimental design, relation between stimulus and response, combination-effect analysis, and mathematical modeling to help to develop and optimize therapeutic combinations rationally (Loh *et al.*, 2018b).

The characteristic specificity of the model is in the principle of orthogonality that implies the independent varying of such factors as dose or concentration of different compounds. Through very well-developed study designs which isolate all the variables, scientists would be able to determine the contribution of each element to the overall effect of the therapeutic intervention. The design paradigm does not only reduce the bias in the experiment, but it also improves the efficiency of operations by allowing a wider range of combinations to be experimented with a lower cost of the resources (Tan *et al.*, 2017b; Loh *et al.*, 2018b).

It is also necessary to incorporate stimulus-response relationships relating how specific inputs (e.g. the concentration of a herbal extract) change biological outputs (e.g. vasodilation or enzymatic inhibition). Through the clarification of these associations, researchers are capable of measuring the potency and efficacy of a given substance or a combination with its respective substances. This observation also guides the development of the optimal dose ranges that would provide therapeutic effects (Tan *et al.*, 2017b; Yam *et al.*, 2024).

One of the major strengths of this model is the ability to describe dynamic interactions between several elements. The therapeutic effects of herbal medicine are commonly synergistic, additive or antagonistic. The model allows the systematic alteration of the component ratios, and careful examination of the resultant biological responses, hence, a strong framework to validate the traditional formulations which very often are not based on a single isolated compound.

The orthogonal stimulus-response model can be enhanced using the quantitative methods including isobolographic analysis and the CI method in order to facilitate further interpretation. The isobolograms have graphical representation of the effects of different component combinations leading to a given effect, thus the ability to discriminate between the synergies in interactions and simple additivity or antagonism. Besides, the CI paradigm, which is based on Chou-Talalay paradigm model, provides a numerical

measure of drug interaction, thus giving greater clarity and accuracy to the combination evaluation (Chou and Talalay, 1984; Chou, 2006).

The orthogonal stimulus-response model provides a scientifically rigorous yet practical framework for optimizing multi-component therapeutics. Combining experimental design, response mapping, and combinatorial analysis makes such an approach particularly useful in developing traditional herbal medicines in an evidence-based paradigm. The method facilitates a researcher to explain the multifaceted interaction networks by linking traditional information to modern pharmacological validation.

2.10 Introduction to Network Pharmacology

2.10.1 Concept and Principles of Network Pharmacology

Network pharmacology is a methodological framework that tries to understand drug mechanisms in the context of a biological system by studying how compounds, molecular target and disease-related pathways interact with each other. Network pharmacology finds the multi-target therapeutics and compound-disease interactions, unlike traditional pharmacology, and it offers a network-based understanding of therapeutics, diseases, and pharmacotherapy, with its complexity, which encompasses the complexity of living systems, diseases, and pharmacotherapy. On the other hand, conventional pharmacology tends to focus on single-target interactions (Li *et al.*, 2023a). This transition can speed up the process of drug discovery by switching the traditional single-target perspective to a current system that

examines the multi-target action via network theory (Ruchawapol, Fu and Xu, 2022). Network pharmacology can therefore be used to profile the traditional Chinese medicine to determine the active constituents and the potential targets thereby explaining the mechanistic interactions of the herbal therapeutic in a variety of signaling networks (Li *et al.*, 2023a). The structured research strategies such as network construction, data mining, target prediction and pathway analysis are needed to be included in network pharmacology (Li, Li and Ji, 2019).

2.10.2 Advantages over Traditional Pharmacological Approaches

Network pharmacology has specific benefits compared to traditional single-target drug discovery models. It allows itself to be focussed on multi-target interactions and networked systems of biological processes, allowing simultaneous modulation of the activities of multiple signalling cascades, potentially increasing therapeutic efficacy and reducing adverse effects. The paradigm has been especially beneficial in the more difficult polygenic disorders in that they are able to formulate more effective therapeutic plans that have a lower probability of developing drug resistance. Furthermore, network pharmacology is better to discover potential drug targets, which increases the success of the clinical trial and minimizes the expenditure and time spent on drug discovery through other conventional methods. It also supports empirical data about TCM practices and helps in formulating personalized and accurate TCM therapy (Zhang *et al.*, 2013). In general, network pharmacology is a promising interface between conventional

medicine and the contemporary biomedical research undertaking to provide a rich, efficient and predictive system that can enhance our understanding in the field of mechanistic understanding as well as generates therapy innovations.

2.10.3 Application of Network Pharmacology in TCM Research

Traditional Chinese Medicine has a rich and unique historical background, which is based on the usage of multi component herbal preparations, which are meant to treat the conditions of a disease based on multi-targeted actions. However, the fact these herbal compounds are intrinsically complex compounds makes it difficult to identify active constituents, clarify their action mechanism, develop a general safety profile, variables that collaborate to restrain the wider scientific consensus. The concept of system-level network pharmacology has become a modern tool that is in line with the TCM holistical paradigm. The methodological framework will support the identification of bioactive compounds, prediction of molecular targets, and defining of the therapeutic outcomes through mapping interactions in complex biological systems. Since contemporary pathophysiological disease processes, including cardiovascular diseases, are often associated with multifactorial etiologies, network pharmacology provides a relevant and integrative framework in the further comprehension and empirical confirmation of the multi-target treatment solutions in the TCM of these complex diseases (Zhou *et al.*, 2020).

CHAPTER 3

MATERIAL AND METHODOLOGY

3.1 Chemicals and Materials

3.1.1 Chemicals

Eupatorin, sinensetin, and 3'-hydroxy-5,6,7,4'-tetramethoxyflavone (TMF) were procured from Chengdu Biopurify (China) (Purity >95%). Atropine, barium chloride ($BaCl_2$), glibenclamide, indomethacin, Nω-Nitro-1-arginine methyl ester (L-NAME), sodium chloride (NaCl), tetraethylammonium (TEA), propranolol, 1H-[1,2,4]Ox-adiazolol[4,3-α]quinoxaline-1-one (ODQ), 2-aminoethyl diphenylborinate (2-APB), 4-aminopyrine (4-AP), and Tween 80 were purchased from Sigma Aldrich (USA). Phenylephrine hydrochloride (PE), acetylcholine chloride (ACh) and nifedipine were purchased from Acros Organics (Geel, Belgium). Methylene blue (MB) was sourced from Pro-medipharm Sdn. Bhd (Malaysia). Potassium chloride (KCl), sodium hydrogen carbonate ($NaHCO_3$), and calcium chloride ($CaCl_2$) were acquired from Bendosen Laboratory Chemicals (Malaysia). Glucose anhydrous, magnesium sulphate ($MgSO_4$), methylene blue (MB), and potassium dihydrogen phosphate (KH_2PO_4) were purchased from R&M chemicals (Malaysia). The carboxymethyl cellulose (CMC) was purchased from Fisher Scientific UK Ltd (United Kingdom) while ethylene glycol tetraacetic acid (EGTA) was sourced from Calbiochem (Germany).

3.1.2 Preparation of Blockers and G28

ACh (1 µM), atropine (1 µM), $BaCl_2$ (10 µM), L-NAME (10 µM), MB (10 µM), PE (1 µM), propranolol (1 µM), TEA (1 mM), 4-AP (1 mM) were dissolved in distilled water. Glibenclamide (1 µM), indomethacin (10 µM), nifedipine (1 µM), ODQ (1 µM) and 2-APB (100 µM) were dissolved in a distilled water containing less than 1% Tween 80. The formulations were prepared in a distilled water containing less than 1% Tween 80.

3.1.3 Animals

The *ex vivo* aortic ring vasodilatory investigation utilised mature male Sprague-Dawley (SD) and Spontaneously Hypertensive rats (SHRs) weighing 200-240 g. The *in vivo* antihypertensive investigation was limited to SHRs with 200-220 g. All rats were housed in regulated environmental conditions at an ~25 °C, with 12-hour light-dark cycle, and free access to food and water. The experiment adhered to the protocols outlined in the Care and Use of Laboratory Animals by Universiti Tunku Abdul Rahman. All experimental protocols acquired approval from the Animal Ethics Committee of Universiti Tunku Abdul Rahman (U/SERC/242/2021).

3.2 Methodology

3.2.1 Preparation of Aortic Rings

The experiment protocols were adapted from previous publications (Yam *et al.,* 2016b; Tan and Yam, 2018; Yam, Tan and Shibao, 2018; Tan *et al.,* 2021). Before the commencement of the experiment, the Krebs-Henseleit

physiological solution (KPS) was prepared in a Petri dish, which was composed of 118.0 mM NaCl, 4.7 mM KCl, 25.0 mM $NaHCO_3$, 1.8 mM $CaCl_2$, 1.2 mM KH_2PO_4, 1.2 mM $MgSO_4$, and 11.0 mM glucose was prepared. The KPS was aerated with carbogen (95% O_2 and 5% CO_2). Adult male SD and SHR rats were euthanised with an overdose of CO_2 inhalation. The thoracic aorta was isolated by making a midline incision through the sternum. Subsequently, it was transferred to the Petri dish containing KPS for thorough cleaning to eliminate surrounding connective tissues. Then, the aorta was cut into approximately 5 mm ring segments and incubated in an organ bath chamber containing 10 mL of KPS. The experimental conditions are maintained at 37 °C, with continuous perfusion of carbogen for optimal physiological conditions. The aortic rings were firmly mounted between two stainless-steel hooks, with one attached to an L-shaped support and the other linked to a Force-Displacement Transducer (FT03, GRASS Instruments, USA). For 30 minutes, the aortic rings were left to equilibrate at the optimal baseline tension of 1g, with KPS being refilled every 10 minutes. As needed, the tension was adjusted to 1g.

Aortic rings were exposed to 1 µM PE and then 1 µM ACh to confirm their integrity. Aortic rings demonstrating a minimum contraction of 0.6 g in reaction to PE and subsequent relaxation of minimum 60% upon Ach induced administration, were designated endothelium-intact and earmarked for further experimentation. The endothelium was mechanically removed under specific experimental circumstances, and endothelium-denuded aortic rings,

characterised by ACh relaxation responses of less than 10%, were used. The aortic rings underwent three consecutive rinses with KPS at 10-minute intervals, with simultaneous replacement of KPS, and the tension was maintained at 1 g. These methods were methodically duplicated in SHRs. The assessment of the integrity of the aortic rings in SHRs was excluded due to endothelial dysfunction resulting from prolonged hypertension circumstances.

3.2.2 Orthogonal Stimulus-response Compatibility Group Studies

The concentration-response curves for the individual compounds, sinensetin, eupatorin, and, TMF, were established based on data obtained from previous studies (Yam *et al.*, 2016b; Yam, Tan and Shibao, 2018; Tan *et al.*, 2021). From these curves, the effective concentrations corresponding to 5%, 10%, 15%, 20%, and 25% of maximal relaxation responses (designated as EC_5, EC_{10}, EC_{15}, EC_{20}, and EC_{25}, respectively) were selected as the working concentrations for the subsequent orthogonal compatibility study. An L36 orthogonal array design was employed to systematically evaluate the potential interactions among the three compounds. The L36 array allows the efficient assessment of multiple factors (compounds) at multiple levels (concentration points) while minimizing the number of experimental runs. In this study, each compound was assigned to six concentration levels corresponding to its EC values (EC_5, EC_{10}, EC_{15}, EC_{20}, EC_{25}, and one control level). A dose-response study was the basis of the combination preparation. Particularly, the percentages of the constituent sinensetin, eupatorin and TMF, in a formulation referred to as G28, were allocated the EC_{20}:EC_{15}:EC_5 ratio.

Accordingly, a proportion of 106:172:64 (sinensetin:eupatorin:TMF) was prepared and homogenized. A 1 mg of G28 was dissolved in 1 mL of 0.5% Tween 80 and obtain a final concentration of 1 mg/mL for G28. Then, 100 µL of the solution was pipetted into an organ bath, which containing 10 mL of KPS.

With the help of an L36 orthogonal array design, 36 different compatibility groups (Group1-Group36) were created. Each group was a combination of all possible low-dose interactions of sinenetin, eupatorin, and of TMF, and in each case, there was no duplication of groups, to which this guaranteed a complete coverage of all possible interactions (Table 3.1) (Loh *et al.*, 2017; Tan *et al.*, 2017b). The overall effectiveness of the three-compound combination was estimated to be generally moderate because the large effects would prevent a high degree of complication when estimating the effects of the interaction, with possible synergy.

The expected relaxation percentage of a group of compatibilities was calculated by adding up the total of the predicted relaxations of each of the compositions, based upon their respective concentration response relationships. Actual vascular relaxation was later determined *ex vivo* on isolated rat aortic rings and observed relaxation was compared with the calculated expected relaxation to determine the existence of synergistic, additive or even antagonistic interaction. Efficacy (%) was computed as the ratio of actual relaxation to expected relaxation, expressed as a percentage.

Table 3.1: Compatibility Groups Screening.

Group	Compatibility Groups		
	Sinensetin	**Eupatorin**	**TMF**
G1	EC_{10}	EC_{10}	EC_{10}
G2	EC_{0}	EC_{5}	EC_{5}
G3	EC_{0}	EC_{10}	EC_{10}
G4	EC_{0}	EC_{15}	EC_{15}
G5	EC_{0}	EC_{20}	EC_{20}
G6	EC_{0}	EC_{25}	EC_{25}
G7	EC_{5}	EC_{0}	EC_{5}
G8	EC_{5}	EC_{5}	EC_{10}
G9	EC_{5}	EC_{10}	EC_{15}
G10	EC_{5}	EC_{15}	EC_{20}
G11	EC_{5}	EC_{20}	EC_{25}
G12	EC_{5}	EC_{25}	EC_{0}
G13	EC_{10}	EC_{0}	EC_{10}
G14	EC_{10}	EC_{5}	EC_{15}
G15	EC_{10}	EC_{10}	EC_{20}
G16	EC_{10}	EC_{15}	EC_{25}
G17	EC_{10}	EC_{20}	EC_{0}
G18	EC_{10}	EC_{25}	EC_{5}
G19	EC_{15}	EC_{0}	EC_{15}
G20	EC_{15}	EC_{5}	EC_{20}
G21	EC_{15}	EC_{10}	EC_{25}
G22	EC_{15}	EC_{15}	EC_{0}
G23	EC_{15}	EC_{20}	EC_{5}
G24	EC_{15}	EC_{25}	EC_{10}
G25	EC_{20}	EC_{0}	EC_{20}
G26	EC_{20}	EC_{5}	EC_{25}
G27	EC_{20}	EC_{10}	EC_{0}
G28	EC_{20}	EC_{15}	EC_{5}
G29	EC_{20}	EC_{20}	EC_{10}
G30	EC_{20}	EC_{25}	EC_{15}
G31	EC_{25}	EC_{0}	EC_{25}
G32	EC_{25}	EC_{5}	EC_{0}
G33	EC_{25}	EC_{10}	EC_{5}
G34	EC_{25}	EC_{15}	EC_{10}
G35	EC_{25}	EC_{20}	EC_{15}
G36	EC_{25}	EC_{25}	EC_{20}

Notes: The predicted (expected) combined vasodilatory effects of the formulations in Groups G1–32 were each below 100%, indicating that these combinations were not expected to achieve complete vasodilation under the test conditions.

3.2.3 Vasodilatory Response and Efficacy of the Compatibility Groups

The aortic rings were pre-contracted with PE (1 µM) for 30 minutes until a stable contraction was obtained. Then, 100 µL of the formulation (1 µg/mL) was introduced into the organ bath for 30 minutes. The force transducer identified the alteration in the contractile force of aortic rings. The signals were amplified by Quad Bridge amp (ADinstrument, Australia), and transformed into readable digital signals by PowerLab 26T (ADinstrument, Australia). The signals were depicted using LabChart 7.3.8 software (AD instrument, Australia). The actual relaxation value was calculated. The identical procedure was implemented across all compatibility groups. The expected relaxation (ER) values for each group, associated with each experimental set, must not surpass 100% to ensure the validity of the resultant actual relaxation (AR) (Loh *et al.*, 2017; Tan *et al.*, 2017b). The efficacy can be calculated as follows:

$$\text{Efficacy} = \frac{Actual\ relaxation}{Expected\ relaxation} \times 100\%$$

The mean relaxation values were calculated through the summation of experiment results according to the effective concentration level of each compound and the mean response at each given level was then calculated. In each of the compounds, the experiments that matched to the same concentration were determined, the corresponding percentages of vasorelaxation were obtained and the arithmetic mean was given. The methodology was systematically used in all levels of concentration of sinensetin, eupatorin and TMF to produce their corresponding relaxation

profiles that were utilized to determine the optimal concentration that will be used in further compatibility analysis.

3.2.4 Dose-responses Vasodilatory Effect of the Formulation

The calculated optimum ratio (F1) and the compatibility groups exhibiting efficacy over 100% (G2, G7, G27, and G28) were chosen for further investigation in a dose-response vasodilatory study. 1 µM PE was applied to induced contraction in the aortic rings.

The formulation was cumulatively added into the organ bath (100 µL of 0.125-4 mg/mL) after a stable contraction had been established. The concentration-response curve was constructed, and each formulation group's half maximum concentration (EC_{50}) and maximum relaxation (R_{MAX}) were calculated. The R_{MAX} can be calculated as follows:

$$R_{MAX} : \frac{X-Y}{X} \times 100\%$$

Where X = Contraction force (g) after 30 minutes of PE incubation; Y = Contraction force (g) following 20 minutes of incubation with the final dose of the combination.

3.2.5 Preliminary Screening on the Vasodilatory Effect of G28 in SD rats and SHRs

The vasodilatory potential of G28 was assessed using isolated aortic rings from both SD rats and SHRs. Endothelium-intact aortic rings were pre-contracted with PE at a concentration of 1 µM for 40 minutes to achieve a

plateau phase (Loh *et al.*, 2017; Tan and Yam, 2018; Yam, Tan and Shibao, 2018). Subsequently, approximately 100 µL of G28 was introduced cumulatively into the organ bath at 20 minute intervals, with a cumulative concentration varying from 1.25 µg/mL to 38.75 µg/mL. The contractile force of the aortic rings was detected and recorded using a force transducer. Signal amplification was accomplished via a Quad Bridge amp. The analog signals were subsequently transformed into digital format by the PowerLab 26T and visualized using LabChart 7.3.8 software. Concentration-response curve was constructed based on the recoreded data, whereas the maximum relaxation (R_{MAX}) and half-maximum effective concentration (EC_{50}) of G28 on the aortic rings from SD rats and SHRs were computed and presented in a table. The R_{MAX} was calculated as follows:

$$\text{maximum relaxation (\%)} = \frac{a-b}{a} x100$$

where a=contraction force (g) of aortic rings after 40 minutes PE pre-contraction, and b=contraction force (g) after incubation with G28 formulation. The results obtained in preliminary screening serve as negative controls for subsequent experiments.

3.2.6 Endothelium and Channel-linked Receptors Dependency in the Vasodilatory Actions of G28

Endothelium-denuded aortic rings were used to assess the role of endothelium to the vasodilatory effects elicited by G28. After the equilibration process, endothelium-denuded aortic rings were subjected to PE

incubation for 40 minutes to achieve plateau phase. G28 was incrementally added into the organ bath at 20 minute intervals (Loh *et al.*, 2017; Tan and Yam, 2018; Yam, Tan and Shibao, 2018). The R_{MAX} and EC_{50} values were calculated, and the concentration-response curve was constructed and compared to the negative control.

The impact of channel-linked receptors in G28-induced vasodilation was evaluated by substituting PE with 80 mM KCl for 40 minutes before contraction (Loh *et al.*, 2017; Tew *et al.*, 2020; Tew *et al.*, 2023). Then, cumulative additions of G28 were introduced at 20 minute intervals. The R_{MAX} and EC_{50} values were calculated, and the concentration-response curve was constructed and compared to the negative control.

3.2.7 The Involvement of Endothelium-derived Relaxing Factors in the Vasodilatory Action of G28

Nitric oxide and PGI_2 contribution to the vasodilation induced by G28 was assessed by pre-incubating endothelium-intact aortic rings with 10 µM of L-NAME (an antagonist of endothelial nitric oxide synthase) and 10 µM of indomethacin, a non-selective cyclooxygenase inhibitor, 20 minutes before a 30 minutes PE. The role of the NO downstream signalling cascade further was subdivided by pre-incubation of PE pre-contraction of the endothelium-intact rings with 1 µM of ODQ (selective soluble guanylate cyclase inhibitor) and 10 µM of MB (selective cGMP inhibitor), respectively (Ch'ng *et al.*, 2017; Ch'ng *et al.*, 2018). G28 was subsequently cumulatively

introduced into the organ bath. The R_{MAX} and EC_{50} values were ascertained. The concentration-response curve was constructed and contrasted to the negative control.

3.2.8 Roles of G-proteins Coupled Receptors in the Vasodilatory Action of G28

To investigate the endothelium-dependent G-protein-coupled M3 receptor and endothelium-independent G-protein-coupled 2-receptor, the endothelium-intact rings were pre-treated with 1 µM of atropine, a non-selective M3 muscarinic receptor antagonist, and 1 µM of propranolol, a non-selective 2 adrenergic receptor antagonist during the time period before PE pre-contraction as well as cumulative treatment with G28 (Loh *et al.*, 2021; Loh *et al.*, 2022). The R_{MAX} and EC_{50} values were calculated. The concentration-response curve was developed along with the comparison to the negative control.

3.2.9 Roles of Potassium Channels in the Vasodilatory Action of G28

The contributions of K_{Ca}, K_V, K_{ATP}, and K_{ir} were assessed by exposing the endothelium-intact aortic rings with 1 mM of TEA (a non-selective K_{Ca} blocker), 1 mM of 4-AP (a non-selective K_V blocker), 10 µM of glibenclamide (a selective K_{ATP} blocker), and 10 µM of $BaCl_2$ (a non-selective K_{ir} blocker) respectively, for 20 minutes (Tew *et al.*, 2020; Tew *et al.*, 2023). This was immediately preceded pre-contraction of PE and cumulative addition of G28. The R_{MAX} and EC_{50} values were obtained. The

concentration-response curve was constructed and juxtaposed with the negative control.

3.2.10 The Role of G28 on Voltage-gated Calcium Channels

There were three groups of experiments involved in this section: a negative control group, a positive control group, and the experimental G28 group. Normal KPS was initially employed to stabilise endothelium-intact aortic rings for a duration of 10 minutes following the integrity evaluation. Subsequently, the solution transferred to K^+-rich calcium (Ca^{2+})-free KPS (91.04 mM NaCl, 50.0 mM KCl, 11.9 mM $NaHCO_3$, 1.05 mM $MgSO_4$, and 5.5 mM glucose, pH 7.4), supplemented with 0.2 mM EGTA for 15 minutes to eradicate Ca^{2+}. The aortic rings were then rinsed with high K^+ Ca^{2+}-free KPS (without EGTA) for 20 minutes, with KPS replaced at 10-minute intervals for stabilisation. In the negative control group, the $CaCl_2$ (0.01 mM, 0.03 mM, 0.1 mM, 0.3 mM, 1 mM, 3 mM, and 10 mM) was cumulatively added to the aortic rings at 3-minute intervals. For the positive control group underwent pre-incubation of aortic rings with the L-type Ca^{2+} channel inhibitor, nifedipine (0.1 µM, 0.3 µM, and 1.0 µM), prior to the cumulative addition of $CaCl_2$ (Loh *et al.*, 2021; Tan *et al.*, 2021). The procedure in the G28 group was executed analogous to the positive control, substituting nifedipine with G28 (1.25 µg/mL, 5 µg/mL, and 20 µg/mL). The cumulative concentration-response contraction curves for the respective groups were generated and analyzed for comparison.

3.2.11 The Role of G28 on Inositol Trisphosphate Receptor

The experiment were carried out in three groups a negative control group, a positive control group, and an experimental G28 group. The equilibration procedures similar to those of the G28 in VOCC evaluation, which involved the incubation of endothelium-denuded aortic rings in normal KPS, followed by exposure to high K^+-Ca^{2+}-free KPS containing EGTA, that was to be followed with the high K^+-Ca^{2+}-free KPS-free EGTA incubation. The negative control group of endothelium-denuded aortic rings was subsequently subjected to PE contraction for 20 minutes without prior incubation with antagonist or G28 (Tan *et al.*, 2017a; Tan *et al.*, 2019). In positive control group, aortic rings were pre-incubated with 2-APB (non-competitive IP_3R antagonist) for 20 minutes, followed by PE incubation for 20 minutes. In the G28 group, 2-APB was substituted with G28 (1.25 µg/mL, 5 µg/mL, and 20 µg/mL).

3.2.12 *In vivo* Antihypertensive Study in SHRs Rats

3.2.12.1 Oral Treatment Preparation and Sub-chronic Oral Administration

The oral treatment dosages for G28 included three levels: low dose (15 mg/kg), medium dose (30 mg/kg), and high dose (60 mg/kg) based on a previous publication (Tew *et al.*, 2023). Before oral administration, all compounds were freshly prepared by dissolving them in a 0.5% CMC solution. The dosing volumes were adjusted to accommodate the individual body weights of SHRs, and the oral treatment were administered via gastric

intubation for a period of 21 days. The SHRs were subjected to an 8-hour fasting period before oral treatment. Daily health assessments of each SHR and weekly body weight measurements were performed (Cicero *et al.*, 2012).

3.2.12.2 Blood Pressure Measurement

The tail-cuff method was employed to systematically measure systolic blood pressure (SBP), diastolic blood pressure (DBP), and mean arterial pressure (MAP) in SHRs on a 7-days basis for 4 cycles, from first cycle (week 0) to forth cycle (week 3). The non-invasive blood pressure monitoring system, CODA (Kent Scientific Corporation, Torrington, USA), was used in the study. To enhance tail artery pulsation, 10 minutes pre-warming process at 35 °C were applied to the SHRs prior to the BP measurements. Two replicable measurements were conducted for each SHR, yielding eight valid results (n=8).

3.2.13 Statistical Analysis

The one-way analysis of variance (one-way ANOVA) was utilized to analyze the *ex vivo* study. In contrast, the *in vivo* study underwent a two-way repeated measurement of analysis of variance (two-way repeated ANOVA) using SPSS Version 20 software (IBM Corp, United States). The *in vivo* analysis was performed across the blocked experimental days to account for day-to-day variation, thereby ensuring that treatment effects were evaluated independently of potential temporal influences. The significance level was set at $P<0.05$. The results were presented as mean±S.E.M.

3.3 Network Pharmacology Study of Sinensetin, Eupatorin, and TMF

3.3.1 Chemical Structure Information of Sinensetin, Eupatorin, and TMF

The chemical structures of sinensetin, eupatorin and TMF used in the current study were downloaded in PubChem database (https://pubchem.ncbi.nlm.nih.gov). PubChem is a publicly available and widely recognised chemical information repository by the National Centre of Biotechnology Information (NCBI), a division of the National Library of Medicine (NLM) under the supervision of the National Institute of Health (NIH). The database summarizes chemical structure and other data donated by a very wide range of sources, including pharmaceutical businesses, research facilities, universities, and government services. It serves as a hub to store the experimental information, commercially relevant compounds, proprietary mixtures of chemicals, and extensive chemical information thus becoming very useful in scholarly research as well as industrial use. Moreover, PubChem contains the BioAssay database, which contains major information of pharmacological, toxicological, and biochemical measurements. In the bounds of this research, PubChem Compound Identifiers (CIDs) of sinensetin, eupatorin and TMF were assigned as the 145659, 97214 and 7020615, respectively. Three dimensional (3D) conformer coordinates of each of these compounds were then derived out of PubChem and deposited in SDF format to enable subsequent analyses.

3.3.2 Drug Target Information of Sinensetin, Eupatorin, and TMF

The data on drug target of sinensetin, eupatorin, and TMF were accessed through PharmMapper (https://www.lilab-ecust.cn/pharmmapper/). PharmMapper is an online platform, which is specially designed to find a potential drug target of a small molecule by reversing pharmacophore mapping. The method employs pharmacophore mapping, in which biological targets of compounds are deduced with the outcome of chemical structures. The PharmMapper operates by comparing molecular properties of the target compounds put into it with a curated database of pharmacophore models, derived based on known protein-ligand complexes; as a result, the most compatible potential targets are identified. The method is specifically beneficial in drug discovery and development as it can be employed to understand the mechanism of action, distinguish off-target effects, and reposition drugs on a renewed effort (Ruan *et al.*, 2020).

The SDF file of each compound was uploaded one by one to the PharmMapper submission portal (https://www.lilab-ecust.cn/pharmmapper/submitfile.html) and only human protein targets and drugs Pharmophore were selected. The results of the pharmacophore interpretation have been sent via email address of the submitter in Excel (.xls) format in the event of a successful submission. These Excel spreadsheets were then transformed into plain-text (.txt) files using Perl 5 (version 30) so that they could be annotated to the gene symbols using the annotation table provided. The Perl script that was used in this conversion is described in Appendix 3.

After the process of annotating the gene symbols, data related to sinensetin, eupatorin, and TMF were co-opted into a single excel sheet. All the symbols of the genes were put into one column and the redundant one removed through the option in excel named remove duplicates and thus ensured that only one instance of a gene symbol existed. The filtered data was further exported to Excel (.xls) spreadsheet. The Excel file was later transferred to a plain-text (.txt) form renamed to Drug.txt that the file was further used to run downstream analysis.

3.3.3 Selection of Target Genes for Hypertension Treatment

Genes related to the disease were accessed through GeneCards® (https:// www.genecards.org/). The GeneCards® is an integrative and web based database which provides comprehensive information on all the reported and predicted human genes. It is an aggregation of information on over 150 sources by the Weizmann Institute and includes genomic, proteomic, transcriptomic, genetic and clinical repositories. Every record of a gene includes synonyms, functions, gene expression, illness links, pathway membership, variations, and related literature sources. The GeneCards® are used in the field of biomedical research and clinical practice by making access to gene-based information more rapid to enable diagnosing, drug discovery, and functional genomics applications. It also offers mala cards and path cards which can be used in the analyses of disease and pathways, making it an excellent resource of genomic studies and individualized medicine programs. The associated genes related to antihypertensive activity were downloaded

as .xls format to be Additional to GeneCards®, OMIM® (Online Mendelian Inheritance in Man) (https:/www.omim.org/) was also utilized to retrieve disease-gene information. OMIM® is an in-depth and authoritative catalogue of human genetic disorders and genes. OMIM® is a database that focuses on inherited and heritable disorders and its maintenance is carried out by the McKusick-Nathans Institute of Genetic Medicine at Johns Hopkins University which carries out linkages between phenotypes and genotypes. Each OMIM® record provides detailed data about gene function, molecular pathogenesis, clinical phenotypes, and patterns of inheritance and references to available scientific literature. OMIM® is regularly revised and widely used by scientists, clinicians, and researcher to locate disease-associated genes, thus easing the diagnosis and research in aid of genomic and precision medicine. OMIM® web site (https://www.omim.org/search/advanced/geneMap) was used to identify the genes related to hypertension with the help of the Gene Map Advanced search tool. (Amberger and Hamosh, 2017).

Gene lists obtained from GeneCards® and OMIM® were merged using Microsoft Excel. The gene symbols from both files were put together in a single column in the new worksheet "input.xls." Excel's "Remove Duplicates" feature was used to make sure every gene symbol appeared only once. Finally, the .xls file was turned into a text file, and a Perl 5 script was run on it to eliminate any remaining identical data (Appendix 4). This created the needed "Disease.txt" file for further work.

3.3.4 Venn Diagram Analysis

To create an intersection Venn diagram, the "VennDiagram" package was first installed in R by executing the command install.packages("VennDiagram"). Once the package installation was completed, the function for generating Venn diagrams became available. The Venn diagram illustrating the overlapping gene symbols between the drug target dataset (Drug.txt) and the disease-related genes dataset (Disease.txt) was created using the following R programming source code listed in Appendix 5.

3.3.5 Protein-Protein Interaction (PPI) Analysis

Protein-Protein Interaction analysis was conducted using the STRING database (https://string-db.org/). STRING (Search Tool of the Retrieval of Interacting Genes/Proteins) is an all-inclusive web-based resource that celebrates experimentally tested as well as computationally forecasted protein-protein interactions based on various information repositories, thus providing information about functional relationships among proteins. Understanding biological activities and molecular actions relies on this information.

For the analysis, the "Multiple Proteins" function was selected in the STRING platform. The gene list from "Drug_Disease.txt" was explored, and the gene symbols were copied and pasted into the "List of Names" input box. The analysis was done on *Homo sapiens*. After this selection, a PPI network

diagram was created. Before the exportation of the resulting data, the minimum interaction score was set to 0.7, which is a high-confidence level, and the possibility to hide the unconnected nodes in the network was turned on to enhance clarity (Triggle *et al.,* 2012; Syrovatkina *et al.,* 2016).

The protein-protein interaction network in the form of a high-resolution bitmap image was retrieved, and the data on the interaction were saved into a file named as string_interactions_short.tsv to be analyzed later. The frequency of protein-protein interactions was then plotted within a bar diagram of the above file with the help of R which is displayed in the source code of Appendix 6.

3.3.6 Assessment of CytoNCA for Core Targets

Cytoscape was used to calculate degree, closeness and betweenness centralities of the genes to determine major proteins in the PPI network. First of all, the file of the interactions by the strings between the strings which was received at STRING was imported into Cytoscape to be observed more closely. Upon the data import, the CytoNCA plugin was installed and was used to compute the degree, closeness, and betweenness centrality measures of all the available genes in the network. The data obtained were later exported to.xls and saved in the name of CytoNCA (Kohl, Wiese and Warscheid, 2011; Golbeck, 2015; Ruan *et al.*, 2020). After the exportation of the file, its content was analyzed in order to calculate the mean degree, closeness and betweenness centralities of each gene. The genes that had

values that were above the average in all the three measures were declared as key targets. The following genes were saved in another file named Core_Targets.txt, which was to be used in the future analyses. In order to be able to study gene enrichment, R scripts were subsequently used to provide each gene with its respective Entrez identifier in the list of genes in the file named Core_Targets.txt, thereby generating a file called id.txt, as detailed in Appendix 7. Barplot.tiff and dotplot.tiff along with GO.txt were thereafter created using the R source code in the appendix 8 using id.txt as input file.

3.3.7 Gene ontogy (GO) Analysis

Gene Ontology (GO) enables the description of the roles of genes and their products across several species in a standard set of term (Consortium, 2019). Primary gene functions are biological process, molecular function, and cellular component. In genetics and molecular biology studies, GO can be used to analyze and understand functions of genes from different species. The GO.txt was then converted to GO.exl using perl programming with source code in .pl or .txt format (Appendix 9).

3.3.8 Kyoto Encyclopedia of Genes and Genomes (KEGG) Analysis

Kyoto Encyclopedia of Genes and Genomes provides comprehensive bioinformatics information that can explain the high-level biologic activities and processes. KEGG also provides databases and maps that illustrate the relationship between molecules with metabolism, signals and their diseases occurrence. Researchers turn to KEGG when they work with big omics

datasets to see genes, proteins or metabolites' involvement in various diseases. KEGG consists of various databases, including KEGG Pathway, KEGG Orthology, KEGG Disease, KEGG Drug and KEGG Compound. With KEGG, it is possible to study how pathways influence the functions of genes and the entire cell, organism or ecosystem (Cai *et al.*, 2023; Zhang *et al.*, 2024a) . The id.txt file was then used to generate barplot.tiff, dotplot.tiff and KEGG.txt using the following source code in R programming (Appendix 10). The KEGG.txt was then converted to KEGG.exl using perl programming with source code in .pl or .txt format (Appendix 11).

CHAPTER 4

RESULTS

4.1 Orthogonal Stimulus-Response Compatibility Group Studies

The group compatibility studies were performed to assess the synergistic effects of the three principal compounds in *Orthosiphon stamineus*. The effective concentrations (EC_0, EC_5, EC_{10}, EC_{15}, EC_{20}, and EC_{25}) for each compound were ascertained from the concentration-response vasodilation curve retrieved from the previous studies, with the corresponding concentration levels detailed in Table 4.1. The 36 compatibility groups were systematically generated using the L_{36} formula layout, with their respective actual relaxation, expected relaxation, and efficacy values outlined in Table 4.2. Based on the results, G2 containing sinensetin, eupatorin, and TMF at effective concentrations of EC_0, EC_5, and EC_5, respectively, manifested the most pronounced vasodilatory responses. The efficacy and actual relaxation values were documented at 190% and 19.05±1.46%, respectively (Table 4.2). In order of potency, Group 7 (G7), Group 27 (G27), and Group 28 (G28) demonstrated actual relaxation of 14.80±0.46%, 35.29±2.97%, and 46.45±3.76%, with corresponding efficacies of 148%, 117.6%, and 116.25%, respectively (Table 4.2).

Table 4.1: The effective concentration selected from sinensetin, eupatorin and 3'-hydroxy-5,6,7,4'-tetramethoxyflavone for compatibility group screening.

No	Effective Concentration (%)	Concentration level (µg/mL)		
		SEN	EUP	TMF
1	Without extract	0	0	0
2	5	54	114	64
3	10	68	140	81
4	15	85	172	102
5	20	106	212	128
6	25	133	261	162

Notes: The concentration stated was obtained from each extract's dose-response curve, corresponding to the respective effective concentration. The concentration stated was not the final concentration applied in the organ bath. SEN: sinensetin, EUP: eupatorin, TMF:3'-hydroxy-5,6,7,4'-tetramethoxyflavone.

Table 4.2: Orthogonal stimulus–response compatibility groups screening.

Group	Compatibility Groups			Expected Relaxation (%)	Actual Relaxation (%)	Efficacy (%)
	SEN	EUP	TMF			
G1	EC_{10}	EC_{10}	EC_{10}	30	6.6±3.98	22
G2	EC_{0}	EC_{5}	EC_{5}	10	19.05±1.46	190
G3	EC_{0}	EC_{10}	EC_{10}	20	12.91±2.74	64.55
G4	EC_{0}	EC_{15}	EC_{15}	30	15.03±3.32	50.1
G5	EC_{0}	EC_{20}	EC_{20}	40	12.84±2.30	32.1
G6	EC_{0}	EC_{25}	EC_{25}	50	12.08±3.17	24.16
G7	EC_{5}	EC_{0}	EC_{5}	10	14.80±0.46	148
G8	EC_{5}	EC_{5}	EC_{10}	20	17.74±0.41	88.7
G9	EC_{5}	EC_{10}	EC_{15}	30	13.16±0.58	43.87
G10	EC_{5}	EC_{15}	EC_{20}	40	24.21±0.66	60.53
G11	EC_{5}	EC_{20}	EC_{25}	50	27.41±0.27	54.82
G12	EC_{5}	EC_{25}	EC_{0}	30	17.16±0.40	57.2
G13	EC_{10}	EC_{0}	EC_{10}	20	15.55±1.77	77.75
G14	EC_{10}	EC_{5}	EC_{15}	30	13.63±1.32	45.43
G15	EC_{10}	EC_{10}	EC_{20}	40	15.01±2.25	37.53
G16	EC_{10}	EC_{15}	EC_{25}	50	19.40±1.95	38.8
G17	EC_{10}	EC_{20}	EC_{0}	30	16.10±1.60	53.67
G18	EC_{10}	EC_{25}	EC_{5}	40	19.05±1.83	47.63
G19	EC_{15}	EC_{0}	EC_{15}	30	28.90±1.74	96.33
G20	EC_{15}	EC_{5}	EC_{20}	40	35.13±2.66	88.5
G21	EC_{15}	EC_{10}	EC_{25}	50	20.66±0.99	41.4

Table 4.2: Orthogonal stimulus–response compatibility groups screening. (continue)

Group	Compatibility Groups			Expected Relaxation (%)	Actual Relaxation (%)	Efficacy (%)
	SEN	EUP	TMF			
G22	EC_{15}	EC_{15}	EC_{0}	30	17.96±2.86	59.87
G23	EC_{15}	EC_{20}	EC_{5}	40	25.15±2.27	63
G24	EC_{15}	EC_{25}	EC_{10}	50	40.21±1.39	80.4
G25	EC_{20}	EC_{0}	EC_{20}	40	28.91±2.43	72.25
G26	EC_{20}	EC_{5}	EC_{25}	50	18.83±1.88	37.6
G27	EC_{20}	EC_{10}	EC_{0}	30	35.29±2.97	117.67
G28	EC_{20}	EC_{15}	EC_{5}	40	46.45±3.76	116.25
G29	EC_{20}	EC_{20}	EC_{10}	50	31.64±3.42	63.2
G30	EC_{20}	EC_{25}	EC_{15}	60	26.19±1.53	43.67
G31	EC_{25}	EC_{0}	EC_{25}	50	27.27±3.50	54.54
G32	EC_{25}	EC_{5}	EC_{0}	30	25.29±2.57	84.3
G33	EC_{25}	EC_{10}	EC_{5}	40	32.60±2.21	81.5
G34	EC_{25}	EC_{15}	EC_{10}	50	49.25±2.34	98.5
G35	EC_{25}	EC_{20}	EC_{15}	60	31.02±3.36	51.7
G36	EC_{25}	EC_{25}	EC_{20}	70	40.49±3.56	57.84

Notes: Effective concentration used in compatibility group screening: Efficacy: (Actual Relaxation/Expected Relaxation)x100%, SEN: sinensetin, EUP: eupatorin, TMF:3’-hydroxy-5,6,7,4’-tetramethoxyflavone. The effective concentrations of SEN, EUP, and TMF are shown in Table 4.1. Data are represented as mean±SEM (n=8).

The average relaxation responses of the sinensetin, eupatorin, and TMF, corresponding to their respective EC values, were illustrated in Table 4.3. The most optimum ratio for sinensetin:eupatorin:TMF was determined to be EC_{25}:EC_{15}:$EC_{10,}$ which is designated as F1. Notably, the combination ratio for F1 was comparable to that of Group 34 in the compatibility group (Table 4.2). To delve deeper into the synergistic interactions among these, two additional formulations denoted F2 (sinensetin:eupatorin:TMF=EC_{25}:EC_{15}:EC_5) and F3 sinensetin:eupatorin:TMF=EC_{25}:EC_{15}:EC_{20}), which are close to F1, were selected for additional analysis.

A confirmation test assessing the efficacy of G2, G7, G27, and G28 was conducted alongside three additional formulations (F1, F2, and F3) (Table 4). From Table 4.4, G2 had the best efficacy, with an actual relaxation of 17.07±2.95% and an efficacy of 170.70%. Consequently, the efficacies for F1, F2, F3, G7, G27 and G28 were 88.02%, 47.67%, 34.48%,154%, 108.20%, and 119%, respectively, with corresponding actual relaxation values of 44.01±5.05%, 21.45±4.85%, 20.69±4.04%, 15.40±2.47%, 32.46±5.00%, and 47.60±5.42%, respectively. Notably, the efficacies of F2 and F3 were considerably inferior to that of F1 (Table 4.4). The compatibility groups exhibiting efficacy surpassing 100%, specifically G2, G7, G27, G28, and F1, were selected for a concentration-response vasodilatory study to ascertain the optimal compound ratio.

Table 4.3: Average relaxation of compounds obtained from compatibility groups screening.

Effective Concentration (%)	Average Relaxation (%)		
	SEN	EUP	TMF
Without compound	11.99	19.24	18.64
5	19.08	21.65	26.20
10	16.46	21.61	27.88
15	28.06	28.73	21.32
20	31.22	15.26	26.14
25	34.32	25.86	20.94

Notes: SEN:sinensetin, EUP:eupatorin, TMF:3'-hydroxy-5,6,7,4'-tetramethoxyflavone. To determine the optimum ratio, the highest average relaxation at the effective concentration of each compound was selected. Three optimum formulas, namely F1, F2, and F3, were calculated from the table. F1 (SEN:EUP:TMF=EC_{25}:EC_{15}:EC_{10}); F2 (SEN:EUP: TMF=EC_{25}:EC_{15}:EC_5) and F3 (SEN:EUP:TMF=EC_{25}:EC_{15}:EC_{20}).

Table 4.4: Confirmation test on optimum combination ratio of compounds in exerting highest vasodilation effects.

Group	Optimum combination ratios			Expected relaxation (%)	Actual relaxation (%)	Efficacy (%)
	SEN	EUP	TMF			
G2	EC_0	EC_5	EC_5	10	17.07±2.95	170.70
G7	EC_5	EC_0	EC_5	10	15.40±2.47	154
G27	EC_{20}	EC_{10}	EC_0	30	32.46±5.00	108.20
G28	EC_{20}	EC_{15}	EC_5	40	47.60±5.42	119
F1	EC_{25}	EC_{15}	EC_{10}	50	44.01±5.05	88.02
F2	EC_{25}	EC_{15}	EC_5	45	21.45±4.85	47.67
F3	EC_{25}	EC_{15}	EC_{20}	60	20.69±4.04	34.48

Notes: Efficacy: (Actual Relaxation/Expected Relaxation)x100%, SEN: sinensetin, EUP: eupatorin, TMF:3'-hydroxy-5,6,7,4'-tetramethoxyflavone. The effective concentrations of SEN, EUP, and TMF are shown in Table 4.1. Data are represented as mean±SEM (n=8).

Table 4.5: The maximum relaxation (R_{MAX}) and half maximal effective concentration (EC_{50}) of selected formulations.

Group	R_{MAX} (%)	EC_{50} (µg/mL)
G2	85.78±4.48	15.32±3.07
G7	88.50±4.86	12.59±4.65
G27	91.96±3.75	14.22±1.69
G28	119.05±3.29	6.78±0.70
F1	100.6±3.38	9.56±0.87

Notes: R_{MAX}= Maximum relaxation; EC_{50}=half maximal effective concentration. Data are represented as mean±SEM (n=8).

4.2 Determination of the Most Optimum Combination Ratio through Dose-response Vasodilatory Study

Figure 4.1 illustrates the concentration-response curves for G2, G7, G27, G28, and F1. The result indicates that G28 exhibited the most pronounced vasorelaxant effect among the groups, with the R_{MAX} of 119.05±3.29% and EC_{50} at 6.78±0.70 µg/mL (Figure 4.1 and Table 4.5). The vasodilatory responses were subsequently observed in F1, G27, G7, and G2, with R_{MAX} and EC_{50} values of 100.6±3.38% and 9.56±0.87 µg/mL, 91.96±3.75% and 14.22±1.69 µg/mL, 88.50±4.86% and 12.59±4.56 µg/mL, and 85.78±4.48% and 15.32±3.07 µg/mL, respectively (Figure 4.1 and Table 4.5).

4.3 Preliminary Screening on the Vasodilatory Effects of G28 on the Aorta of SD rats and SHRs

The vasodilatory effects of G28 on endothelium-intact aorta isolated from SD rats and SHRs were graphically illustrated in Figure 4.2. G28 manifested pronounced vasodilatory responses, yielding R_{MAX} and EC_{50} values of 104.28±3.04% and 6.55±0.76 μg/mL, respectively, in the aortic rings isolated from SD rats (Figure 4.2 (a) and Table 4.6) and 104.51±3.79% and 4.82±0.43 μg/mL, respectively, in the aortic rings of SHRs (Figure 4.2 (b) and Table 4.6).

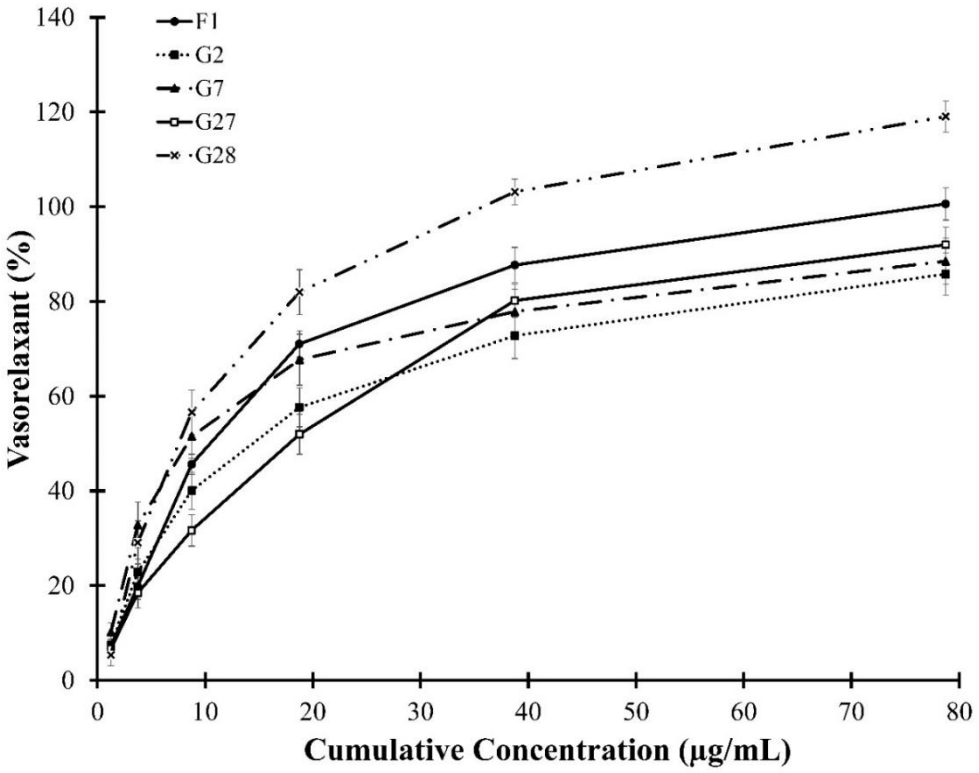

Figure 4.1: Comparison of vasodilation effect of various formulations (n=8).

4.4 Evaluation of Endothelium Dependency and Channel-linked Dependency of G28-induced Vasodilation

The endothelium-denuded aorta tissues were utilized to assess the endothelium's role in G28-induced vasodilation. Figure 4.2 demonstrated that the vasodilatory effects of G28 were markedly diminished following the removal of endothelium, yielding R_{MAX} and EC_{50} values of 43.60±4.57% (P<0.001) and >38.75 μg/mL respectively, in the aortic rings from SD rats (Figure 4.2 (a) and Table 4.6), and 50.37±3.41% (P<0.001) and >38.75 μg/mL in the aortic rings from SHRs (Figure 4.2 (b) and Table 4.6).

To examine the dependence of channel-linked receptors on G28-induced vasodilation, endothelium-intact aortic rings were pre-contracted with 80 mM of KCl for 40 minutes before adding G28. Figure 4.2 highlights a substantial reduction in vasodilatory response elicited by G28 in endothelium-intact aortic rings from SD rats that were pre-contracted with KCl, resulting in R_{MAX} and EC_{50} values of 20.55±3.26% (P<0.001) and >38.75 μg/mL, respectively. The inhibitory effect was also apparent in aortic rings isolated from SHRs, with R_{MAX} and EC_{50} values of 52.82±6.76% (P<0.001) and >38.75 μg/mL (Figure 4.2 (a) and Table 4.6).

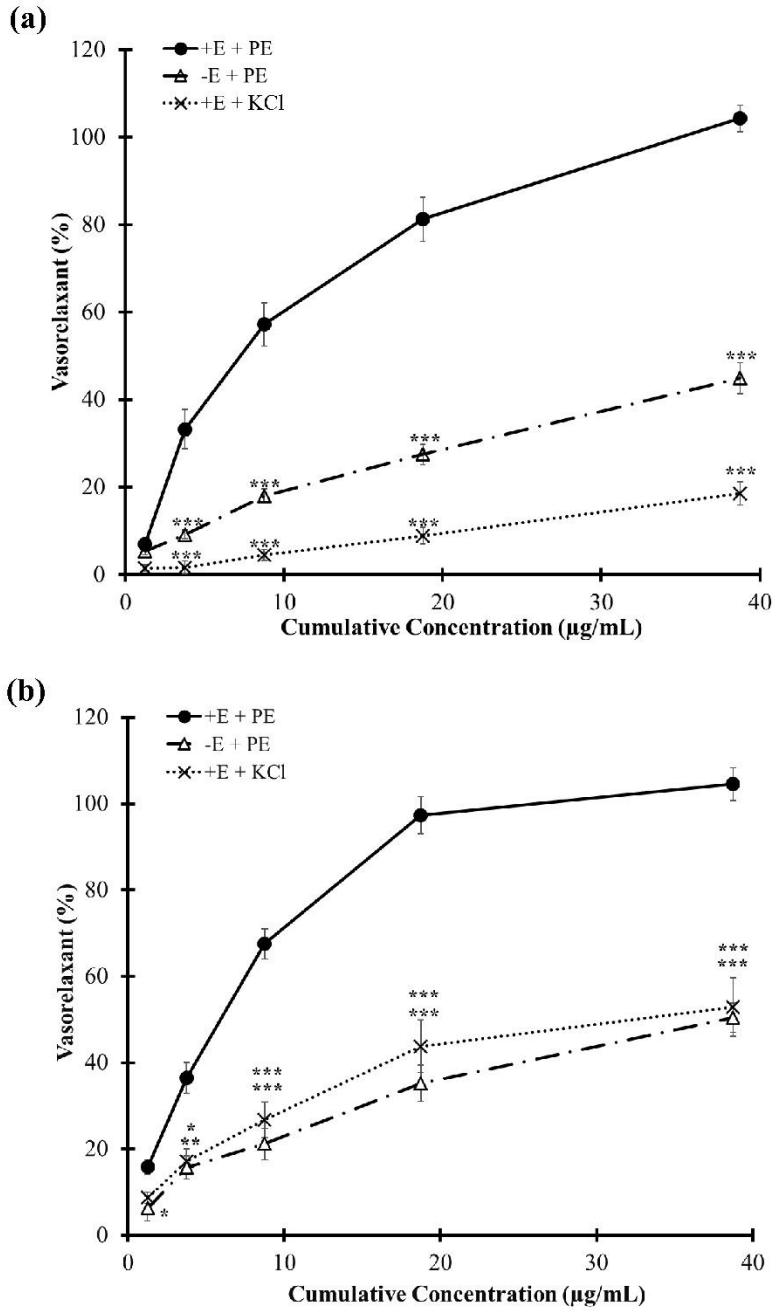

Figure 4.2: Cumulative concentration-response curves of G28-induced vasodilatory effects on PE pre-contracted endothelium-intact (+E), endothelium-denuded (-E) or KCl pre-contracted endothelium-intact rat aortic rings isolated from Sprague-Dawley rats (a) and Spontaneously Hypertensive rats (b) (n=8). Significance at *P<0.05; **P<0.01; ***P<0.001, in comparison to the negative control.

Table 4.6: Comparison of the maximum relaxation (R_{MAX}) and half-maximum effective concentration (EC_{50}) of G28 in different conditions.

Condition of aortic rings	Sprague-Dawley rats		Spontaneously hypertensive rats	
	EC_{50} (µg/mL)	R_{MAX} (%)	EC_{50} (µg /mL)	R_{MAX} (%)
Intact	6.55±0.76	104.28±3.04	4.82±0.43	104.51±3.79
Denuded	>38.75	43.60±4.57***	>38.75	50.37±3.41***
KCl	>38.75	20.55±3.26***	>38.75	52.82±6.76***
L-NAME	12.88±2.99	69.30±3.76***	4.94±1.03	75.31±2.73**
Methylene Blue	>38.75	53.85±2.33***	12.77±2.22	68.25±2.84***
ODQ	9.38±1.22	82.03±2.75**	>38.75	47.56±4.44***
Indomethacin	15.87±1.40	74.81±3.88***	6.48±0.92	87.67±7.93
Propranolol	6.60±0.72	95.17±1.57	1.18±0.37	99.97±5.76
Atropine	4.74±0.70	91.49±3.32	2.63±0.63	64.94±7.18***
Glibenclamide	10.65±1.51	85.31±5.45*	18.31±10.29	76.73±6.18**
$BaCl_2$	19.73±4.66	78.92±4.08***	8.86±2.97	68.42±3.66***
4-AP	19.71±5.72	70.77±4.88***	4.35±0.56	69.76±1.78***
TEA	31.57±7.47	64.32±4.18***	7.19±1.39	70.66±5.29***

Notes: Results are expressed as mean±S.E.M ; $^{*}P<0.05$, $^{**}P<0.01$, and $^{***}P<0.001$ compared to absence of antagonist; R_{MAX}= Maximum relaxation ; EC_{50}= half-maximum effective concentration.

4.5 Involvement of Endothelium-dependent Relaxing Factors (EDRFs) in G28-induced Vasodilation

Figures 4.3 (a) and (b) illustrate the influence of L-NAME, methylene blue, ODQ, and indomethacin on the vasodilatory effects induced by G28 in aortic rings isolated from SD rats and SHRs. Figure 4.3 (a) indicates that L-NAME, methylene blue, ODQ, and indomethacin significantly attenuated G28's vasodilatory activity in aortic rings from SD rats. Methylene blue had the most robust inhibitory effects, demonstrating significant inhibition at a G28 concentration of 3.85 µg/mL, resulting in R_{MAX} and EC_{50} values of 53.85±2.33% (P<0.001) and >38.75 µg/mL (Table 4.6), respectively. The inhibitory effects of L-NAME, ODQ, and indomethacin resulted in R_{MAX} values of 69.30±3.76% (P<0.001), 82.03±2.75% (P<0.01), and 74.81±3.88% (P<0.001), respectively, with matching EC_{50} values of 12.88±2.99 µg/mL 9.38±1.22 µg/mL, and 15.87±1.40 µg/mL (Table 4.6).

Figure 4.3 (b) illustrates the unique inhibitory patterns of EDRF antagonists in SHRs' aortic rings. Among the antagonists, ODQ had the most pronounced inhibitory effects on G28-induced vasodilation, with R_{MAX} and EC_{50} values of 47.56±4.44% (P<0.001) and >38.75 µg/mL (Table 4.6). The inhibitory effects of methylene blue were substantial when the cumulative concentration of G28 reached 8.75 µg/mL, yielding an R_{MAX} of 68.25±2.84% (P<0.001) with an EC_{50} of 12.77±2.22 µg/mL (Table 4.6). The inhibitory impact of L-NAME's was negligible at early concentrations of G28 (1.25 to 8.75 µg/mL). Substantial inhibition was noted at cumulative G28 concentrations of 18.75

μg/mL and above, resulting in an R_{MAX} of 75.31±2.73% (P<0.01) and EC_{50} of 4.94±1.03 μg/mL (Table 4.6). In contrast to the inhibitory effects shown in the aortic rings of SD rats, indomethacin exhibited a subtle inhibitory influence on the vasodilatory responses elicited by G28. This inhibition did not reach statistical significance, as indicated by R_{MAX} and EC_{50} values of 87.67±7.93% and 6.48±0.92 μg/mL (Table 4.6).

4.6 Involvement of G-protein Coupled Receptors in G28-induced Vasodilation

Figures 4.4 (a) and (b) depict the vasodilatory responses of G28 when the atropine and propranolol were present separately. Propranolol demonstrated minimal impact on G28-induced vasodilation in the aortic rings of SD rats and SHRs, with R_{MAX} values of 95.17±1.57% and 99.97±5.76%, and EC_{50} recorded at 6.60±0.72 μg/mL and 1.18±0.37 μg/mL (Table 4.6), respectively. Atropine exhibited unnotable inhibitory influence on the vasodilatory actions of G28 in SD rats, with R_{MAX} and EC_{50} values of 91.49±3.32% and 4.74±0.70 μg/mL (Figure 4.4(a) and Table 4.6). In aortic rings isolated from SHRs, the inhibitory effects of atropine on G28-induced vasodilation were negligible at lower concentrations of G28. Nonetheless, its suppressive effect became significant when the cumulative concentration of G28 reached 18.75 μg/mL, yielding R_{MAX} and EC_{50} values of 64.94±7.18% (P<0.001) and 2.63±0.63 μg/mL (Figure 4.4(b) and Table 4.6).

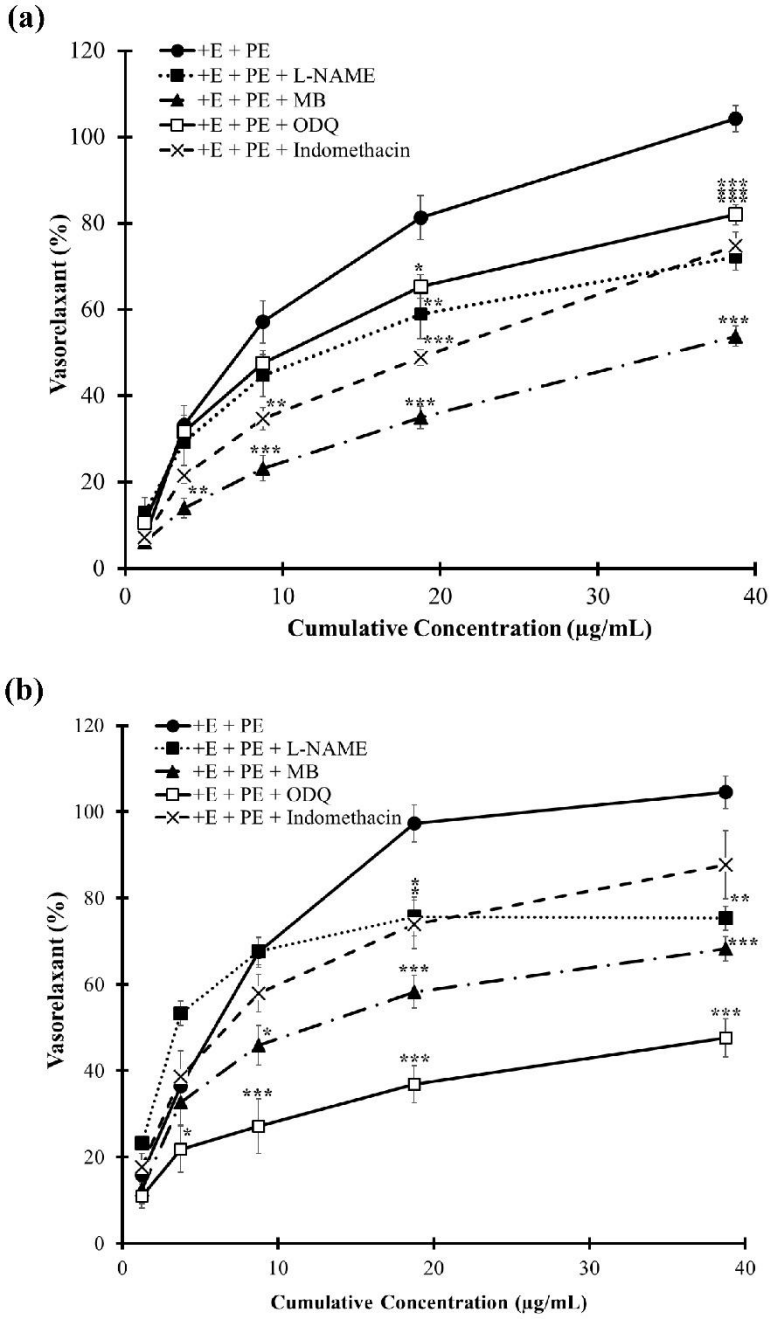

Figure 4.3: Cumulative concentration-response curves of G28-induced vasodilatory effects in the presence of L-NAME, indomethacin, methylene blue or ODQ on PE pre-contracted endothelium-intact (+E) aortic rings isolated from Sprague-Dawley rats (a) and Spontaneously Hypertensive rats (b) (n=8). Significance at *P<0.05; **P<0.01; ***P<0.001, in comparison to the negative control.

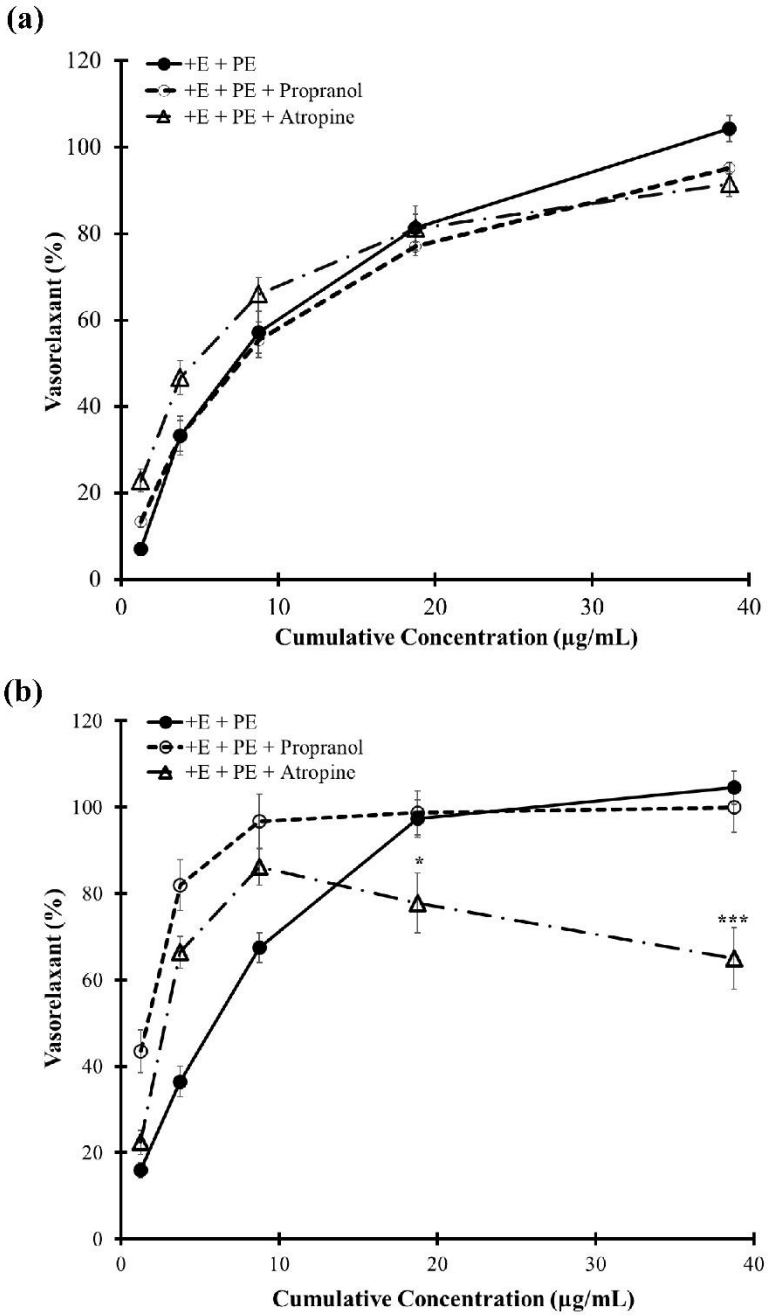

Figure 4.4: Cumulative concentration-response curves of G28-induced vasodilatory effects in the presence of atropine or propranolol on PE pre-contracted endothelium-intact (+E) aortic rings isolated from Sprague-Dawley rats (a) and Spontaneously Hypertensive rats (b) (n=8). Significance at *P<0.05; **P<0.01; ***P<0.001, in comparison to the negative control.

4.7 Involvement of Potassium Channels in G28-induced Vasodilation

Figures 4.5 (a) and (b) elucidate the effect of glibenclamide, $BaCl_2$, 4-AP, and TEA on G28-induced vasodilation. In the aortic rings of SD rats, $BaCl_2$, 4-AP, and TEA exhibited dramatically inhibition when G28 reached a cumulative concentration of 3.75 μg/mL. The subsequent R_{MAX} values obtained were 78.92±4.08%, 70.77±4.88%, and 64.32±4.18%, with associated EC_{50} values of 19.73±4.66 μg/mL (P<0.001), 19.71±5.72 μg/mL (P<0.001), and 31.57±7.47 μg/mL (P<0.001) (Table 4.6). The inhibitory effects of glibenclamide were negligible at initial concentrations of G28 (3.75 μg/mL and lower). However, a notable inhibitory response was detected when the cumulative concentration of G28 attained 8.75 μg/mL, yielding an R_{MAX} value of 85.31±5.45% (P<0.05) and an EC_{50} value of 10.65±1.51 μg/mL (Table 4.6).

In SHRs' aortic rings, glibenclamide, $BaCl_2$, 4-AP, and TEA markedly impede G28-induced vasodilation, exhibiting minor variations in inhibitory trends related to SD rats (Figure 4.5 (b)). The inhibitory effect of glibenclamide became significant at a G28 concentration of 8.75 μg/mL, resulting in an R_{MAX} value of 76.73±6.18% (P<0.01) and an EC_{50} value of 18.31±10.29 μg/mL (Table 4.6). The inhibitory effects of $BaCl_2$, 4-AP, and TEA became pronounced upon the introduction of 18.75 μg/mL of G28, resulting in R_{MAX} values of 68.42±3.66% (P<0.001), 69.76±1.78% (P<0.001), and 70.66±5.29% (P<0.001), respectively, with corresponding EC_{50} values of 8.86±2.97 μg/mL, 4.35±0.56 μg/mL, and 7.19±1.39 μg/mL (Table 4.6).

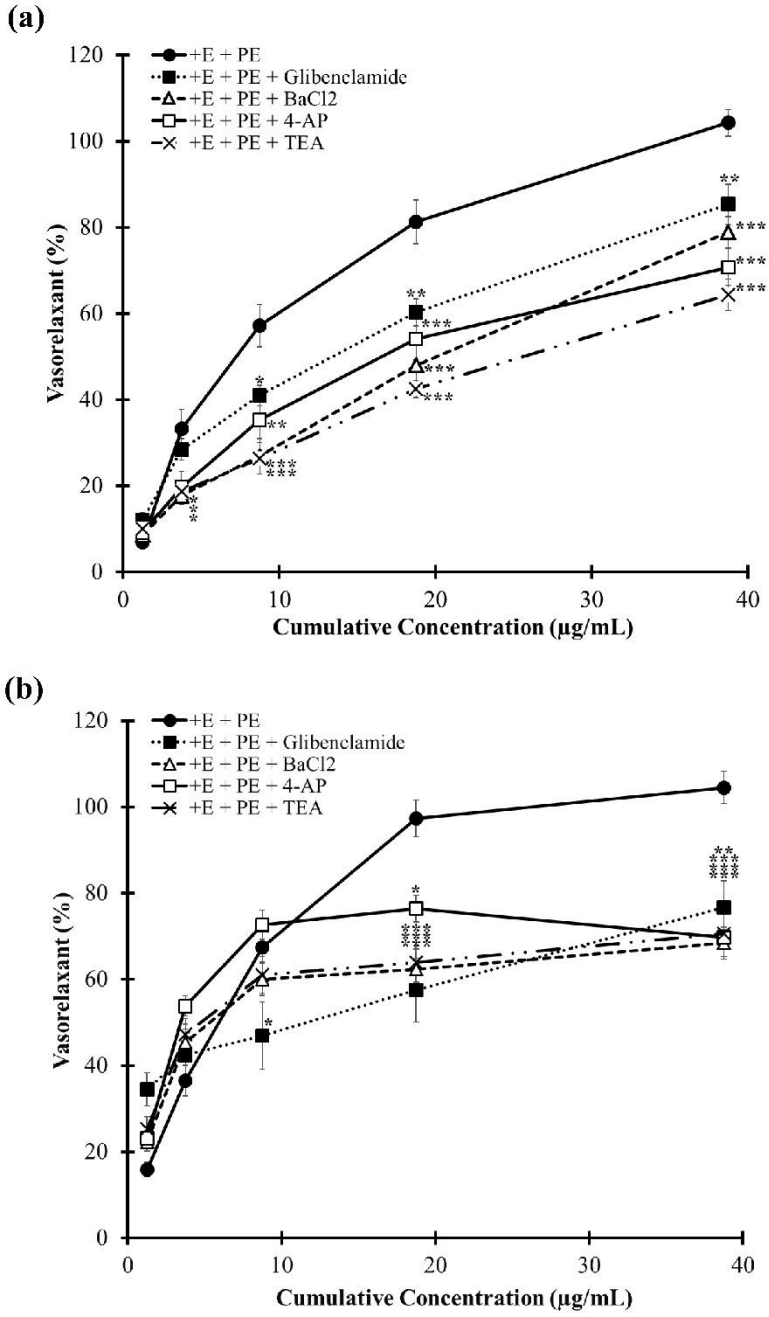

Figure 4.5: Cumulative concentration-response curves of G28-induced vasodilatory effects in the presence of TEA, glibenclamide, 4-AP or $BaCl_2$ on PE pre-contracted endothelium-intact (+E) aortic rings isolated from Sprague-Dawley rats (a) and Spontaneously Hypertensive rats (b) (n=8). Significance at *P<0.05; **P<0.01; ***P<0.001, in comparison to the negative control.

4.8 Actions of G28 on Voltage-gated Calcium Channels

The aortic rings were exposed to $CaCl_2$ at cumulative concentrations ranging from 0.01 mM to 10 mM while being incubated in a Ca^{2+}-free environment to assess the involvement of VOCCs. When the cumulative concentration of $CaCl_2$ in the organ bath reached 3 mM, the maximum contraction tone of 0.92±0.05 g was achieved in the aortic rings excised from SD rats that were not given nifedipine or G28 (Figure 4.6 (a) and Table 4.7). The contraction caused by extracellular $CaCl_2$ was nearly eliminated by the VOCC blocker nifedipine (0.1 µM, 0.3 µM, or 1.0 µM). When the concentration of $CaCl_2$ in the organ bath reached 10 mM, the peak contraction forces were 0.16±0.01 g (P<0.001), 0.11±0.01 g (P<0.001), and 0.05±0.01 g (P<0.001), respectively (Figure 4.6(a) and Table 4.7). Figure 4.6 (a) shows that when the cumulative concentration of $CaCl_2$ reached 3 mM (Table 4.7), 1.25 µg/mL, 5 µg/mL, and 20 µg/mL of G28 significantly inhibited aortic contraction induced by $CaCl_2$. The peak contraction forces were 0.55±0.03 g (P<0.001), 0.34±0.03 g (P<0.001), and 0.27±0.04 g (P <0.001), respectively.

When the cumulative concentration of $CaCl_2$ reached 10 mM, extracellular $CaCl_2$ produced the maximum contraction force of 0.83±0.02 g in the aortic rings of SHRs, free from the effects of nifedipine and G28 (Figure 4.6 (b) and Table 4.7). The antagonizing effect of nifedipine (0.1 µM, 0.3 µM, or 1.0 µM) almost ceased the aortic contractions. When the cumulative concentration of $CaCl_2$ reached 10 mM, the highest contractile tone was recorded at 0.14±0.01 g (P<0.001), 0.12±0.02 g (P<0.001), and 0.06±0.01 g (P<0.001, respectively

(Figure 4.6 (b) and Table 4.7). In aortic rings separated from SHRs, G28's inhibitory effect on extracellular calcium-induced contraction was marginally different from what was achieved in SD rats. When the concentration of $CaCl_2$ in the organ bath reached 10 mM, the most tremendous contraction force of 0.83±0.03 g was obtained, indicating that the 1.25 μg/mL of G28 had minimal inhibitory effects (Figure 4.6 (b) and Table 4.7). When exposed to 10 mM $CaCl_2$, the aortic rings produced the maximum contraction force at 0.53±0.05 g (P<0.001) and 0.46±0.05 g (P<0.001), respectively. The presence of 5 μg/mL and 20 μg/mL of G28 significantly decreased the extracellular calcium-induced contraction (Figure 4.6 (b) and Table 4.7).

4.9 Actions of G28 on inositol triphosphate receptor (IP_3R)

In the endothelium-denuded aortic rings obtained from SD rats, PE induced a transient contraction under Ca^{2+}-free circumstances, resulting in a contract tension of 0.95±0.04 g (Figure 4.7(a) and Table 4.7). The presence of 2-APB markedly suppressed the contraction, reducing the force to 0.03±0.01 g (P<0.001). G28 at concentrations of 5 μg/mL and 20 μg/mL, manifested substantial inhibitory effects on PE-induced vasoconstriction, leading to decreased contractile tones of 0.71±0.03 g (P<0.001) and 0.52±0.03 g (P<0.001), respectively (Figure 4.7 (a) and Table 4.7). However, G28 at the minimal concentration (1.25 μg/mL) did not demonstrate pronounced suppressive effects on PE-induced vasoconstriction (Figure 4.7 (a) and Table 4.7).

In the SHRs' aortic rings, PE triggered a transient contractile tension in endothelium-denuded aortic rings, culminating in a final contraction of 0.32±0.07 g (Figure 4.7 (b) and Table 4.7). Substantially mitigated the vasoconstrictive effects induced by PE, yielding a contraction force of 0.004±0.006 g (P<0.001) (Figure 4.7 (b) and Table 4.7). Concentrations of 1.25 µg/mL, 5 µg/mL, and 20 µg/mL significantly diminished PE-induced vasoconstriction, yielding contractile tones at 0.20±0.05 g (P<0.001), 0.20±0.05 g (P<0.001), and 0.19±0.05 g (P<0.001), respectively (Figure 4.7 (b) and Table 4.7).

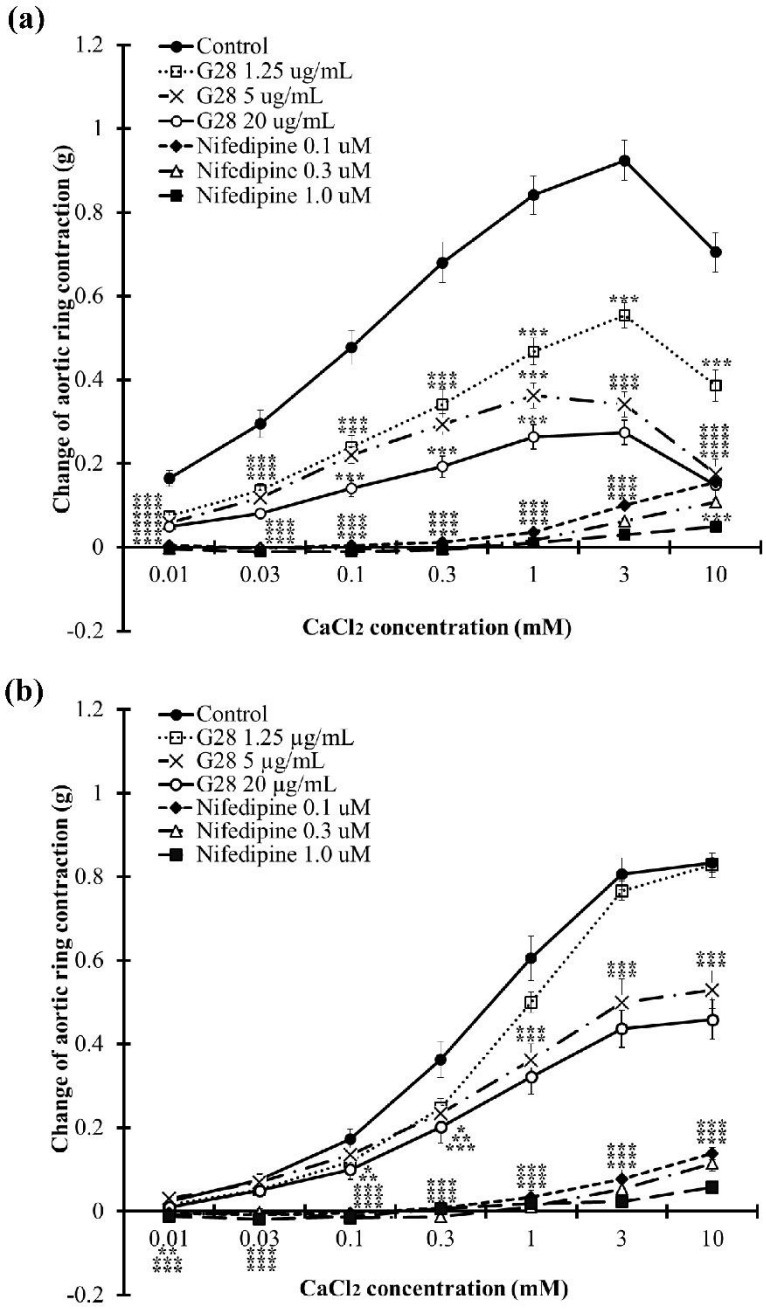

Figure 4.6: Effect of voltage-gated calcium channel antagonist, nifedipine (0.1, 0.3, 1.0 µM) and G28 (1.25 µg/mL, 5 µg/mL and 20 µg/mL) on $CaCl_2$-induced contraction in endothelium-intact (+E) aortic rings isolated from Sprague-Dawley rats (a) and Spontaneously Hypertensive rats (b), in high K^+ and Ca^{2+} free KPS (n=8). Significance at *P<0.05; **P<0.01; ***P<0.001, in comparison to the negative control.

Table 4.7: Comparison of calcium-induced contraction responses (g) in among different conditions.

Treatments	Concentration	C_{MAX} (g)	
		Sprague-Dawley Rats	Spontaneously Hypertensive Rats
VOCC			
Negative control	-	0.92±0.05	0.83±0.02
Nifedipine	0.1 µM	0.55±0.03***	0.83±0.03
Nifedipine	0.3 µM	0.34±0.03***	0.53±0.05***
Nifedipine	1.0 µM	0.27±0.03***	0.46±0.05***
G28	1.25 µg/mL	0.10±0.01***	0.14±0.01***
G28	5 µg/mL	0.06±0.01***	0.12±0.02***
G28	20 µg/mL	0.03±0.01***	0.06±0.01***
IP_3R			
Negative control	-	0.95±0.04	0.32±0.07
2-APB	100 µM	0.03±0.01***	0.004±0.006***
G28	1.25 µg/mL	0.80±0.03	0.20±0.05***
G28	5 µg/mL	0.71±0.03***	0.19±0.05***
G28	20 µg/mL	0.52±0.03***	0.19±0.05***

Notes: Results are expressed as mean±S.E.M; $P<0.05^{*}$, $P<0.01^{**}$, and $P<0.001^{***}$, compared to negative control; C_{MAX}= Maximum contraction; VOCC=voltage-operated calcium channel, IP_3R=inositol triphosphate receptor.

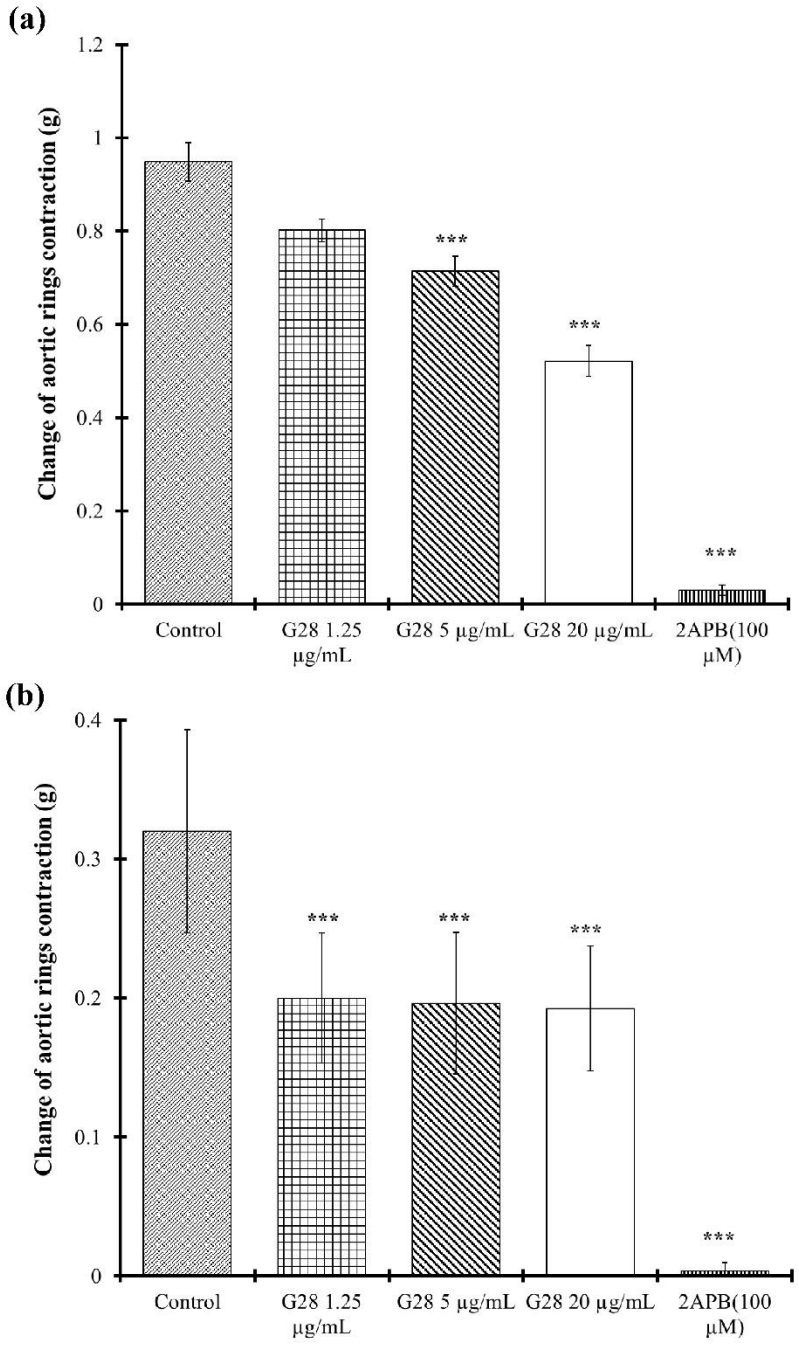

Figure 4.7: Effect of different concentrations G28 (1.25 µg/mL, 5 µg/mL and 20 µg/mL) and 2-APB (100 µM) on intracellular Ca^{2+} release in endothelium-intact (+E) aortic rings isolated from Sprague-Dawley rats (a) and Spontaneously Hypertensive rats (b), in high K^{+} and Ca^{2+} free KPS (n=8). Significance at *P<0.05; **P<0.01; ***P<0.001, in comparison to the negative control.

4.10 The anti-hypertensive effects of G28 on SHRs

Blood pressure dynamics in SHRs were monitored over a 21-day period of oral administration during the *in vivo* study. The negative control group demonstrated no statistically significant alterations in SBP, DBP, and MAP over the 21 days, recording values of 204.73±4.22 mmHg, 143.94±5.36 mmHg, and 163.79±4.94 mmHg, respectively, after 21 days of oral treatment (week 3), compared to initial measurements of 206.42±4.02 mmHg, 143.67±7.20 mmHg, and 164.23±6.06 mmHg before the initiation of oral administration (week 0) (Figure 4.8 and Table 4.8). In contrast, the groups treated with propranolol (80 mg/kg) and the G28 (15 mg/kg, 30 mg/kg, and 60 mg/kg) markedly reduced the BP of SHRs in a time-dependent manner during 21 days of treatment. The initial SBP of propranolol-treated and G28-treated groups (15 mg/kg, 30 mg/kg, and 60 mg/kg) were documented at 213.83±3.82 mmHg, 210.94±5.31 mmHg, 213.23±5.31 mmHg, and 205.98±2.04 mmHg, respectively, and substantially decreased to 178.10±2.71 mmHg (P<0.001), 189.79±4.17 mmHg (P<0.05), 189.40±2.87 mmHg (P<0.05), and 180.75±1.67 mmHg (P<0.001), respectively, after a 21-day of oral treatment period (Figure 4.8 (a) and Table 4.8), in comparison to the negative control. The initial DBP levels of the propranolol-treated (80 mg/kg) and the G28-treated groups (15 mg/kg, 30 mg/kg, and 60 mg/kg) were recorded at 156.02±6.13 mmHg, 152.67±9.34 mmHg, 154.56±9.09 mmHg, and 139.46±4.64 mmHg, respectively, prior to oral administration. After 21 days of oral treatment, the levels were 122.35±4.13 mmHg (P<0.005), 133.83±4.68 mmHg, 138.25±3.12 mmHg, and 129.67±3.12 mmHg, in

comparison to the negative control (Figure 4.8 (b) and Table 4.8). The MAP trend was similar to that of DBP in the propranolol-treated and G28-treated groups (15 mg/kg, 30 mg/kg, and 60 mg/kg). The initial MAP values for these groups were recorded at week 0, measuring 174.92±5.31 mmHg, 171.73±7.95 mmHg, 173.75±7.82 mmHg, and 160.33±4.11 mmHg. After 21 days of treatment, the values decreased to 140.56±3.60 mmHg (P<0.005), 152.13±4.41 mmHg, 155.04±2.62 mmHg, and 146.56±2.13 mmHg (P<0.05) (Figure 4.8 (c) and Table 4.8), respectively, in comparison to the negative control.

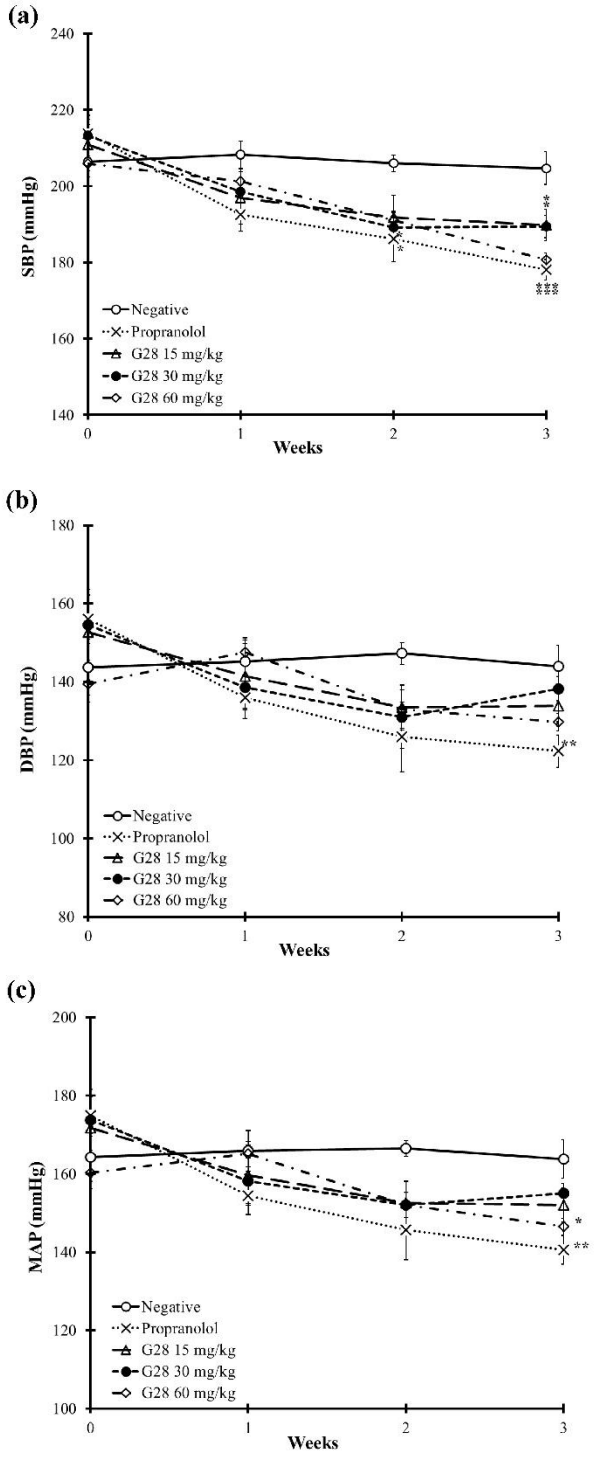

Figure 4.8: The SBP (a), DBP (b), and MAP (c) of Spontaneously Hypertensive rats after 21 day oral administration with distilled water (negative control), 80 mg/kg propranolol (positive control), and G28 (15 mg/kg, 30 mg/kg, and 60 mg/kg) (n=8). Significance at *P<0.05; **P<0.01; ***P<0.001, in comparison to the negative control.

Table 4.8: **The SBP, DBP and MAP of SHRs for 21 days oral administration.**

Groups	Blood pressure (mmHg)			
	Week 0	**Week 1**	**Week 2**	**Week 3**
SBP				
Negative control	206.42±4.02	208.31±3.54	206.02±2.25	204.73±4.22
Propranolol 80 mg/kg	213.83±3.82	192.52±4.42	186.25±6.06	178.10±2.71***
G28 15 mg/kg	210.94±5.31	196.98±6.78	191.85±5.83	189.79±4.17*
G28 30 mg/kg	213.23±5.31	198.56±6.12	189.25±3.92*	189.40±2.87*
G28 60 mg/kg	205.98±2.04	201.25±3.34	191.04±2.36*	180.75±1.67***
DBP				
Negative control	143.67±7.20	145.21±6.02	147.29±2.74	143.94±5.36
Propranolol 80 mg/kg	156.02±6.13	136.00±5.29	125.94±8.81	122.35±4.13**
G28 15 mg/kg	152.67±9.34	141.46±8.23	133.42±5.79	133.83±4.68
G28 30 mg/kg	154.56±9.09	138.56±5.70	131.00±8.08	138.25±3.12
G28 60 mg/kg	139.46±4.64	147.50±3.26	133.02±8.08	129.67±3.12
MAP				
Negative control	164.23±6.06	165.88±5.31	166.54±2.04	163.79±4.94
Propranolol 80 mg/kg	174.92±5.31	154.48±4.85	145.69±7.61	140.56±3.60**
G28 15 mg/kg	171.73±7.95	159.69±7.71	152.56±5.69	152.13±4.41
G28 30 mg/kg	173.75±7.82	158.23±5.79	152.04±6.09	155.04±2.62
G28 60 mg/kg	160.33±4.11	165.10±3.27	152.06±3.19	146.56±2.13*

Notes: SBP: systolic blood pressure; DBP: diastolic blood pressure and MAP: mean arterial blood pressure. The SBP, DBP and MAP are in mm/Hg. Results are expressed as mean±S.E.M (n=8); $^{*}P<0.05$, $^{**}P<0.01$, and $^{***}P<0.001$ compared to negative control.

4.11 Network Pharmacology Study of Sinensetin, Eupatorin, and TMF

4.11.1 Potential Targets of Sinensetin, Eupatorin, and TMF

The results from PharmMapper showed that a total of 288, 286, and 271 of target genes was obtained from sinensetin, eupatorin, and TMF. Among these genes a total of 341 no repeated target genes were identified through target prediction analysis (Table 4.9). These genes represent a wide array of molecular classes, including enzymes, receptors, kinases, transcription factors, and structural proteins. Among the identified targets, several are key regulators of enzymatic metabolism (e.g., CYP19A1, AKR1C3, DHFR, GSTP1), hormonal pathways (e.g., ESR1, AR, NR3C1), and intracellular signaling transducers (e.g., MAPK1, AKT1, JAK2, PIK3R1).

The gene set also includes several members of the mitogen-activated protein kinase family (MAPK8, MAPK14, MAP2K1) and phosphodiesterases (PDE4B, PDE5A, PDE3B), as well as regulators of nitric oxide and redox balance (NOS3, SOD2, NQO1). Apoptosis-related genes such as CASP1, CASP3, and CASP7, and matrix remodeling enzymes like MMP1, MMP2, MMP3, and MMP9 are also present in the list.

Additionally, various nuclear receptors and transcriptional regulators (RXRA, RARA, PPARA, NR1H3, PPARG) were included, highlighting potential modulatory effects on gene expression. A number of metabolic regulators and

transport-related genes were identified, such as FABP3, FABP4, ALB, and SLC family members (e.g., SLC22A5 and inferred SLC transporters).

Table 4.9: Target genes was obtained from sinensetin, eupatorin, and TMF.

No	Gene	No	Gene	No	Gene	No	Gene
1	BCHE	36	MAPK8	71	KIF11	106	TYMS
2	BACE1	37	SHBG	72	NR3C2	107	CTNNA1
3	CYP19A1	38	ESRRG	73	DUSP6	108	PPARD
4	AR	39	QPCT	74	PDE4B	109	EGFR
5	NR1H2	40	ADAM17	75	GC	110	PTPN11
6	PPIA	41	CFD	76	LCK	111	CCNT1
7	CA1	42	MAPK14	77	AKR1C1	112	HSD11B1
8	F2	43	NOS3	78	F10	113	C8G
9	ESR1	44	PAH	79	JAK3	114	NR1I2
10	PNP	45	CHEK1	80	FNTA	115	ADH5
11	CA2	46	PDE4D	81	APCS	116	CASP7
12	FAP	47	AMY1A	82	CES1	117	DHODH
13	GSTP1	48	BCAT2	83	NQO2	118	RHOA
14	CCNA2	49	SRC	84	PLAU	119	REG1A
15	PGR	50	CBR1	85	NQO1	120	SHMT1
16	GBA	51	LSS	86	FGFR2	121	PDE3B
17	TTR	52	HSD17B1	87	MMP3	122	FHIT
18	PIM1	53	MIF	88	GSK3B	123	AKR1C2
19	CDK2	54	CSNK1G2	89	BMP7	124	IGF1R
20	AKR1C3	55	AKR1B1	90	HSPA8	125	CSNK2A1
21	CTSS	56	PYGL	91	PCK1	126	ABO
22	KDR	57	MAOB	92	DHFR	127	MET
23	MAPK10	58	PDPK1	93	HK1	128	ME2
24	STS	59	ANXA5	94	DPP4	129	PDE5A
25	APOA2	60	RXRA	95	IMPDH2	130	TGFBR1
26	CFB	61	PTPN1	96	ADH1C	131	ADK
27	ALB	62	SULT2A1	97	SERPINA1	132	MAPKAPK2
28	GSR	63	MTAP	98	MMP8	133	CDA
29	MMP13	64	PLK1	99	ISG20	134	NR1H3
30	SORD	65	IGLV2-8	100	AHCY	135	AKT1
31	CTSD	66	AZGP1	101	XIAP	136	REN
32	CASP3	67	FGFR1	102	LGALS7	137	RAC2
33	ANG	68	MMP12	103	EPHX2	138	BHMT
34	EPHB4	69	LTA4H	104	F7	139	BST1
35	CDK6	70	HSP90AA1	105	SOD2	140	RNASE4

Table 4.9: Target genes was obtained from sinensetin, eupatorin, and TMF (continue).

No	Gene	No	Gene	No	Gene	No	Gene
141	LDHB	178	AMD1	215	FABP3	252	MMP2
142	NCS1	179	CRABP2	216	CHIT1	253	ARL5A
143	GSTT2B	180	RBP4	217	PTK2	254	TGFB2
144	THRB	181	SULT1E1	218	MAPK1	255	GSTM1
145	PDHB	182	GSTA1	219	PITPNA	256	FDPS
146	MTHFD1	183	RAB11A	220	MMP9	257	VDR
147	ELANE	184	UCK2	221	SDS	258	S100A9
148	HPN	185	LYZ	222	ALDH2	259	AKT2
149	ARHGAP1	186	THRA	223	CTSG	260	DCPS
150	CTSK	187	AMY2A	224	GNPDA1	261	OAT
151	PDK2	188	GPI	225	GSTA3	262	CTSF
152	PPARG	189	MAN1B1	226	LGALS3	263	IL2
153	FABP4	190	RHEB	227	CDK7	264	KIT
154	HCK	191	ARSA	228	HPRT1	265	GSTO1
155	CYP2C9	192	HEXB	229	PPCDC	266	TAP1
156	RNASE3	193	NMNAT1	230	EPHA2	267	F11
157	FKBP1A	194	LGALS2	231	BIRC7	268	MMP1
158	PLA2G2A	195	SULT2B1	232	ARG1	269	CD209
159	HDAC8	196	RARA	233	ABL1	270	DPEP1
160	ITK	197	GSTZ1	234	GSTM2	271	CMA1
161	PPARA	198	OTC	235	ARG2	272	CDC42
162	DTYMK	199	NR1H4	236	TGM3	273	GCK
163	SEC14L2	200	NR3C1	237	RAB5A	274	PNMT
164	TNK2	201	STAT1	238	HRAS	275	FOLH1
165	CCL5	202	CLK1	239	PRKCQ	276	MAP2K1
166	ACP3	203	SELP	240	B3GAT1	277	KAT2B
167	TPI1	204	HINT1	241	TPH1	278	FABP7
168	INSR	205	IMPDH1	242	ACE	279	GP1BA
169	ZAP70	206	APRT	243	ACADM	280	TK1
170	ERBB4	207	PAPSS1	244	HNF4G	281	GCDH
171	TRAPPC3	208	CBS	245	NT5M	282	PKLR
172	SYK	209	CYP2C8	246	HMGCR	283	PIK3R1
173	PAK6	210	HAGH	247	SETD7	284	AURKA
174	CDK5R1	211	JAK2	248	DUT	285	GALE
175	DCK	212	EIF4E	249	CASP1	286	PARP1
176	CD1A	213	FABP6	250	ATIC	287	SELE
177	ALDOA	214	MME	251	FECH	288	GM2A

Table 4.9: Target genes was obtained from sinensetin, eupatorin, and TMF (continue).

No	Gene	No	Gene	No	Gene	No	Gene
289	TEK	303	TRDMT1	317	ERI1	331	RAC1
290	TPSB2	304	FGG	318	RAP2A	332	HNMT
291	CTSB	305	NMNAT3	319	PMS2	333	BTK
292	PPP1CC	306	APAF1	320	HADH	334	AK1
293	ARF4	307	UAP1	321	TREM1	335	EEA1
294	RARB	308	RFK	322	ESR2	336	TTPA
295	GMPR2	309	CLEC4M	323	DAPK1	337	PROCR
296	LCN2	310	RARG	324	MMP7	338	FKBP3
297	AGXT	311	WARS1	325	C1S	339	DCXR
298	RNASE2	312	RAB9A	326	UMPS	340	CRYZ
299	FKBP1B	313	RAF1	327	SULT1A1	341	SPR
300	DDX39B	314	NDST1	328	RXRB		
301	GMPR	315	NOS2	329	RORA		
302	GLO1	316	ADAM33	330	RND3		

4.11.2 Core antihypertensive and target genes from sinensetin, eupatorin, and TMF

After eliminating duplicates there were a total of 2345 anti-hypertensive-related genes obtained from the GeneCards® and OMIM® database. A total of 75 gene targets were identified as potentially involved in hypertension-related pathways for sinensetin, eupatorin, and TMF（Table 4.10 and Figure 4.9). These targets encompass genes involved in vasomotor regulation, endothelial function, vascular remodeling, hormonal response, oxidative stress, inflammation, and lipid metabolism.

The list includes several key enzymes and receptors involved in blood pressure regulation, such as NOS3, ACE, REN, and PDE5A, which contribute to nitric oxide production, renin-angiotensin system activity, and cyclic nucleotide signaling. Genes involved in vascular remodeling and matrix turnover such as MMP1, MMP2, MMP3, MMP9, and MMP12 were also identified.

Transcriptional regulators and nuclear receptors like PPARG, PPARA, NR3C1, NR3C2, NR1I2, NR1H3, and VDR were included, reflecting modulation of gene expression related to vascular inflammation and metabolic balance. Signal transduction components such as MAPK1, MAPK10, AKT1, JAK2, PIK3R1, and PTK2 were also found, indicating involvement in vascular cell signaling and growth regulation.

Genes related to oxidative and metabolic balance, including SOD2, NQO1, GSTM1, GSR, ALDH2, and MAOB, were present, alongside transport and adhesion molecules such as KDR, EGFR, SELE, and SELP, which contribute to endothelial integrity and leukocyte recruitment.

Table 4.10: Core antihypertensive and target genes from sinensetin, eupatorin, and TMF.

No	Target Gene	No	Target Gene	No	Target Gene	No	Target Gene
1	BCHE	21	NR3C2	41	PPARG	61	ACADM
2	CYP19A1	22	PDE4B	42	CYP2C9	62	HNF4G
3	AR	23	CES1	43	PLA2G2A	63	HMGCR
4	CA1	24	PLAU	44	PPARA	64	MMP2
5	F2	25	NQO1	45	INSR	65	GSTM1
6	ESR1	26	MMP3	46	ERBB4	66	VDR
7	CA2	27	DPP4	47	SULT1E1	67	MMP1
8	GSTP1	28	EPHX2	48	LYZ	68	CMA1
9	PGR	29	SOD2	49	NR3C1	69	PNMT
10	TTR	30	PPARD	50	SELP	70	KAT2B
11	KDR	31	EGFR	51	CYP2C8	71	PIK3R1
12	MAPK10	32	NR1I2	52	JAK2	72	SELE
13	ALB	33	ABO	53	MME	73	NOS2
14	GSR	34	PDE5A	54	PTK2	74	SULT1A1
15	SHBG	35	NR1H3	55	MAPK1	75	PROCR
16	NOS3	36	AKT1	56	MMP9		
17	PDE4D	37	REN	57	ALDH2		
18	MAOB	38	BST1	58	ABL1		
19	SULT2A1	39	THRB	59	ARG2		
20	MMP12	40	ELANE	60	ACE		

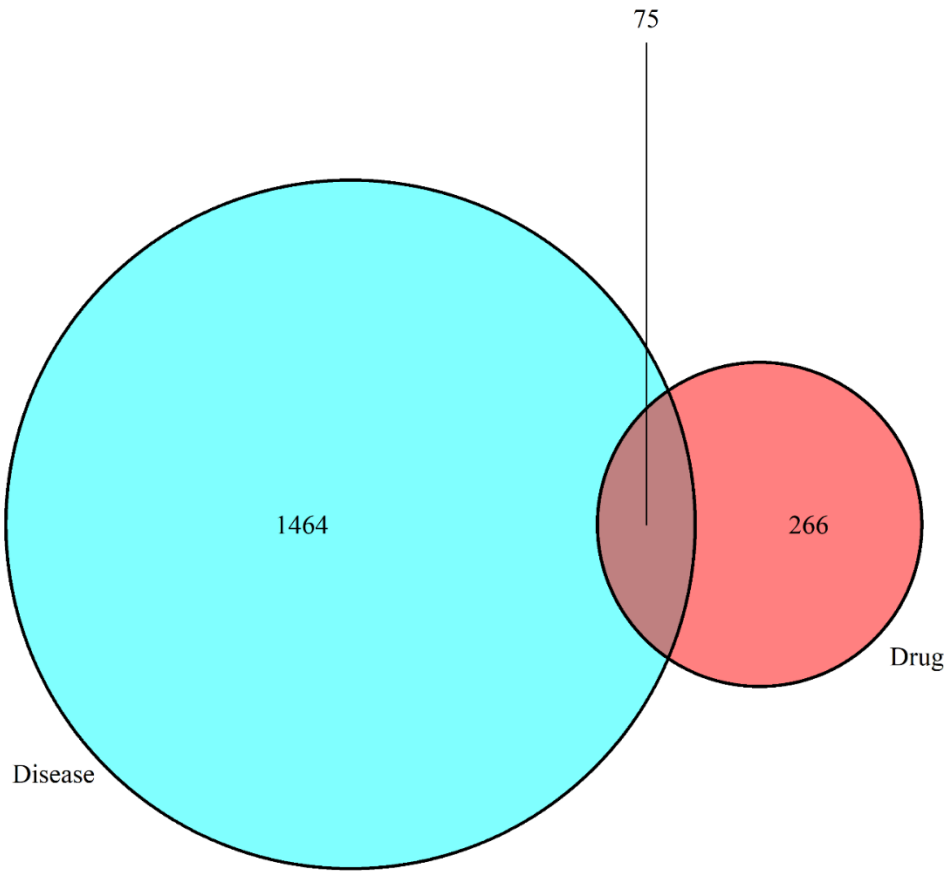

Figure 4.9: Venn diagram showing the overlap between hypertension-related genes (Disease) and the predicted target genes of sinensetin, eupatorin, and TMF (Drug). A total of 1,464 genes were associated with hypertension, and 266 genes were predicted as compound targets. The intersection represents 75 common genes, indicating potential molecular targets through which the compounds may exert antihypertensive effects.

4.11.3 Protein-protein interaction (PPI) Network of Anti-hypertension-associated and Target Genes of Sinensetin, Eupatorin, and TMF

The PPI network presented illustrates the interconnected targets of sinensetin, eupatorin, and TMF, likely constructed using STRING analysis. Each node in the network represents a protein, while the edges reflect predicted or validated interactions derived from experimental data, curated databases, co-expression patterns, or text mining. The three flavonoids are mediated by a group of central nodes with high degree connectivity which serves as important regulatory proteins.

Markedly, such proteins as ESR1, PPARG, EGFR, and matrix metalloproteinase family members (MMP1, MMP2, and MMP9) can be considered major hubs in the network. In vascular remodelling, extracellular matrix regulation, upon inflammatory reactions, metabolic regulation and hormonal signalling, these proteins are intensively implicated. The discovery of INSR, JAK2 and MAPK1 also confirms that the compounds have the potential to regulate metabolic and inflammatory pathways (Figure 4.10).

Figure 4.11 refers to the bar chart which shows degree centrality of a number of genes in a PPI network therefore indicating the frequency of interaction of the given genes with other proteins. The highest degree of the node in this dataset is 18, which is the highest degree of AKT1 that is why this node is the most

important central node. This dominance suggests that there should be a central regulatory position of AKT1, especially in cell survival, metabolism and vascular regulation signalling cascades. Following are the EGFR and ESR1; these two proteins are highly reported in the process of controlling cell proliferation, hormone receptiveness and oncogenesis. Other interesting genes involve the ALB and MMP9 that are respectively linked with the transportation of proteins and the reconstruction of the extracellular matrix. Intermediately linked genes include PIK3R1 and ACE which also underscore their role in intracellular signalling and blood pressure regulation. Genes with lower degree NR3C2, NR3C1, GSTP1, CYP2C9, CYP19A1 having a grade of 6, respectively, show fewer interactions, but still a possible contribution to particular biological activity, such as xenobiotic metabolism and hormonal regulation. Together, this distribution illuminates a hierarchical structure of the interaction network where high connection hub genes could serve as critical control nodes and potential therapeutic targets in diseases of interest of disease-modifying interventions. (Figure 4.11).

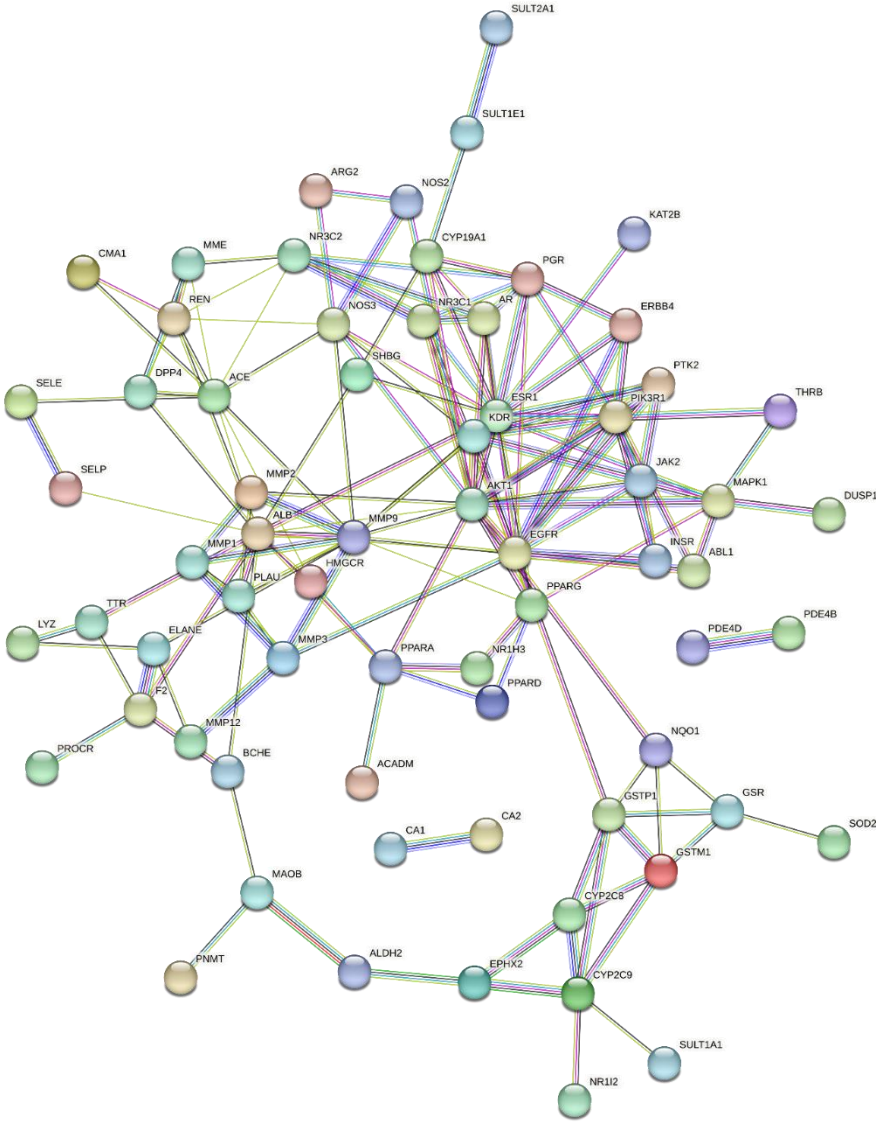

Figure 4.10: Protein-protein interaction (PPI) network of predicted targets for sinensetin, eupatorin, and TMF, constructed using STRING database. Each node represents a protein, while edges indicate functional and physical associations based on evidence from curated databases, experimental data, and text mining.

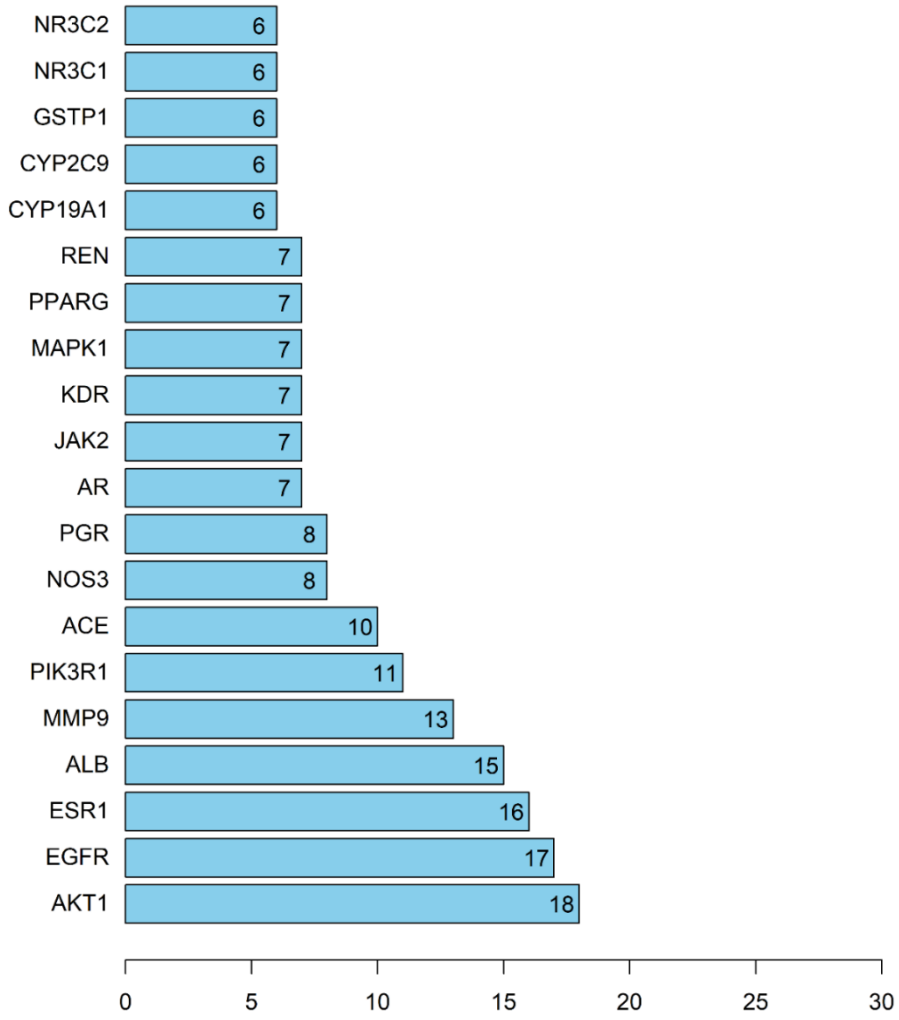

Figure 4.11: Bar chart illustrating the degree centrality of genes within PPI network. Degree values represent the number of direct interactions each gene has with others in the network. AKT1, EGFR, and ESR1 emerged as the top hub genes, suggesting their central regulatory roles in key biological processes such as cell signaling, proliferation, and vascular function.

4.11.4 Gene Ontology analysis from sinensetin, eupatorin, and TMF

The Gene Ontology (GO) enrichment analysis reveals that there are a number of molecular functions that are greatly over-represented among the targets of the gene and with a heavy focus on transcriptional regulation, receptor binding, and even enzymatic action. The main mechanisms are the activity of nuclear receptors, the activity of ligand-based transcription factors, and the activity of transcription co-activator/coregulator, which suggest a regulatory effect on the expression of genes. Other functions include serine -endopeptidase activity, ATPase binding, and calmodulin binding implying that it is involved in proteolytic activities, as well as intracellular signalling. Moreover, the nuclear steroid receptor activity and estrogen -response element bind to hormo-mediated transcriptional regulation. It is noteworthy that a number of enriched words are related to binding activities and metabolic processes such as monocarboxylic acid binding, organic acid binding, and fatty acid binding that can be potentially related to metabolic regulation. Such terms as the activity of the metallopeptidase, kinase regulator, and phosphoinositide binding show the signal transduction and protein turnover modulation (Figure 4.12).

Bubble plot illustrates the GO enrichment analysis of molecular functions that are explained to the target genes, which presented significant biological roles of activity of sinensetin, eupatorin and TMF (Figure 4.13). Endopeptidase activity, with the largest gene ratio and the highest level of statistical information,

represents one of the most enriched functions and argues in its favor is a prevailing part in proteolytic functions, including, but not limited to, extracellular matrix reorganization and anti-inflammatory regulation. Additional very overrepresented functions are nuclear receptor activity, ligand-activated transcription factor activity, and transcription coregulator binding indicating the role of the genes in hormonal signalling and gene-expression regulation. Their existence as serine-type peptidase activity, ATPase binding, and calmodulin binding also indicates that they would be used as signalling mediators in the cell, followed by regulation of the enzyme activity. Terms of metabolism like monocarboxylic acid binding, organic acid binding and fatty acid binding were also enriched, which may suggest a potential impact on lipid metabolism and energy homeostasis. What is more, the presence of such terms as the metallopeptidase activity, binding of phosphotyrosine residues and oxygen indicates the possibility of the participation in redox regulation and in the metallopeptidase–tyrosine-modified pathways. Altogether, these findings suggest that the target genes are mainly involved in enzymatic functions, transcriptional regulation, hormone, and metabolic regulation that overall justify the augmentation of the therapeutic prospects of the compounds in regulating inflammation, vascular tone, and metabolic activity.

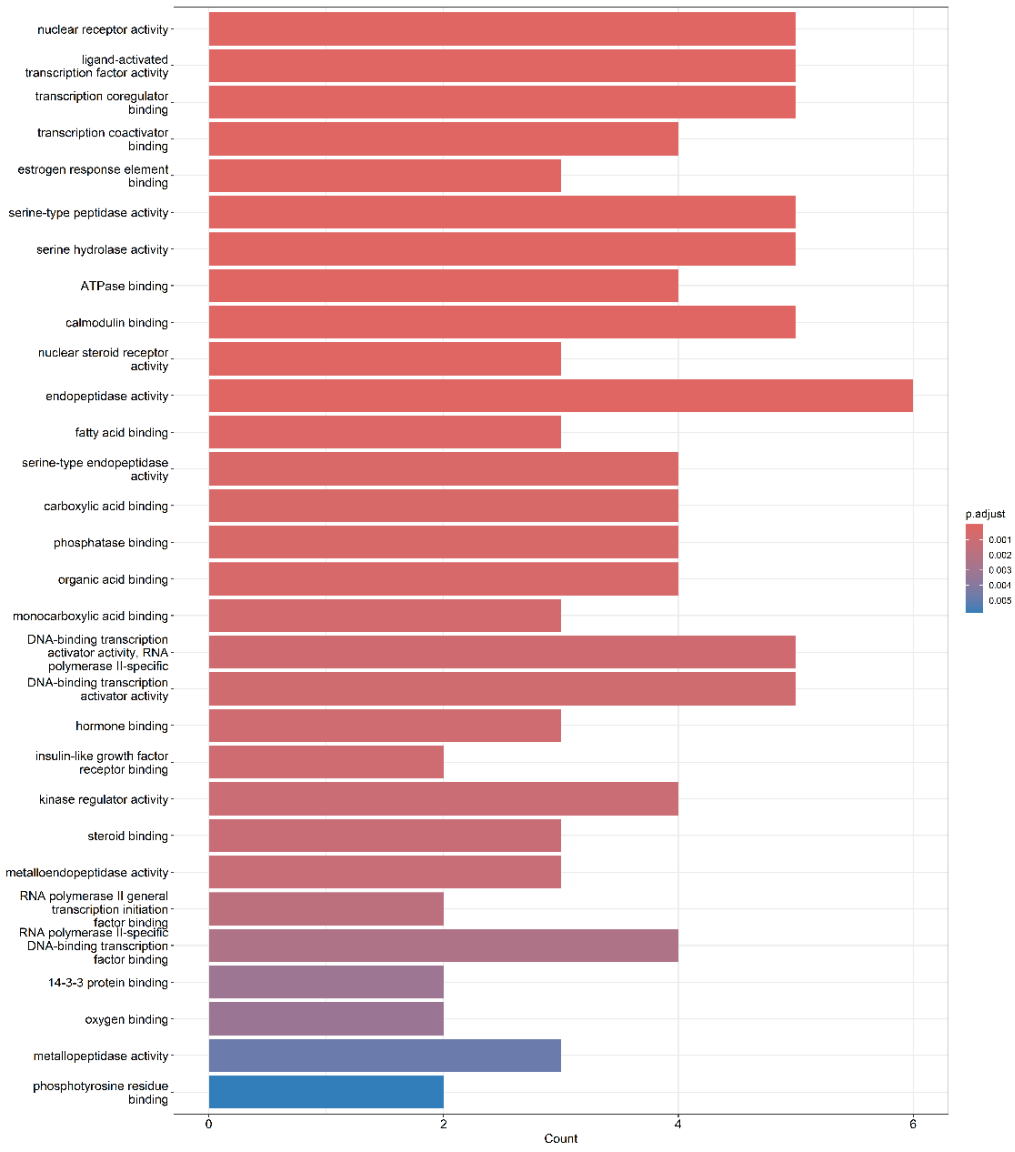

Figure 4.12: Gene Ontology (GO) enrichment analysis of molecular function terms associated with the target genes. The bar lengths represent the number of genes enriched in each GO category, while the color gradient reflects the adjusted p-values, indicating statistical significance.

Figure 4.13: Bubble plot of GO enrichment analysis for molecular function terms. The y-axis lists significantly enriched GO terms, while the x-axis shows the gene ratio (the proportion of input genes associated with each term). Bubble size indicates the number of genes and color reflects the adjusted p-value, with darker red indicating higher statistical significance.

4.11.5 KEGG Analysis from Sinensetin, Eupatorin, and TMF

Analysis of enrichment of the KEGG paths reveals a number of biologically important pathways that might be involved in the antihypertensive property of the following compounds that are under investigation. It is worth mentioning that the lipid and atherosclerosis are cardiovascular-related pathways, diabetic cardiomyopathy, and the relaxin signaling pathway are directly linked to the cardiovascular functions and vascular tone regulation. Such pathways as the relaxin one, in particular, are already known to promote vasodilation and ensure better endothelial performance by controlling the levels of NO, and endothelin. Equally, the enrichment of the hypoxia-inducible factor 1 **(**HIF-1) signaling and TNF signaling pathways indicates that the compounds might cause alterations in vascular remodelling and inflammation that is closely related to the hypertension pathophysiology. The emergence of the estrogen signaling pathway also contributes towards the presence of hormonal regulation in vascular protection as estrogen is a vasodilator. Also, the platelet activation pathway is enriched, which means that it may affect endothelial integrity and thrombotic risk which is often increased in hypertensive conditions. Even though a variety of cancer related pathways are also enriched, it is possible that because they overlap on molecular targets associated with oxidative stress, calcium signaling, or angiogenesis, which are applicable to blood pressure regulation. All in all it can be proposed that the compounds of interest can have antihypertensive effects via

multifaceted actions that include: endothelial (function), inflammatory, lipid metabolic, and vascular remodeling (Figure 4.14). These signaling pathways somewhat illuminate the dot plot that may form the basis of the antihypertenses action of compounds being investigated. The cardiovascular-related pathways including lipid and atherosclerosis, diabetic cardiomyopathy, fluid shear stress and atherosclerosis, and relaxin signaling are particularly highly enriched, with all associated with the mechanistic pathways of the vascular functionality, endothelial integrity, and blood pressure. As an example, the relaxin signaling pathway has been known to increase the bioavailability of nitric oxide and vasodilation, whereas pathways associated with atherosclerosis highlight the contribution of inflammation in the vascular/vessel as well as the lipid metabolism to hypertension. The increase in the TNF and HIF-1 signaling pathways also promotes the anti-inflammatory and angiogenic roles that are fundamental in controlling the vascular resistance. There is also the estrogen signaling pathway, which has a large gene ratio and count, which is an indication of a hormonal regulating mechanism which is specifically applicable to sex-based differences in blood pressure. Although the cancer-related pathways are predominant, numerous have overlapping targets in oxidative stress, receptor signaling (e.g., VEGF, PI3K), and calcium homeostasis -mechanisms that are central to tumorigenesis and to hypertension (Figure 4.15).

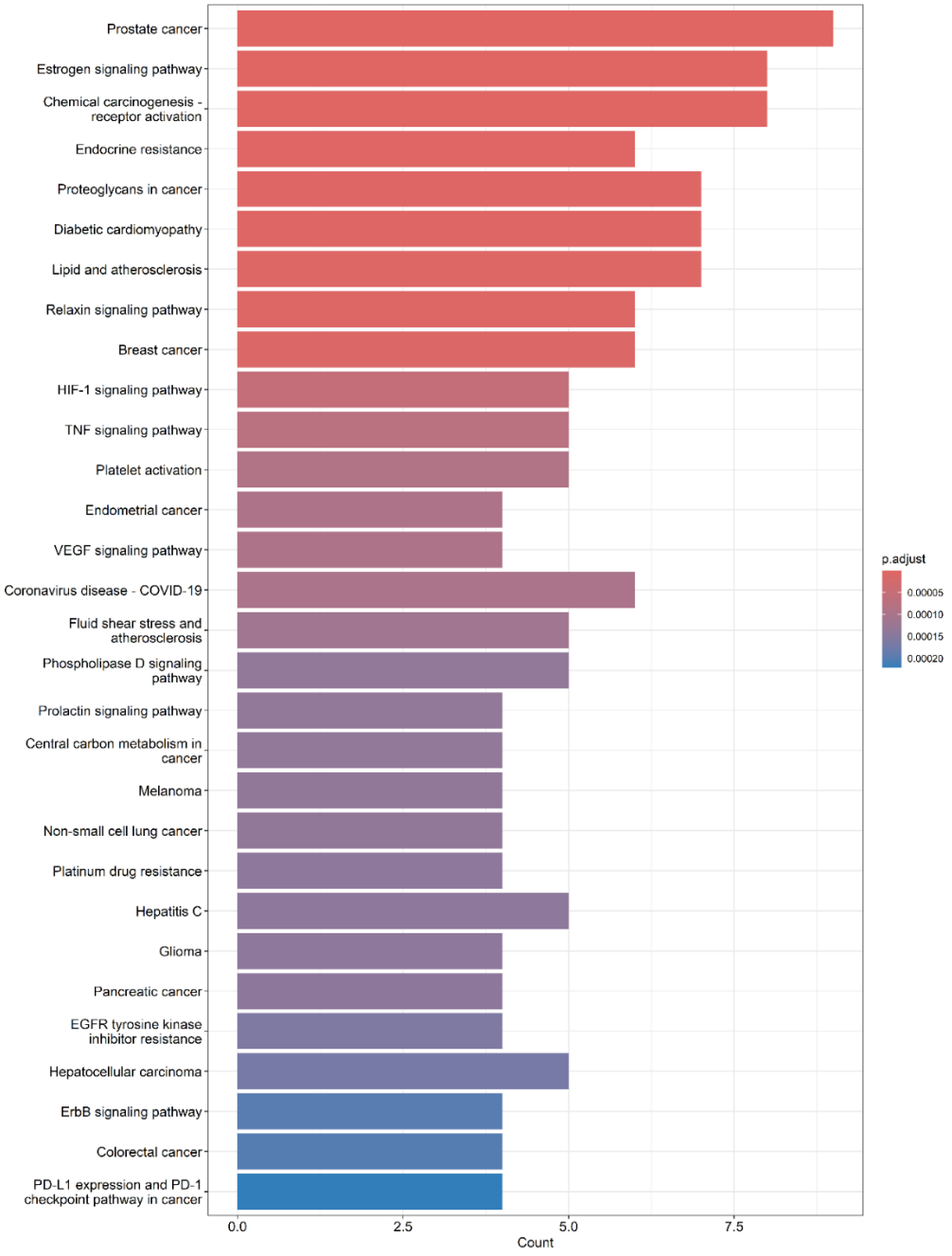

Figure 4.14: Bar chart of KEGG pathway enrichment analysis, showing the biological pathways significantly associated with a set of target genes—likely those modulated by sinensetin, eupatorin, and TMF.

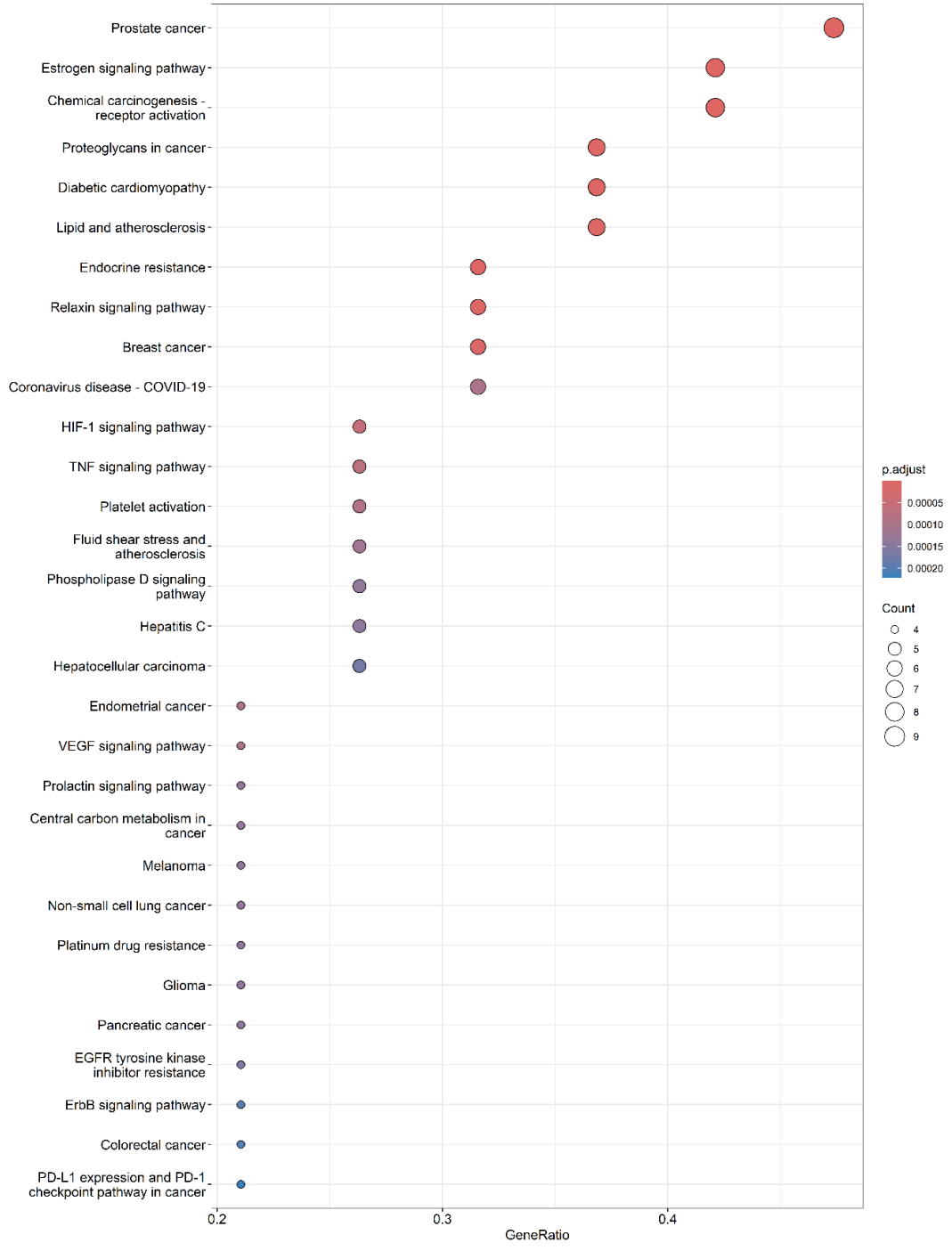

Figure 4.15: **Bubble plot of KEGG pathway enrichment analysis, specifically visualizing the biological pathways most significantly associated with a set of target genes—likely modulated by flavonoids such as sinensetin, eupatorin, and TMF.**

CHAPTER 5

DISCUSSION

A large paradigm shift in modern medicine can be explained by an active preference to use combination therapy, which is largely conditioned by the complexity of diseases and restrictions of the paradigm of single-compound, single-target (Loh *et al.*, 2018b). As a result, an in-depth insight into drug interactions will be critical in streamlining the use of drugs. Non-linear interactions between chemicals refer to the situation where aggregate effects of several substances are identical to their individual effects. These interactions are mainly in form of synergies or antagonises. When the cumulative activity is greater than the predicted or expected cumulative activity, this represents a synergistic interaction whereas when the cumulative activity is less than was expected, this is antagonistic interaction (Pezzani *et al.*, 2019; Twarog, Connelly and Shelat, 2020).

The orthogonal stimulus response compatibility design has been shown to have a few serious strengths in the case of evaluating complicated interactions between multiple substances at different concentrations. This design offered an effective, rational, and scientifically sound framework in the current study of the potential synergistic effects of sinensetin, eupatorin, and TMF on the vasodilatory

properties. Its main benefit is the ability to minimize the work load of experiments. The L36 orthogonal array would have been inefficient in terms of the number of compounds tested but it is clear that all the most significant interactions could be studied with only 36 experimental groups, a saving of 83 per cent when compared to using a full factorial design of three compounds with six concentrations. This not only conserved resources and time and lab animals, but also followed ethical research principles that are in line with the 3Rs (Reduction, Replacement, and Refinement).

Furthermore, the orthogonal design guarantees that the concentrations of all the compounds are balanced and represented separately in the experimental matrix without redundancy. This design enhances the chances of finding synergistic and antagonistic effect in lower sub-maximal concentrations (EC_5–EC_{25}), such that mixture effects are less pronounced as compared to a high dose model. With the actual effect of vasodilation compared with what could theoretically be predicted, it was even possible to ascertain which formulations can produce more or less effect than their individual actions. The design of the study additionally allowed the easy statistical analysis of the study, which could clearly interpret the data and provide high-quality measures of efficacy of each studied group. The other merit of the orthogonal design is that it is flexible and scalable. It is also easy to add more conditions or levels of concentration in case the future research needs to be increased.

Another advantage of the orthogonal design is its flexibility and scalability. It can easily include additional factors or concentration levels if future studies require expansion. This may provide a sustainable framework for broader investigation for future. Overall, the use of orthogonal stimulus-response design supported not only scientific precision and experimental efficiency but also ethical and environmental sustainability by optimizing resource usage.

This analysis used the orthogonal stimulus-responses compatibility approach to build a robust framework for studying the synergism between sinensetin, eupatorin, and TMF. Each compound's six effective concentration (EC) values were chosen for the orthogonal stimulus-response compatibility studies. The findings revealed that G2 demonstrated the highest efficacy (190%) of vasodilation in a rat aortic model. Interestingly, the absence of sinensetin in the vasodilatory actions of G2 indicates that the pronounced vasodilatory effects were exclusively attributed to the synergistic action of eupatorin and TMF at their respective EC_5 concentrations. Likewise, G7 demonstrated a vasodilatory efficacy surpassing 100% through the synergistic actions of TMF and sinensetin at respective EC_5 concentrations. This observation underscores that TMF at a concentration of 64 µg/mL synergistically interacts with 114 µg/mL of eupatorin or 54 µg/mL of sinensetin, resulting in a significantly enhanced vasodilatory impact beyond the anticipated level. The G27 and G28 elicited vasodilatory efficacy over 100%, however, their levels are significantly lower than those of

G2. This signifies that the different ratio of sinensetin, eupatorin, and TMF in G27 and G28 demonstrate diminished synergistic interaction compared to G2.

The quest to achieve the best ratio of combination in formulations is crucial in many fields of operation particularly in the pharmaceutical industry. This process aims to optimise the efficacy hence will ensure that formulation attains its optimum potential, a requirement in drug development, medical therapeutics and therapeutic interventions (Kofi-Tsekpo, 1994). The ratios of the optimum combination were computed in relying on the mean relaxation value based on orthogonal stimulus response compatibility research. It is worth noting that the ratios of F1 and G34 were alike. Both F1 and G34 showed a close approximability of the actual relaxation values of the anticipated values and along with almost 100% efficacy. This observation indicates the ratios of sinensetin, eupatorin, and TMF in these groups had an additive and not a synergistic effect. Conversely, F2 and F3 had actual relaxation values that were lower than the anticipated ones, which means that they had antagonistic interactions (Yin *et al.*, 2014).

An experiment of graded concentration-response was used to examine the vasodilatory action of G2, G7, G27, G28, and F1 on thoracic aorta of rats. Interestingly, G2 and G7 had high effects in the orthogonal stimulus response compatibility study but with lowest effects vasodilatory effect in this concentration response vasodilatory study. This low anticipated vasodilation

(10%) is a probable explanation of the insignificant effect, despite higher levels. On the other hand, G28 had the highest vasodilatory effect at all the concentrations. This phenomenon indicates that sinensetin is essential for inducing vasodilation in a concentration-dependent manner. The absence of G2, without sinensetin, may have reduced its effectiveness across concentration. The concentration-response study may have revealed the optimal concentration for G28, resulting a stronger effect. Repeated exposure might also make receptors more sensitive, and G28 may counteract receptor regulatory mechanisms that arise from extended or recurrent exposure to these compounds. This finding highlighted the complex nature of compound interactions in vascular tissues and the importance of using different research methods for fully understand their effects.

Sinensetin, eupatorin, and TMF have demonstrated substantial vasodilatory effects in a range of 1.25 to 40 µg/mL (Yam *et al.*, 2016b; Tan and Yam, 2018; Yam, Tan and Shibao, 2018). This study further explored the synergistic effects of these three compounds on vasodilation within a defined concentration range. The G28 formulation demonstrated a concentration-dependent vasodilatory response, achieving maximum relaxation (R_{MAX}) of 119.05±3.29%. The effects was slightly stronger than those demonstrated by individual compounds (with R_{MAX} values of 108±9.83% for sinensetin, 99.72±6.39% for eupatorin, and 98.78±8.13% for TMF) (Yam *et al.*, 2016b; Tan and Yam, 2018; Yam, Tan and Shibao, 2018) within the comparable concentration range of 1.25 to 40 µg/mL.

This synergistic action was notably pronounced at specific concentration levels, emphasizing their cooperative vasodilatory actions nuanced and concentration-dependent nature.

Previous research has revealed that the chloroform fraction of *Orthosiphon stamineus* displays significant vasodilatory effects in rat's aortic rings model (Yam *et al.*, 2016a). This preliminary investigation led to a subsequent focus on the three key components within the chloroform fraction: sinensetin, eupatorin, and TMF, each demonstrating potent vasodilatory properties (Yam *et al.*, 2016b; Tan and Yam, 2018; Yam, Tan and Shibao, 2018). Intriguingly, the chloroform fraction's vasodilatory activity surpassed its principal components' combined effects. The results of the initial studies inspired a multifaceted orthogonal experimental study of synergistic relations between the three main components, which led to the discovery of compound G28 (Yam *et al.*, 2024). Although every constituent has its own vasodilatory effects, G28 seems to have a different mechanism and its mechanism should be studied further in terms of its mechanics.

Vasodilation is a complex physiological process that is regulated by a variety of different mechanisms that encompass endothelium, vascular smooth muscle cells, and various receptor systems. Such mechanisms are typically divided into endothelium-dependent and endothelium-independent (Yam *et al.*, 2016b). The current paper has shown that G28 produces a significant vasodilatory action on intact endothelium, aortic rings of Sprague-Dawley and spontaneously

hypertensive rats pre-contracted with phenylephrine. The evidence shows that the effect of the G28 induced vasodilation was significantly reduced, but not eliminated, in response to endothelial denudation or pre-contraction with potassium chloride. These findings indicate G28 to mediate and cause vasodilation by acting on a number of mechanistic pathways, involving endothelium-dependent and endothelium-independent processes.

The endothelial layer, which is the inner coating of vascular tissue, is centrally involved in the vasodilatory process through the discharge of the EDRFs, such as NO, PGI_2, and EDHFs (Kang, 2014). Among them, NO is the main vasodilator in conduit arteries, thus, acting as the main mediator of VSMCs relaxation. Endothelial eNOS forms NO out of its precursor L arginine. After the synthesis, NO spreads to neighboring VSMCs where it opens sGC, thus elevating the levels of cGMP. This signal transduction pathway then triggers PKG that enhances the action of MLCP which eventually causes the relaxation of the vasoreceptor (Liu, Xu and Cheng, 2008; Yamamoto, Suzuki and Hase, 2008).

This study elucidates the role of the NO/sGC/cGMP signaling pathway in G28-induced vasodilation in the aortic ring of both SD rats and SHRs. This finding is consistent with a previous study that demonstrating the ability of the chloroform fraction of *O. stamineus* extracts enhances NO production and activates its downstream signaling pathway (Yam *et al.*, 2016a). Interestingly, G28-induced vasodilatory response in aortic rings of spontaneously hypertensive rats (SHRs)

showed a different pattern compared to the response in Sprague -Dawley (SD) rats mediating through the nitric-oxide/sGC/ cGMP signaling pathway. Chronic hypertension is often linked to endothelial dysfunction and diminished nitric-oxide synthesis that leads to the compensatory responses of increased enzyme or receptor activity to maintain the vascular homeostasis (Bernatova *et al.*, 2009; Bernatova, 2014). NO is responsible in regulation of vascular tone by activating the sGC that can be found in the vascular smooth muscle (Chen, Pittman and Popel, 2008). Most NO synthesis takes place in the endothelium and is catalysed by eNOS, which activates its calmodulin-binding domain when cytosolic Ca^{2+} levels rise (Forstermann and Sessa, 2012). L-arginine is then converted by eNOS into NO when activated. This is one of the major pathway of NO through which vasodilation occurs, operating by subsequent activation of cGMP-dependent pathways downstream of soluble guanylyl cyclase, which in turn activates the protein kinase G (PKG) that decreases intracellular calcium levels responsible for its vasodilatory effect. The compensatory mechanisms may explain the observed variations in responsiveness between SHRs and SD rats in this study.

The network pharmacological study showed that the relaxin signaling pathway plays a pivotal role in mediating vasodilation through multiple molecular targets, several of which were significantly upregulated in our dataset. Notably, the activation of the PI3K/AKT/eNOS constitutes a primary mechanism by which relaxin promotes endothelium-dependent vasorelaxation. Upon receptor binding, relaxin stimulates PI3K, which activates AKT, leading to phosphorylation and

activation of eNOS (Appendix 16). This causes amplified NO synthesis, which is an important mediator that can cause vasodilation via soluble guanylyl cyclase activation and subsequent elevation of cyclic levels of GMP to the vascular smooth-muscle cells (Dschietzig *et al.*, 2001; Conrad, 2010).

Furthermore, the microarray results indicated the upregulation of BRAF and ERK1/2 (MAPK1/3) in the MAPK signaling cascade as these proteins are known to regulate endothelial survival, as well as enhance the eNOS expression through transcriptional activation (Dschietzig *et al.*, 2001; Conrad, 2010; Ng *et al.*, 2019). These are also associated with the maintenance of vasodilatory action and vascular protection.

In addition, the significant increase in the expression of MMP2, MMP9, and MMP13 highlights the importance of relaxin in the remodeling of the vascular. These matrix metalloproteinases break down the extracellular matrix scaffolds including collagen, thus enhancing arterial compliance and decreasing vascular stiffness which is important determinants in the long run regulation of blood-pressure (Samuel *et al.*, 2019). The overexpression of these genes, as a whole, well substantiates the assumption that relaxin signaling facilitates acute and chronic vasodilation, so that the potential to apply relaxin signaling therapeutically in antihypertensive interventions is significant.

Besides the relaxin signaling pathway, network-pharmacological outcomes also depicted that fluid shear stress and the atherosclerosis pathway also mediate the effect of vasodilatory effect mainly via the NO signaling cascade (Appendix 17). In laminar shear stress conditions, eNOS can be activated by endothelial cells via multiple upstream pathways, in particular, the PI3K/Akt and AMPK signaling modules. This causes phosphorylation and activation of eNOS, which causes the increase of NO production (Boo and Jo, 2003; Li, Haga and Chien, 2005). An action of NO is that it enters adjacent vascular smooth-muscle cells and activates soluble guanylyl cyclase, rises the concentration of cyclic GMP (cGMP), and leads to smooth-muscle relaxation, which eventually results in dilation of vessels and a drop in blood-pressure (Förstermann and Sessa, 2012). In addition to its vasodilatory activity, NO has anti-inflammatory and anti- thrombotic properties and inhibits platelet aggregation and adherence of leukocytes to the endothelium, which are usually enhanced during hypertension (Förstermann and Sessa, 2012). eNOS and its upstream pathological regulators, including PI3K and Akt are indicated to be increased in the KEGG map (Appendix 17), so the compounds of interest have a possibility to increase the NO bioavailability and endothelial activity. In addition to that, NO aids with oxidative balance by decreasing the reactive oxygen species, and indirectly promotes antioxidant defense via cross-talk with the Nrf2 pathway. Therefore, it is important to note that, temporary alterations of NO pathway: especially by means of activation of eNOS, is a vital pathway of regulation of vascular tone, and is one of the primary therapeutically targets in hypertension.

The other network-pharmacology outcome showed existence of the lipid and atherosclerosis pathway, and presented a network of molecular processes directly connected to vasodilation, dysfunctioning of the endothelium, and vasodilation activating of the smooth-muscle-cell. One of the characteristics is the release of the PI3K/Akt signaling pathway that is stimulated in the KEGG map (Appendix 18), supporting the vascular tone preservation through the activation of eNOS and NO generation, which are essential in the prevention of vasoconstriction and in preserving the tone of the vasculature (Förstermann and Sessa, 2012).

The synthetic production of Prostacyclin (PGI_2), which is another widely known endothelial-derived relaxing factor, is an endothelial cell-based synthesis derived through the enzymes of the synthesis of arachidonic acid to PGI_2 mediated by COX and PGI_2 synthase. After synthesis, the PGI_2 is released through the endothelium binding to the IP receptor on the smooth-muscle-cell membrane. Tumblr activation of the IP receptor leads to a downstream signaling pathway, which involves adenylyl cyclase, cAMP and protein kinase A. The consequence of this cascade is the inhibition of MLCK, which prevents vasoconstriction (Berumen *et al.*, 2012; Kang, 2014). The effective attenuation of vasodilatory effects upon COX inhibition in the aorta of SD rats implies that G28 elicits PGI_2 production, triggering the AC/cAMP/PKA signaling cascade. This experimental observation, in concordance with prior investigations, substantiates the capability of the chloroform fraction of *O. stamineus* extract to enhance PGI_2 production

and induce vasodilation. This significant inhibitory effect was not observed in aortic ring of SHRs. Other studies have demonstrated that SHRs secrete more PGI_2 (Uehara *et al.*, 1987; Osanai *et al.*, 1990), which could be the cause of the elevated baseline PGI_2 levels and one of the reasons of the attenuated inhibitory effects in this group.

In addition to the EDRFs, GPCRs are also crucial in regulating the vasodilation. The AC/cAMP/PKA signaling cascade may be triggered through endothelium independent mechanisms. A Gs2 -adrenergic receptor (a Gs2 -protein-coupled receptor present in vascular smooth muscle cells) is analogous to IP receptors because it sources the AC/cAMP/PKA pathway during activation (Loh *et al.*, 2018a). Moreover, muscarinic acetylcholine receptors (and M3 in particular) found in endothelium and VSMCs, play a role in the multifaceted control of vascular tone, which is a cholinergic receptor that causes vasodilation by releasing PLC and its subsequent signalling cascades (Ishii and Kurachi, 2006; Baltoumas, Theodoropoulou and Hamodrakas, 2013). In the current experiment, both propranol and atropine did not cause a notable inhibitory effect on vasodilation induced by G28 on aortic ring of SD rats. This finding is in contrast to other previous studies that suggested that the 2 -adrenergic receptors and muscarinic M3 receptors were involved in the vasodilatory action of chloroform extracts of *O. stamineus*, eupatorin, sinensetin and TMF (Yam *et al.*, 2016b; Tan and Yam, 2018; Yam, Tan and Shibao, 2018). These differences can be explained by the fact that the ratios or concentrations of eupatorin, sinensetin, and TMF

might also differ a bit and, therefore, affect the synergistic interactions and vasodilatory processes.

The current results indicate that the inhibitory action of atropine on aortic ring of SHRs does differ with SD rats. Activation of M3 receptors in VSMCs which seem to have an increased role in regulation of vascular tone under hypertensive conditions (Luscher and Vanhoutte, 1986; Saternos *et al.*, 2018), seems to explain the significant vasodilation induced by G28 in SHR aortic rings after the administration of atropine. In SHRs, endothelial dysfunction may impair the vasodilatory response mediated by M_3 receptors in the endothelium, thereby unmasking the typically subdued vasocontractile effect of M_3 receptors in VSMCs. In this study, atropine caused only a slight, statistically insignificant reduction in G28-induced vasodilation in the aortic ring of SD rats, suggesting that G28 may interact with M_3 receptors, but only to a limited degree. This interpretation is supported by previous research demonstrating that high concentration of Ach can cause vasoconstriction in the aorta of SHRs (Luscher and Vanhoutte, 1986).

In addition to EDRFs and GCPRs, channel-linked receptors also play an important role in regulating of vascular tone. Preliminary screening using aortic rings pre-contracted with KCl demonstrated that G28-induced vasodilation is partially mediated through activation of these receptors. Among them, potassium channels are particular important serving as key regulators of vascular tone.

Potassium channels, widely expressed ion channels, are crucial regulators of vascular tone and membrane potential in VSMCs. Four major types of potassium channels, which are: K_{Ca}, K_V, K_{ATP}, and K_{ir} are of significant concern to vascular tone regulation. The opening of K_V, K_{ATP}, and K_{Ca} channels leads to effluxion of K^+, resulting in membrane hyperpolarization, inhibiting the voltage-gated Ca^{2+}channels, weakening the entrance of Ca^{2+}, and causing vasodilation. K_{ir} channels are, in contrast, the only channels through which K^+ enters and causes repolarisation of the membrane potential. The large-conductance BKCa subtype is highly expressed in VSMCs and is opened by an increase in intracellular Ca^{2+}, protein PKA, or PKG the end result being vasodilation. The small intermediary conductance SSKCa channels, i.e. IKCa is expressed mostly in the vascular endothelium and mediate the indirect action of vasodilation changes on EDHF signaling and intracellular Ca^{2+} dynamics. They facilitate the translocation of K^+ across cell membranes, resulting in a hyperpolarising current that ultimately leads to vasodilation (Edwards and Weston, 1995; Jackson, 2000; Jackson, 2017; Loh *et al.*, 2018a). The current article shows that the four major spaces of K^+ channels play an active role in the vasodilatory impact of G28 in the aorta of SD rats and SHRs. These data are indicative that G28 can stimulate K^+ channels, leading to membrane hyperpolarization and the resulting vasodilation. The findings have been consistent with the literature that demonstrates the contribution of K_{Ca}, K_V, K_{ATP}, and K_{ir} channels to the vasodilatory effects of the chloroform fraction of the extracts of *O. stamineus* (Yam *et al.*, 2016a).

Calcium is a critical intracellular second messenger in the vascular smooth muscle cells (VSMCs), thus, acting as a key regulator of vascular tone, especially by regulating action potentials (Gorlach *et al.*, 2015). VSMCs changes in cytosolic Ca^{2+} concentrations are the key determinants of the contractile state of VSMCs. There are two pathways through which the calcium ions accumulate in the cytosol, through extracellular influx using VOCCs, or intracellular release using calcium stores through IP_3Rs (McFadzean and Gibson, 2002). Ca^{2+} increases in VSMCs in combination with calmodulin to create Ca^{2+}calmodulin complexes, which then stimulate MLCK. MLCK becomes phosphorylated and thus the formation of actin-myosin cross-bridges occurs, which is one of the crucial processes that occur during the contraction of muscle due to the cyclic interaction of myosin and actin and is known as the sliding filament theory (Hill-Eubanks *et al.*, 2011; Kuo and Ehrlich, 2015).

In VSMCs, extracellular KCl can cause depolarize the membrane and trigger L-type calcium channels, a subtype of VOCC, facilitating the influx of extracellular Ca^{2+} (Kuo and Ehrlich, 2015). The partially diminished vasodilatory effects of G28, noted when aortic rings were pre-contracted with KCl suggests, in part, the involvement of G28 with VOCC. The detrimental effect of G28 on VOCC was further verified in the experiment where aortic rings isolated from both SD rats and SHRs were subjected to the extracellular introduction of $CaCl_2$ under Ca^{2+}-free and high KCl conditions. This interpretation is corroborated by previous research that demonstrated the potent attenuation of the contractile effects of

$CaCl_2$ by chloroform fraction of *O. stamineus* extracts (Yam *et al.*, 2016a). The present study demonstrated a reduction in contractions in SD rats subjected to 10 mM of $CaCl_2$, however no reduction was noted in SHRs. Literature indicates similar expression levels of VOCCs in normotensive rats and SHRs (Fukuda *et al.*, 2014). However, another report emphasized enhanced VOCC activity in SHRs relative to normotensive rats (Yamada *et al.*, 1992). The subtle discrepancy observed in the 10 mM $CaCl_2$-induced contraction in the aorta of SD rats and SHRs may be ascribed to the enhanced activity of VOCCs in SHRs. Comprehensive investigations are required to comprehend the activity of VOCCs in SHRs fully.

As aforementioned, the intricate modulation of muscle contraction entails the release of intracellular Ca^{2+} from the sarcoplasmic reticulum (SR). In VSMCs, calcium release from the SR is mainly controlled by IP_3R. When PE activates of alpha-1 (α1) adrenergic receptors on the cell surface, it G_q-protein, hence activates an PLC to produce a signaling molecule known as inositol trisphosphate (IP_3), which subsequently travels to SR and binds to IP_3R to promote Ca^{2+} release from the SR store (Stansfield *et al.*, 2014). This cascade increases cytosolic Ca^{2+} in VSMCs and results in contraction. The current findings demonstrated the antagonistic effects of G28 on IP_3R. This observation was confirmed by finding that there was a significant decrease in PE-evoked contraction at both at 5 µg/mL and 20 µg/mL of G28 in the aorta of both SD rats and SHRs under Ca^{2+}-free circumstances substantiated this observation. The findings are in accordance with

the existing literature that has proven the vasodilatory action of the extracts of *O. stamineus* to mediate the intracellular release of Ca^{2+} (Manshor *et al.*, 2013; Yam *et al.*, 2016a). Interestingly, the PE-induced contraction in SHRs was significantly lower than that in SD rats, which was also reinforced by another study that found the acute PE-induced contraction to be consistently lower in SHRs (Fukuda *et al.*, 2014). The low contractile force in SHRs could explain the high level of inhibition at 1.25 µg/mL of G28 on PE-induced contraction, in contrast to the lack of substantial inhibition in SD rats' aorta. When the overall contractile force is reduced, even small changes can appear more pronounced compared to situations with higher maximum values.

The intrinsic strength of a vasodilator does not necessarily involve its efficacy as a strong antihypertensive agent in living creatures due to the multifactorial interaction of pharmacoking factors and the fluctuating physiological processes that are involved in the life of organisms.

A potent vasodilator is not always an effective antihypertensive agent *in vivo*, since its impact depends on pharmacokinetic behavior and the multifaceted physiological responses of the organism. Given that G28 has significant vasodilatory effects in the conduit arteries of both SD rats and SHRs, *in vivo* antihypertensive studies were solely performed in SHRs to ascertain their therapeutic impact. The *in vivo* studies showed statistically significant decrease in blood pressure in all groups of treatment after 21 days of oral intake. This

effect on blood pressure could be explained by possible simultaneous stimulation of several vasodilatory processes which are inherent to the G28 formulation. In addition to this, previous literature indicates that *O. stamineus* ethanolic extracts have a possible role in inhibiting angiotensin-converting enzyme (ACE), and thus in vasodilation (Shafaei *et al.*, 2016). Thus, the effect of G28 on blood-pressure reduction in SHRs can be attributed to the activation of multiple signalling pathways such as the effects of NO/sGC/cGMP axis and AC/cAMP/PKA pathway, as well as the regulation of potassium channels and inactivation of calcium channel functions. It is also reasonable to expect that the concerted efforts of these mechanisms are behind the strong antihypertensive effect of G28. However, more extensive studies are justified, which should explain the mechanisms of its antihypertensive effect.

CHAPTER 6

CONCLUSION

The studies identified substantial cooperative relationships between three flavonoids including sinensetin, eupatorin, and TMF in their ability to expand blood vessels. Rat aortic rings treated with G2 and G7 demonstrated superior vasodilatory outcomes as G2 caused the maximum relaxation reaching 190% among all samples tested. The studies established that eupatorin and TMF in G2 and TMF and sinensetin in G7 produced these synergistic effects when used at their individual EC_5 levels. Tests determined that formulation G28 represented the most effective formulation by showing a vasodilatory response which exceeded the effects of its component compounds based on concentration level. Experimental findings show that G28 contains potent synergistic properties from its components which indicate strong potential for therapeutic use in vascular conditions.

The studies showed that vasodilation caused by G28 utilizes two different pathways including mechanisms which require endothelial cells and those that do not. NO triggers venous smooth muscle relaxation through its activation of sGC which processes cGMP to achieve endothelium-dependent vasodilation. PGI_2 activate the AC to produce cyclic adenosine monophosphate cAMP that

works with PKA in a cascade which results in vasodilation. Endothelium-independent vasodilation affects multiple potassium channels such as K_{Ca} and K_V channels and K_{ATP} channels and K_{ir} channels while simultaneously blocking VOCCs. The muscle relaxation occurs when these actions lower intracellular calcium content inside cells. Laboratory research on live animals confirmed the clinical ability of G28 to serve as a therapeutic agent. A 21-day oral treatment of G28 to spontaneously hypertensive rats resulted in the reduction of systolic pressure combined with diminished levels of diastolic pressure and mean arterial pressure. G28 shows antihypertensive properties because it executes various vasodilatory actions while possibly disrupting ACE activity. The research demonstrates that G28 shows great potential as a phytopharmaceutical agent which targets multiple hypertension treatment points.

Limitation of the study

Although the current study has a strict design and implementation, the current study has a number of limitations that may be inherent and can guide further studies. Use of isolated thoracic aortic segments of Sprague Dawley and spontaneously hypertensive rats (SHRs) limits the application to translation. *Ex vivo* vasodilatory can be a poor model of *in vivo* phenomena, whereby metabolic, pharmacokinetic, and systemic effects have a major impact. Isolated rat aortic observations therefore ought to be cautiously applied to the entire animal or clinical conditions. There was a restriction in the concentration range as well. Using fixed EC values of sinensetin, eupatorin and TMF could have masked

other effective ratios. It is necessary to expand the concentration range as well as perform extensive dose response studies to define the best synergistic combinations.

More informative yet inconclusive evidence came about by mechanistic inquiries that relied predominantly on pharmacological inhibitors (e.g., L-NAME, ODQ, atropine, propranolol). The partial inhibition of vasodilation which is seen after endothelium ablation and potassium channels blockage indicates redundancy of the pathways. More definitive mechanistic understanding would be possible with the use of molecular biology techniques, e.g. silencing of genes or the use of knockout models. The focus on short-term, acute experimental models restricts the knowledge of long-term drug pharmacodynamics, receptor desensitization, and tolerance generation. The longitudinal exposure investigations are required to determine the long-term effectiveness and safety. In addition to it, the use of SHR models, though providing valuable information, may not be able to reproduce human pathophysiology fully.

The presentation of species-specific differences in receptor expression, enzyme activities and cardiovascular control needs to be approached cautiously and with a gradual transition to human-relevant models. Focus on large conduit arteries only (e.g. aorta) is even more restrictive on generalizability. Since smaller resistance arteries play a more direct role in blood-pressure regulation, future studies need to include mesenteric or coronary microvessels in order to obtain a

more comprehensive vascular evaluation. Lastly, a lack of pharmacokinetic data is a major gap. The careful evaluation of absorption, distribution, metabolism, and excretion (ADME) cannot be ignored as a tool of correlating pharmacodynamics observations with the results achieved *in vivo*. Overall, this study is important, as it significantly advances the effects of sinensetin, eupatorin, and TMF in vasodilation, despite these methodological inadequacies, which can be addressed to improve rendering the topic translationally relevant and therapeutically meaningful through extending concentration testing, molecular analyses, chronological studies, and incorporation of other models.

Future study

To eliminate the revealed limitations, the subsequent studies will combine the orthogonal stimulus response with cumulative dose response designs in order to provide the higher predictive validity and reliability. Pharmacokinetic-pharmacodynamics (PK-PD) modeling can be further used to enhance the transfer of experimental results to biologically useful conclusions. It should be encouraged to adopt wider animal models, such as a rabbit or a pig to facilitate the clinical application, because these models are more closely related to humans in terms of cardiovascular systems. Cross and species comparison of studies are also expected to enhance the rigor and extraneous validity of the results. It is necessary to increase the concentration ranges and ratios of various compounds in the test, to ensure that possible synergetic and antagonistic effects are accounted. The overall application of dose response matrices and use of the

highly sophisticated statistical models like response surface methodology (RSM) will facilitate identification of the best combinations of sinensetin, eupatorin and TMF in order to achieve more precise formulation design. Molecular and genetic methodologies and their application such as CRISPR/Cas9-mediated gene editing and knockout models have the potential to help to better understand and elucidate the underlying mechanism by distinguishing between primary and secondary signaling pathways.

A combination of these methods with pharmacological inhibitors can help improve our knowledge of what precise pathways are involved in the process of vasodilatory activity. Experiments of chronic exposure are mandatory in assessing long-term pharmacodynamic effects, desensitization of receptor, and tolerance. Determining both conduit and resistance arteries, including mesenteric or coronary microvessels will provide a better insight into vascular response. The relationship between systemic exposure and pharmacodynamic outcomes will be clarified by using pharmacokinetic research with methods like liquid chromatography-mass spectrometry (LC-MS) or radiolabeled tracers. The use of humanvascular tissues or engineered organ -on-a-chip systems could be used to close the gap between preclinical observation and clinical application, enhancing predictive validity. All these measures have the potential to enhance mechanistic insights, enhance formulation development, and help mechanistic sinensetin-, eupatorin-, and TMF-based vasodilatory therapies to reach the clinical realm.

REFERENCES

Adam, Y. *et al.* (2009) 'Diuretic properties of *Orthosiphon stamineus* Benth', *Journal of Ethnopharmacology*, 124(1), pp. 154-158. Available at: https://doi.org/10.1016/j.jep.2009.04.014

Ahmad, H. *et al.* (2023) 'Angiotensin-converting enzyme and hypertension: a systemic analysis of various ACE inhibitors, their side effects, and bioactive peptides as a putative therapy for hypertension', *Journal of the Renin-Angiotensin-Aldosterone System*, 21(2023) Available at: https://doi.org/10.1155/2023/7890188

Ahumada-Castro, U. *et al.* (2021) 'In the right place at the right time: regulation of cell metabolism by IP3R-mediated inter-organelle Ca^{2+} Fluxes.', *Frontiers in cell and Developmental Biology*, 9, p. 629522. Available at: https://doi.org/10.3389/fcell.2021.629522

Al-Makki, A. *et al.* (2022) 'Hypertension pharmacological treatment in adults: a world health organization guideline executive summary', *Hypertension* 79(1), pp. 293-301.

Amberger, J.S. and Hamosh, A. (2017) 'Searching online mendelian inheritance in man (OMIM): A knowledgebase of human genes and genetic phenotypes', *Current Protocols in Bioinformatics*, 58, pp. 1.2.1-1.2.12. Available at: https://doi.org/10.1002/cpbi.27

Baltoumas, F.A., Theodoropoulou, M.C. and Hamodrakas, S.J. (2013) 'Interactions of the alpha-subunits of heterotrimeric G-proteins with GPCRs, effectors and RGS proteins: a critical review and analysis of interacting surfaces, conformational shifts, structural diversity and electrostatic potentials', *Journal of Structural Biology*, 182(3), pp. 209-218. Available at: https://doi.org/10.1016/j.jsb.2013.03.004

Beghi, S. *et al.* (2022) 'Calcium signalling in heart and vessels: role of calmodulin and downstream calmodulin-dependent protein kinases', *International Journal of Molecular Sciences*,, 23(24), p. 16139. Available at: https://doi.org/10.3390/ijms232416139

Berenbaum, M.C. (1989) 'What is synergy?', *Pharmacological Reviews*, 41(2), pp. 93-141.

Bernatova, I. (2014) 'Endothelial dysfunction in experimental models of arterial hypertension: cause or consequence?', *BioMed Research International*, 2014, p. 598271. Available at: https://doi.org/10.1155/2014/598271

Bernatova, I. *et al.* (2009) 'Endothelial dysfunction in spontaneously hypertensive rats: focus on methodological aspects', *Journal of Hypertension*, 27(6), pp. S27-S31. Available at: https://doi.org/10.1097/01.hjh.0000358834.18311.fc

Berumen, L.C. *et al.* (2012) 'Serotonin receptors in hippocampus', *The Scientific World Journal*, 2012, p. 823493. Available at: https://doi.org/10.1100/2012/823493

Boo, Y.C. and Jo, H. (2003) 'Flow-dependent regulation of endothelial nitric oxide synthase: role of protein kinases', *American Journal of Physiology-Cell Physiology*, 285(3), pp. C499-508. Available at: https://doi.org/10.1152/ajpcell.00122.2003Boo

Brozovich, F.V. *et al.* (2016) 'Mechanisms of Vascular Smooth Muscle Contraction and the Basis for Pharmacologic Treatment of Smooth Muscle Disorders', *Pharmacological Reviews*, 68(2), pp. 476–532. Available at: https://doi.org/10.1124/pr.115.010652

Cai, M. *et al.* (2023) 'Network pharmacology and molecular docking predictions of the active compounds and mechanism of action of Huangkui capsule for the treatment of idiopathic membranous nephropathy', *Medicine* 102(37), p. e35214. Available at: https://doi.org/10.1097/MD.0000000000035214

Ch'ng, Y.S. *et al.* (2017) 'Vasorelaxant properties of *Vernonia amygdalina* ethanol extract and its possible mechanism', *Pharmaceutical Biology*, 55(5), pp. 2083-2094.

Ch'ng, Y.S. *et al.* (2018) 'Vasodilation and Antihypertensive Activities of *Swietenia macrophylla* (Mahogany) Seed Extract', *Journal of Medicinal Food*, 21(3), pp. 289-301.

Chen, K., Pittman, R.N. and Popel, A.S. (2008) 'Nitric oxide in the vasculature: where does it come from and where does it go? A quantitative perspective', *Antioxidants & Redox Signaling*, 10(7), pp. 1185–1198. Available at: https://doi.org/10.1089/ars.2007.1959

Cheung, H.T. and Terry, D.S. (1980) 'Effects of nocodazole, a new synthetic microtubule inhibitor, on movement and spreading of mouse peritoneal macrophages', *Cell Biology International Reports*, 4(12), pp. 1125-1129. Available at: https://doi.org/10.1016/0309-1651(80)90050-8

Chou, T.C. (2006) 'Theoretical basis, experimental design, and computerized simulation of synergism and antagonism in drug combination studies',

Pharmacological Reviews, 58(3), pp. 621-681. Available at: https://doi.org/10.1124/pr.58.3.10

Chou, T.C. (2010) 'Drug combination studies and their synergy quantification using the Chou-Talalay method', *Cancer Research*, 70(2), pp. 440-446. Available at: https://doi.org/10.1158/0008-5472

Chou, T.C. and Talalay, P. (1984) 'Quantitative analysis of dose-effect relationships: the combined effects of multiple drugs or enzyme inhibitors', *Advances in Enzyme Regulation*, 22, pp. 27-55. Available at: https://doi.org/10.1016/0065-2571(84)90007-4

Cicero, A.F. *et al.* (2012) 'Effect of a combined nutraceutical containing *Orthosiphon stamineus* effect on blood pressure and metabolic syndrome components in hypertensive dyslipidaemic patients: a randomized clinical trial', *Complementary Therapies in Clinical Practice*, 18(3), pp. 190-194. Available at: https://doi.org/10.1016/j.ctcp.2012.02.002

Collaboration, T.B.P.L.T.T. (2021) 'Pharmacological blood pressure lowering for primary and secondary prevention of cardiovascular disease across different levels of blood pressure: an individual
participant-level data meta-analysis', *Lancet*, 397(10288), p. 1884. Available at: https://doi.org/10.1016/S0140-6736(21)01069-2

Conrad, K.P. (2010) 'Unveiling the vasodilatory actions and mechanisms of relaxin', *Hypertension*, 56(1), pp. 2-9. Available at: https://doi.org/10.1161/HYPERTENSIONAHA.109.133926

Consortium, T.G.O. (2019) 'The Gene Ontology Resource: 20 years and still GOing strong', *Nucleic Acids Research*, 47(D1), pp. D330-D338. Available at: https://doi.org/10.1093/nar/gky1055

Cushnie, T.P. and Lamb, A.J. (2005) 'Antimicrobial activity of flavonoids', *International Journal of Antimicrobial Agents*, 26(5), pp. 343-356. Available at: https://doi.org/10.1016/j.ijantimicag.2005.09.002

Dolečková, I. *et al.* (2012) 'Antiproliferative and antiangiogenic effects of flavone eupatorin, an active constituent of chloroform extract of Orthosiphon stamineus leaves', *Fitoterapia*, 83(6), pp. 1000-1007. Available at: https://doi.org/10.1016/j.fitote.2012.06.002

Dschietzig, T. *et al.* (2001) 'The pregnancy hormone relaxin is a player in human heart failure', *The FASEB Journal*, 15(12), pp. 2187-2195. Available at: https://doi.org/10.1096/fj.01-0070com

Edwards, G. and Weston, A.H. (1995) 'Pharmacology of the potassium channel openers', *Cardiovascular Drugs and Therapy*, 9, pp. 185-193. Available at: https://doi.org/10.1007/BF00878465

Ekor, M. (2014) 'The growing use of herbal medicines: issues relating to adverse reactions and challenges in monitoring safety', *Frontiers in Pharmacology*, 4 Available at: https://doi.org/10.3389/fphar.2013.00177

Falzone, M.E. and MacKinnon, R. (2023) 'The mechanism of Gα q regulation of PLCβ3 -catalyzed PIP2 hydrolysis', *Proceedings of the National Academy of Sciences*, 120(48), p. e2315011120. Available at: https://doi.org/10.1073/pnas.2315011120

Félétou, M. (2009) 'Calcium - activated potassium channels and endothelial dysfunction: therapeutic options?', *British Journal of Pharmacology* 156(4), pp. 545–562. Available at: https://doi.org/10.1111/j.1476-5381.2009.00052.x

Feng, F. *et al.* (2023) 'Structural changes and anti-hepatocellular carcinoma activity of interferon-γ after interaction with sinensetin', *International Journal of Biological Macromolecules*, 253 Available at: https://doi.org/10.1016/j.ijbiomac.2023.126392

Forstermann, U. and Sessa, W.C. (2012) ' Nitric oxide synthases: Regulation and function', *European Heart Journal*, 33(7), pp. 829–837. Available at: https://doi.org/10.1093/eurheartj/ehr304

Förstermann, U. and Sessa, W.C. (2012) 'Nitric oxide synthases: regulation and function', *European Heart Journal*, 33(7), pp. 829-837. Available at: https://doi.org/10.1093/eurheartj/ehr304

Fukuda, T. *et al.* (2014) 'Attenuation of L-type Ca^{2+} channel expression and vasomotor response in the aorta with age in both Wistar-Kyoto and spontaneously hypertensive rats', *PLoS One*, 9(2), p. e88975. Available at: https://doi.org/10.1371/journal.pone.0088975

Gao, N. *et al.* (2013) 'Signaling through myosin light chain kinase in smooth muscles ', *Journal of Biological Chemistry*, 288(11), pp. 7596–7605. Available at: https://doi.org/10.1074/jbc.M112.427112

Gericke, A. *et al.* (2014) 'Role of the M_3 muscarinic ccetylcholine receptor subtype in murine ophthalmic arteries after endothelial removal', *Investigative Opthalmology & Visual Science*, 55(1), p. 625. Available at: https://doi.org/10.1167/iovs.13-13549

Gheibi, S. *et al.* (2018) 'Regulation of vascular tone homeostasis by NO and H2S: implications in hypertension', *Biochemical Pharmacology*, (149), pp. 42–59. Available at: https://doi.org/10.1016/j.bcp.2018.01.017

Golbeck, J. (2015) 'Chapter 21 - Analyzing networks', in J. Golbeck (ed.) *Introduction to Social Media Investigation*. USA: Syngress, pp. 221-235. doi: https://doi.org/10.1016/B978-0-12-801656-5.00021-4.

González-Cortazar, M. *et al.* (2022) 'Eupatorin and Salviandulin-A, with Antimicrobial and Anti-Inflammatory Effects from Salvia lavanduloides Kunth Leaves', *Plants*, 11(13), p. 1739. Available at: https://doi.org/10.3390/plants11131739

Gorlach, A. *et al.* (2015) 'Calcium and ROS: A mutual interplay', *Redox Biology*, 6, pp. 260-271. Available at: https://doi.org/10.1016/j.redox.2015.08.010

Guerrero-García, C. and Rubio-Guerra, F. (2018) 'Combination therapy in the treatment of hypertension', *Drugs in Context*, 7, pp. 1-9. Available at: https://doi.org/0.7573/dic.212531

Haddy, F.J., Vanhoutte, P.M. and Feletou, M. (2006) 'Role of potassium in regulating blood flow and blood pressure', *American Journal of Physiology-Regulatory, Integrative and Comparative Physiology* 290(3), pp. R546–R552. Available at: https://doi.org/10.1152/ajpregu.00491.2005

Hill-Eubanks, D.C. *et al.* (2011) 'Calcium signaling in smooth muscle', *Cold Spring Harbor Perspectives in Biology*, 3(9), pp. 1-20. Available at: https://doi.org/10.1101/cshperspect.a004549

Hossain, M.A. *et al.* (2012) 'Cytotoxic effects of polymethoxyflavones isolated from *Kaempferia parviflora*', *Journal of the Korean Society for Applied Biological Chemistry*, 55, pp. 471-476. Available at: https://doi.org/10.1007/s13765-012-2026-4

Huang, B. *et al.* (2020) 'Sinensetin flavone exhibits potent anticancer activity against drug-resistant human gallbladder adenocarcinoma cells by targeting PTEN/PI3K/AKT signalling pathway, induces cellular apoptosis and inhibits cell migration and invasion', *Journal of BUON*, 25(2), pp. 1251-1256.

Ishii, M. and Kurachi, Y. (2006) 'Muscarinic acetylcholine receptors', *Current Pharmaceutical Design*, 12(28), pp. 3573-3581. Available at: https://doi.org/10.2174/138161206778522056

Jackson, W.F. (2000) 'Ion channels and vascular tone', *Hypertension*, 35(1-2), pp. 173-178. Available at: https://doi.org/10.1161/01.hyp.35.1.173

Jackson, W.F. (2017) 'Potassium channels in regulation of vascular smooth muscle contraction and growth', in R. A. Khalil (ed.) *Vascular Pharmacology-Smooth Muscle, Vol. 78*. 20160817 edn. United State of America: Academic Press, pp. 89-144. doi: https://doi.org/10.1016/bs.apha.2016.07.001.

Jung, T. and Cheon, C. (2024) 'Synergistic and additive effects of herbal medicines in combination with chemotherapeutics: a scoping review', *Integrative Cancer Therapies*, 23 Available at: https://doi.org/10.1177/15347354241259416

Kamato, D. *et al.* (2015) 'Structure, function, pharmacology, and therapeutic potential of the G protein, $G\alpha/_{q,11}$', *Frontiers in Cardiovascular Medicine*, 2(4) Available at: https://doi.org/10.3389/fcvm.2015.00014

Kang, K.T. (2014) 'Endothelium-derived relaxing factors of small resistance arteries in hypertension', *Toxicological Research*, 30(3), pp. 141-148. Available at: https://doi.org/10.5487/TR.2014.30.3.141

Kang, S.I., Shin, H.S. and Kim, S.J. (2015) 'Sinensetin enhances adipogenesis and lipolysis by increasing cyclic adenosine monophosphate levels in 3T3-L1 adipocytes', *Biological and Pharmaceutical Bulletin*, 38(4), pp. 552-558. Available at: https://doi.org/10.1248/bpb.b14-00700

Kim, S. *et al.* (2020) 'Sinensetin induces autophagic cell death through p53-related AMPK/mTOR signaling in hepatocellular carcinoma HepG2 cells', *Nutrients*, 12(8), p. 2462. Available at: https://doi.org/10.3390/nu12082462

Kofi-Tsekpo, M.W. (1994) 'Optimization of pharmaceutical formulations for therapy', *African Journal of Health Sciences*, 1(1), pp. 13-19. Available at: https://www.ncbi.nlm.nih.gov/pubmed/12150638.

Kohl, M., Wiese, S. and Warscheid, B. (2011) 'Cytoscape: software for visualization and analysis of biological networks', in M. Hamacher, M. Eisenacher and C. Stephan (eds.) *Data Mining in Proteomics - Methods in Molecular Biology, Vol. 696*. USA: Humana Press, pp. 291-303. doi: https://doi.org/10.1007/978-1-60761-987-1_18.

Kong, Z. *et al.* (2023) 'Sinensetin ameliorates high glucose-induced diabetic nephropathy via enhancing autophagy *in vitro* and *in vivo*', *Journal of Biochemical and Molecular Toxicology*, 37(10), p. e23445. Available at: https://doi.org/10.1002/jbt.23445

Koon, C.M. *et al.* (2011) '*Salviae Miltiorrhizae* Radix and *Puerariae Lobatae* Radix herbal formula mediates anti-atherosclerosis by modulating key atherogenic events both in vascular smooth muscle cells and endothelial cells. ',

Journal of Ethnopharmacology, 138(1), pp. 175-183. Available at: https://doi.org/10.1016/j.jep.2011.08.073

Kuo, I.Y. and Ehrlich, B.E. (2015) 'Signaling in muscle contraction', *Cold Spring Harbor Perspectives in Biology*, 7(2), pp. 1-14. Available at: https://doi.org/10.1101/cshperspect.a006023

Lam, I.K. *et al.* (2012) 'In vitro and in vivo structure and activity relationship analysis of polymethoxylated flavonoids: identifying sinensetin as a novel antiangiogenesis agent', *Molecular Nutrition & Food Research*, 56(6), pp. 945-956. Available at: https://doi.org/10.1002/mnfr.201100680

Lee, H.J. *et al.* (2020) 'Sinensetin: An insight on its pharmacological activities, mechanisms of action and toxicity', *Frontiers in Pharmacology*, 11, pp. 1-16. Available at: https://doi.org/10.3389/fphar.2020.553404

Li, C. *et al.* (2022) 'Multi-compound and drug-combination pharmacokinetic research on Chinese herbal medicines', *Acta Pharmacologica Sinica* 43, pp. 3080–3095. Available at: https://doi.org/10.1038/s41401-022-00983-7

Li, L. *et al.* (2023a) 'Network pharmacology: a bright guiding light on the way to explore the personalized precise medication of traditional Chinese medicine', *Chinese Medicine*, 18(1), p. 146. Available at: https://doi.org/10.1186/s13020-023-00853-2

Li, R., Li, Q. and Ji, Q. (2019) 'Molecular targeted study in tumors: From western medicine to active ingredients of traditional Chinese medicine.', *Biomedicine and Pharmacotherapy*, 121, p. 109624. Available at: http://doi:10.1016/j.biopha.2019.109624

Li, Y. *et al.* (2023b) 'Natural flavonoid sinensetin inhibits cisplatin-induced pyroptosis and attenuates intestinal injury', *Biochimica et Biophysica Acta-Molecular Basis of Disease*, 1869(166637) Available at: https://doi.org/10.1016/j.bbadis.2023.166637

Li, Y.S., Haga, J.H. and Chien, S. (2005) 'Molecular basis of the effects of shear stress on vascular endothelial cells', *Journal of Biomechanics*, 38(10), pp. 1949-1971. Available at: https://doi.org/10.1016/j.jbiomech.2004.09.030

Lin, L. *et al.* (2023) 'Sinensetin attenuated macrophagic NLRP3 inflammasomes formation via SIRT1-NRF2 signaling', *ACS Omega*, 8(37), pp. 33514–33525. Available at: https://doi.org/10.1021/acsomega.3c03319

Liu, L., Xu, D.M. and Cheng, Y.Y. (2008) 'Distinct effects of naringenin and hesperetin on nitric oxide production from endothelial cells', *Journal of*

Agricultural and Food Chemistry, 56(3), pp. 824-829. Available at: https://doi.org/10.1021/jf0723007

Loh, Y.C. *et al.* (2021) 'Discovery of trans-3,4,4′ -trihydroxystilbene as new lead vasorelaxant agent for antihypertensive drug development', *Life Sciences*, 278, p. 119560.

Loh, Y.C. *et al.* (2022) 'The predominance of endothelium-derived relaxing factors and beta-adrenergic receptor pathways in strong vasorelaxation induced by 4-hydroxybenzaldehyde in the rat aorta', *Biomedicine & Pharmacotherapy*, 150, p. 112905.

Loh, Y.C. *et al.* (2017) 'Vasodilatory effects of combined traditional Chinese medicinal herbs in optimized ratio', *Journal of Medicinal Food*, 20(3), pp. 265-278. Available at: https://doi.org/10.1089/jmf.2016.3836

Loh, Y.C. *et al.* (2018a) 'Overview of the microenvironment of vasculature in vascular tone regulation', *International Journal of Molecular Sciences*, 19(1) Available at: https://doi.org/10.3390/ijms19010120

Loh, Y.C. *et al.* (2018b) 'Orthogonal stimulus-response as a tool to formulate traditional Chinese medicinal herbal combination', *Journal of Pharmacopuncture*, 21(3), pp. 203-206. Available at: https://doi.org/doi.org/10.3831/KPI.2018.21.024

Luscher, T.F. and Vanhoutte, P.M. (1986) 'Endothelium-dependent contractions to acetylcholine in the aorta of the spontaneously hypertensive rat', *Hypertension*, 8(4), pp. 344-348. Available at: https://doi.org/10.1161/01.hyp.8.4.344

Lyckander, I.M. and Malterud, K.E. (1996) 'Lipophilic flavonoids from Orthosiphon spicatus prevent oxidative inactivation of 15-lipoxygenase', *Prostaglandins, Leukotrienes and Essential Fatty Acids*, 54(4), pp. 239-246.

Majed, B.H. and Khalil, R.A. (2012) 'Molecular Mechanisms Regulating the Vascular Prostacyclin Pathways and Their Adaptation during Pregnancy and in the Newborn', *Pharmacological Reviews*, 64(3), pp. 540–582. Available at: https://doi.org/10.1124/pr.111.004770

Mancia, G. *et al.* (2019) 'Two-drug combinations as first-step antihypertensive treatment', *Circulation Research*, 124(7), pp. 1113–1123. Available at: https://doi.org/10.1161/CIRCRESAHA.118.313294

Manshor, N.M. *et al.* (2013) 'Vascular reactivity concerning *Orthosiphon stamineus* Benth-mediated antihypertensive in aortic rings of spontaneously

hypertensive rats', *International Journal of Vascular Medicine*, 2013, pp. 1-8. Available at: https://doi.org/10.1155/2013/456852

Martinsen, A., Dessy, C. and Morel, N. (2014) 'Regulation of calcium channels in smooth muscle: New insights into the role of myosin light chain kinase', *Channels*, 8(5), pp. 402–413. Available at: https://doi.org/10.4161/19336950.2014.950537

McFadzean, I. and Gibson, A. (2002) 'The developing relationship between receptor-operated and store-operated calcium channels in smooth muscle', *British Journal of Pharmacology*, 135(1), pp. 1-13. Available at: https://doi.org/10.1038/sj.bjp.0704468

Mitchell, J.A. *et al.* (2008) 'Role of nitric oxide and prostacyclin as vasoactive hormones released by the endothelium', *Experimental Physiology*, 93(1), pp. 141-147. Available at: https://doi.org/10.1113/expphysiol.2007.038588

Mohamed, E. *et al.* (2012) 'Potent α-glucosidase and α-amylase inhibitory activities of standardized 50% ethanolic extracts and sinensetin from Orthosiphon stamineus Benth as anti-diabetic mechanism', *BMC Complementary Medicine and Therapies*, 12(176) Available at: https://doi.org/10.1186/1472-6882-12-176

Nelson, M.T. and Quayle, J.M. (1995) 'Physiological roles and properties of potassium channels in arterial smooth muscle', *American Journal of Physiology-Cell Physiology*, 268(4), pp. C799–C822. Available at: https://doi.org/10.1152/ajpcell.1995.268.4.C799

Ng, H.H. *et al.* (2019) 'Relaxin and extracellular matrix remodeling: Mechanisms and signaling pathways', *Molecular and Cellular Endocrinology*, 487, pp. 59-65. Available at: https://doi.org/10.1016/j.mce.2019.01.015

Osanai, T. *et al.* (1990) 'Changes in vascular wall production of prostacyclin and thromboxane A2 in spontaneously hypertensive rats during maturation and the concomitant development of hypertension', *Japanese Circulation Journal*, 54(5), pp. 507-514. Available at: https://doi.org/10.1253/jcj.54.507

Pezzani, R. *et al.* (2019) 'Synergistic effects of plant derivatives and conventional chemotherapeutic agents: an update on the cancer perspective', *Medicina*, 55(4), pp. 1-16. Available at: https://doi.org/10.3390/medicina55040110

Razak, N.A. *et al.* (2019) 'Cytotoxicity of eupatorin in MCF-7 and MDA-MB-231 human breast cancer cells via cell cycle arrest, anti-angiogenesis and induction of apoptosis.', *Scientific Report*, 9(1514) Available at: https://doi.org/10.1038/s41598-018-37796-w.

Rizou, A.E.I. *et al.* (2023) 'A Multilevel Study of Eupatorin and Scutellarein as Anti-Amyloid Agents in Alzheimer's Disease', *Biomedicines*, 11(5) Available at: https://doi.org/10.3390/biomedicines11051357

Ruan, X. *et al.* (2020) 'Mechanism of dayuanyin in the treatment of coronavirus disease 2019 based on network pharmacology and molecular docking', *Chinese Medicine*, 15(62) Available at: https://doi.org/10.1186/s13020-020-00346-6

Ruchawapol, C., Fu, W.W. and Xu, H.X. (2022) 'A review on computational approaches that support the researches on traditional Chinese medicines (TCM) against COVID-19', *Phytomedicine*, 104, p. 154324. Available at: https://doi.org/10.1016/j.phymed.2022.154324

Samuel, C.S. *et al.* (2019) 'Anti-fibrotic actions of relaxin', *British Journal of Pharmacology*, 174(10), pp. 962-976. Available at: https://doi.org/10.1111/bph.13529

Sandoo, A. *et al.* (2010) 'The endothelium and its role in regulating vascular tone', *The Open Cardiovascular Medicine Journal*, 4(1), pp. 302–312. Available at: https://doi.org/10.2174/1874192401004010302

Saternos, H.C. *et al.* (2018) 'Distribution and function of the muscarinic receptor subtypes in the cardiovascular system', *Physiological Genomics*, 50(1), pp. 1-9. Available at: https://doi.org/10.1152/physiolgenomics.00062.2017

Shafaei, A. *et al.* (2016) 'Flavonoids-rich *Orthosiphon stamineus* extract as new candidate for angiotensin I-converting enzyme inhibition: A molecular docking study', *Molecules*, 21(11) Available at: https://doi.org/10.3390/molecules21111500

Shi, Z. *et al.* (2024) 'Sinensetin inhibits the movement ability and tumor immune microenvironment of non-small cell lung cancer through the inactivation of AKT/β-catenin axis', *Journal of Biochemical and Molecular Toxicology*, 38(11), p. e70024. Available at: https://doi.org/10.1002/jbt.70024

Sobey, C.G. (2001) 'Potassium channel function in vascular disease', *Arteriosclerosis, Thrombosis, and Vascular Biology*, 21(1), pp. 28–38. Available at: https://doi.org/10.1161/01.ATV.21.1.28

Spinella, M. (2002) 'The importance of pharmacological synergy in psychoactive herbal medicines', *Alternative Medicine Review*, 7(2), pp. 130-137.

Stansfield, W.E. *et al.* (2014) 'The pathophysiology of cardiac hypertrophy and heart failure', in M. S. Willis, J. W. Homeister and J. R. Stone (eds.) *Cellular and*

Molecular Pathobiology of Cardiovascular Disease. USA: Academic Press, pp. 51-78. doi: https://doi.org/10.1016/b978-0-12-405206-2.00004-1.

Sun, H.J. *et al.* (2020) 'Role of endothelial dysfunction in cardiovascular diseases: the link between inflammation and hydrogen sulfide', *Frontiers in Pharmacology*, 10(1568) Available at: https://doi.org/10.3389/fphar.2019.01568

Syrovatkina, V. *et al.* (2016) 'Regulation, Signaling, and Physiological Functions of G-Proteins', *Journal of Molecular Biology*, 428(19), pp. 3850–3868. Available at: https://doi.org/10.1016/j.jmb.2016.08.002

Tan, C.S. *et al.* (2017a) 'Vasorelaxation effect of *Glycyrrhizae uralensis* through the endothelium-dependent Pathway', *Journal of Ethnopharmacology*, 199, pp. 149-160.

Tan, C.S. *et al.* (2017b) 'Decomposition and reformulation of Banxia Baizhu Tianma decoction: a vasodilatory approach', *Chinese Herbal Medicines*, 9(2), pp. 134-146. Available at: https://doi.org/10.1016/s1674-6384(17)60087-x

Tan, C.S. *et al.* (2019) 'Vasorelaxant and chemical fingerprint studies of *Citrus reticulatae* pericarpium extracts', *Journal of Ethnopharmacology*, 232, pp. 135-144.

Tan, C.S. *et al.* (2021) 'Vasorelaxant effect of 5,7,4′ - Trihydroxyflavanone (Naringenin) via endothelium dependent, potassium and calcium channels in Sprague Dawley rats: Aortic ring model', *Chemico-Biological Interactions*, 348, p. 109620.

Tan, C.S. and Yam, M.F. (2018) 'Mechanism of vasorelaxation induced by 3'-hydroxy-5,6,7,4'-tetramethoxyflavone in the rats aortic ring assay', *Naunyn-Schmiedeberg's Archives of Pharmacology*, 391(6), pp. 561-569. Available at: https://doi.org/10.1007/s00210-018-1481-9

Tang, J., Wennerberg, K. and Aittokallio, T. (2015) 'What is synergy? The Saariselkä agreement revisited', *Frontiers in Pharmacology*, 6(181) Available at: https://doi.org/10.3389/fphar.2015.00181

Tangsucharit, P. *et al.* (2016) 'Muscarinic acetylcholine receptor M1 and M3 subtypes mediate acetylcholine-induced endothelium-independent vasodilatation in rat mesenteric arteries ', *Journal of Pharmacological Sciences*, 130(1), pp. 24–32. Available at: https://doi.org/10.1016/j.jphs.2015.12.005

Tarkin, J.M. and Kaski, J.C. (2016) 'Vasodilator therapy: nitrates and nicorandil', *Cardiovascular Drugs and Therapy*, 30(4), pp. 367–378.

Tew, W.Y. *et al.* (2020) 'Underlying mechanism of vasorelaxant effect exerted by 3,5,7,2′ ,4′ -pentahydroxyflavone in rats aortic ring', *European Journal of Pharmacology*, 880, p. 173123.

Tew, W.Y. *et al.* (2023) 'Evaluation of vasodilatory effect and antihypertensive effect of chrysin through *in vitro* and sub-chronic *in vivo* study ', *Biomedicine & Pharmacotherapy* 157, p. 114020.

Triggle, C.R. *et al.* (2012) 'The endothelium: Influencing vascular smooth muscle in many ways.', *Canadian Journal of Physiology and Pharmacology*, 90(6), pp. 713–738. Available at: https://doi.org/10.1139/y2012-073

Trimarco, V. *et al.* (2012) 'Nutraceuticals for blood pressure control in patients with high-normal or grade 1 hypertension', *High Blood Pressure & Cardiovascular Prevention*, 19(3), pp. 117-122. Available at: https://doi.org/10.2165/11632160-000000000-00000

Twarog, N.R., Connelly, M. and Shelat, A.A. (2020) 'A critical evaluation of methods to interpret drug combinations', *Scientific Reports*, 10(1), p. 5144. Available at: https://doi.org/10.1038/s41598-020-61923-1

Uehara, Y. *et al.* (1987) 'Prostacyclin synthase and phospholipases in the vascular wall of experimental hypertensive rats', *Prostaglandins*, 34(3), pp. 423-442. Available at: https://doi.org/10.1016/0090-6980(87)90087-6

Ushio-Fukai, M. (2009) 'Vascular signaling through G protein-coupled receptors: new concepts', *Current Opinion in Nephrology and Hypertension*, 18(2), pp. 153–159. Available at: https://doi.org/10.1097/MNH.0b013e3283252efe

Vikram, A. *et al.* (2010) 'Suppression of bacterial cell-cell signalling, biofilm formation and type III secretion system by citrus flavonoids', *Journal of Applied Microbiology*, 109(2), pp. 515-527. Available at: https://doi.org/10.1111/j.1365-2672.2010.04677.x

Wang, H. *et al.* (2023) 'Advancing herbal medicine: enhancing product quality and safety through robust quality control practices', *Frontiers in Pharmacology*, 14(1265178) Available at: https://doi.org/10.3389/fphar.2023.1265178

Xiong, X. *et al.* (2013a) 'Trends in the treatment of hypertension from the perspective of traditional Chinese medicine', *Evidence-Based Complementary and Alternative Medicine*, Available at: https://doi.org/10.1155/2013/275279

Xiong, X. *et al.* (2013b) ' Chinese herbal formulas for treating hypertension in traditional Chinese medicine: perspective of modern science', *Hypertension Research*, 36, pp. 570-579.

Yam, M.F. *et al.* (2016a) 'Vasorelaxant action of the chloroform fraction of *Orthosiphon stamineus* via NO/cGMP pathway, potassium and calcium channels', *The American Journal of Chinese Medicine*, 44(7), pp. 1413-1439. Available at: https://doi.org/10.1142/S0192415X16500798

Yam, M.F. *et al.* (2016b) 'Mechanism of vasorelaxation induced by eupatorin in the rats aortic ring', *European Journal of Pharmacology*, 789, pp. 27-36. Available at: https://doi.org/10.1016/j.ejphar.2016.06.047

Yam, M.F., Tan, C.S. and Shibao, R. (2018) 'Vasorelaxant effect of sinensetin via the NO/sGC/cGMP pathway and potassium and calcium channels', *Hypertension Research*, 41(10), pp. 787-797. Available at: https://doi.org/10.1038/s41440-018-0083-8

Yam, M.F. *et al.* (2024) 'Investigation of synergistic interaction of sinensetin, eupatorin, and 3′ -hydroxy-5,6,7,4′ -tetramethoxyflavone in vasodilation efficacy', *Hypertension Research*, Available at: https://doi.org/10.1038/s41440-024-01907-0

Yamada, K. *et al.* (1992) 'Alterations of calcium channels in vascular smooth muscle cells from spontaneously hypertensive rats', *Japanese Heart Journal*, 33(5), pp. 727-734. Available at: https://doi.org/10.1536/ihj.33.727

Yamamoto, M., Suzuki, A. and Hase, T. (2008) 'Short-term effects of glucosyl hesperidin and hesperetin on blood pressure and vascular endothelial function in spontaneously hypertensive rats', *Journal of Nutritional Science and Vitaminology*, 54(1), pp. 95-98. Available at: https://doi.org/10.3177/jnsv.54.95

Yin, N. *et al.* (2014) 'Synergistic and antagonistic drug combinations depend on network topology', *PLoS One*, 9(4), p. e93960. Available at: https://doi.org/10.1371/journal.pone.0093960

Zhang, G.B. *et al.* (2013) 'Network pharmacology: a new approach for chinese herbal medicine research', *Evidence-Based Complementary and Alternative Medicine*, 2013, p. 621423. Available at: https://doi.org/10.1155/2013/621423

Zhang, X.T. *et al.* (2024a) 'Screening of active components of *Ganoderma lucidum* and decipher its molecular mechanism to improve learning and memory disorders', *Bioscience Reports*, 44(7), p. BSR20232068. Available at: https://doi.org/10.1042/BSR20232068

Zhang, Z. *et al.* (2024b) 'Integration of traditional, complementary, and alternative medicine with modern biomedicine: the scientization, evidence, and challenges for integration of traditional Chinese medicine', *Acupuncture and Herbal Medicine*, 4(4), pp. 68-78. Available at: https://doi.org/10.1097/HM9.0000000000000089

Zhou, X. *et al.* (2016) 'Synergistic Effects of Chinese Herbal Medicine: A Comprehensive Review of Methodology and Current Research', *Frontiers in Pharmacology*, 7(201) Available at: https://doi.org/10.3389/fphar.2016.00201

Zhou, Z. *et al.* (2020) 'Applications of network pharmacology in Traditional Chinese Medicine research', *Evidence-Based Complementary and Alternative Medicine*, 2020, p. 1646905. Available at: https://doi.org/10.1155/2020/1646905

Zsolnay, V., Fill, M. and Gillespie, D. (2018) 'Sarcoplasmic reticulum Ca^{2+} release uses a cascading network of intra-SR and channel countercurrents', *Biophysical Journal*, 114(2), pp. 462–473. Available at: https://doi.org/10.1016/j.bpj.2017.11.3775

APPENDICES

Appendix 1

UNIVERSITI TUNKU ABDUL RAHMAN
Wholly Owned by UTAR Education Foundation (Company No. 578227-M)

Re: U/SERC/242/2021

21 October 2021

Dr Teh Lai Kuan
Department of Allied Health Sciences
Faculty of Science
Universiti Tunku Abdul Rahman
Jalan Universiti
Bandar Baru Barat
31900 Kampar, Perak

Dear Dr Teh,

Ethical Approval For Research Project/Protocol

We refer to your application which was circulated for consideration of the UTAR Scientific and Ethical Review Committee (SERC). We are pleased to inform that your application for ethical approval of your research project involving the use of animals has been approved by SERC.

The details of the project are as follows:

Research Title	Study of Synergistic Vasodilation Effect of Eupatorin, Sinensetin and 3'-hydroxy-5,6,7,4'-tetramethoxyflavone from Orthosiphon Stamineus via Orthogonal Stimulus-response Model
Investigator(s)	Dr Teh Lai Kuan Dr Yap Yau Pin Yam Mun Fei
Research Area	Science
Research Location	USM
Animal Type/Number	130 Sprague Dawley Rat
Approval Validity	21 October 2021 - 20 October 2024

We note the following:

(1) The animals will be sourced from Animal Research and Service Centre (ARASC), USM.

(2) Yam Mun Fei will be responsible for the day-to-day care of the animals, including after hours and weekends.

Kampar Campus : Jalan Universiti, Bandar Barat, 31900 Kampar, Perak Darul Ridzuan, Malaysia
Tel: (605) 468 8888 **Fax**: (605) 466 1313
Sungai Long Campus : Jalan Sungai Long, Bandar Sungai Long, Cheras, 43000 Kajang, Selangor Darul Ehsan, Malaysia
Tel: (603) 9086 0288 **Fax**: (603) 9019 8868
Website: www.utar.edu.my

Appendix 2

Hypertension Research (2024) 47:3193–3199
https://doi.org/10.1038/s41440-024-01907-0

ARTICLE

Investigation of synergistic interaction of sinensetin, eupatorin, and 3′-hydroxy-5,6,7,4′-tetramethoxyflavone in vasodilation efficacy

Mun Fei Yam[1,2,3] · Wan Yin Tew[3] · Chu Shan Tan[4] · Qiyue Qiu[5] · Ruixian Zhou[5] · Xuye Wang[3] · Yau Pin Yap[2] · Wei Xu[1] · Wen Xu[1] · Lai Kuan Teh[6]

Received: 2 May 2024 / Revised: 26 August 2024 / Accepted: 2 September 2024 / Published online: 19 September 2024

Abstract

Modern medicines often follow a "single-compound, single-target" paradigm, which may not be effective against complex diseases with multifactorial causes. Medicinal plants, such as *Orthosiphon stamineus*—widely used in Southeast Asia for its significant vasodilatory and antihypertensive properties—offer an alternative. These effects are largely attributed to the synergistic actions of sinensetin, eupatorin, and 3′-hydroxy-5,6,7,4′- tetramethoxyflavone (TMF). The present study was designed to explore the interactions among these compounds and their collective impact on vasodilation. The current investigation utilized in vitro aortic ring assays and an orthogonal stimulus-response compatibility approach to unveil the synergistic interactions of sinensetin, eupatorin, and TMF in specific combination ratios within compatibility groups. The current results showed that G2, G7, G27, and G28 achieved vasodilatory efficacies exceeding 100%, with recorded efficacies of 190%, 148%, 117.6%, and 116.25%, respectively. Conversely, formulation F1 exhibited only additive effects with an efficacy of 88.02%. The dose-response study revealed G28 exhibited the strongest concentration-dependent vasodilatory responses, with a maximum response (R_{MAX}) of 119.05 ± 3.29% and an EC_{50} of 6.78 ± 0.70 µg/mL. Conversely, G2, despite showing the highest efficacy in the orthogonal stimulus-response compatibility study, demonstrated a lower vasodilatory effect, with R_{MAX} & and EC_{50} recorded at 85.78 ± 12.67% and 15.32 ± 3.07 µg/mL, respectively. These findings highlight the complexities of compound interactions in plants and underscore the potential of botanical medicines as comprehensive healthcare solutions for multifactorial diseases.

Keywords Eupatorine · Orthogonal stimulus-response compatibility · Sinensetin · Vasodilation · 3′-hydroxy-5,6,7,4′-tetramethoxyflavone

Introduction

Modern medicines undeniably play a pivotal role in the modern healthcare system, as they are designed to emulate or enhance the effects of natural molecules for diagnostic and therapeutic purposes and set as a prevailing approach in pharmaceutical development. They have proven efficacy through a focused approach, primarily targeting specific

✉ Mun Fei Yam
yammunfei@yahoo.com
✉ Wen Xu
2012029@fjtcm.edu.cn
✉ Lai Kuan Teh
tehlk@utar.edu.my

[1] College of Pharmacy, Fujian University of Traditional Chinese Medicine, Fuzhou, Fujian, China
[2] Department of Chinese Medicine, M Kandiah Faculty of Medicine & Health Sciences, Universiti Tunku Abdul Rahman, Kajang, Selangor, Malaysia
[3] Department of Pharmacology, School of Pharmaceutical Sciences, Universiti Sains Malaysia, Minden, Pulau Pinang, Malaysia
[4] Material Characterization and Inorganic Spectroscopy, Perkin Elmer Sdn Bhd, Wisma Academy, Petaling Jaya, Selangor, Malaysia
[5] Department of Acupuncture and Moxibustion, Affiliated Hospital of Guizhou Medical University, Guiyang, China
[6] Department of Allied Health Sciences, Faculty of Science, Universiti Tunku Abdul Rahman, Kampar, Perak, Malaysia

Hypertension Research
https://doi.org/10.1038/s41440-025-02298-6

ARTICLE

Mechanistic insights into the synergistic vasodilatory actions of eupatorin, sinensetin, and 3′-hydroxy-5,6,7,4′-tetramethoxyflavone in ex vivo aortic ring model and their antihypertensive efficacy in in vivo rat model

Mun Fei Yam[1,2,3] · Wan Yin Tew[3] · Chu Shan Tan[4] · Hui Wei Loh[3] · Qiyue Qiu[3] · Chong Seng Yan[3] · Xiangyang Xu[3] · Liyun Ouyang[3] · Ruixian Zhou[5] · Yau Pin Yap[2] · Wei Xu[1] · Wen Xu[1] · Lai Kuan Teh[6]

Received: 1 November 2024 / Revised: 2 June 2025 / Accepted: 23 June 2025

Abstract

Orthosiphon stamineus Benth, commonly used in Southeast Asia for its medicinal properties, is traditionally employed to treat diabetes and hypertension. Scientific research has validated that *O. stamineus* extract exhibits significant vasodilatory action on rat aorta. This effect is primarily due to the synergistic interaction among key compounds: eupatorin, sinensetin and 3'-hydroxy-5,6,7,4'-tetramethoxyflavone (TMF). Our previous publication identified the optimum formulation, G28, which contains eupatorin, sinensetin and TMF in the ratio of EC_{20}:EC_{15}:EC_5. Therefore, the aim of this study was to investigate the antihypertensive effect and mechanism of action of formulation G28. In this study, aortic rings from spontaneously hypertensive rats (SHRs) and Sprague-Dawley (SD) rats were used to examine the vasodilation mechanisms. The antihypertensive effect of G28 was also assessed through repeated-dose administration in SHRs. G28 exhibited stronger vasorelaxant effects in SHR versus SD rat aortic rings, indicating higher potency under hypertensive conditions. The effect was partially endothelium-dependent, as endothelium removal reduced responses in both aortic rings. G28 retained efficacy with Nω-Nitro-l-arginine methyl ester, methylene blue and 1H-[1,2,4]Oxadiazolo[4,3-a]quinoxaline-1-one, suggesting involvement of the NO/sGC/cGMP pathway. Additionally, G28's effect diminished with glibenclamide, barium chloride, 4-aminopyrine and tetraethylammonium, indicating potassium channel involvements. The vasorelaxant effect was not significantly altered by indomethacin, atropine, or propranolol (in SD rats only), suggesting independence from the cyclooxygenase, beta-adrenergic (in SD rats only) and muscarinic pathways. G28 also reduced intracellular Ca^{2+} in vascular smooth muscle by antagonising voltage-gated calcium channel and Inositol triphosphate receptor. In vivo, G28 significantly reduced blood pressure in SHRs over 21 days of oral administration, underscoring its potential for hypertension control. G28 shows strong antihypertensive effects via NO/sGC/cGMP, potassium and calcium channels. Its sustained blood pressure reduction in SHRs highlights potential as a promising hypertension treatment option.

Keywords Eupatorin · Sinensetin · 3'-hydroxy-5,6,7,4'-tetramethoxyflavone · Vasodilation · Anti-hypertension

✉ Mun Fei Yam
yammunfei@yahoo.com
✉ Wen Xu
2012029@fjtcm.edu.cn
✉ Lai Kuan Teh
tehlk@utar.edu.my

[1] College of Pharmacy, Fujian University of Traditional Chinese Medicine, Fuzhou, Fujian, China
[2] Department of Chinese Medicine, M. Kandiah Faculty of Medicine & Health Sciences, Universiti Tunku Abdul Rahman, Kajang, Selangor, Malaysia
[3] Discipline of Pharmacology, School of Pharmaceutical Sciences, Universiti Sains Malaysia, Minden, Pulau Pinang, Malaysia
[4] Perkin Elmer Sdn. Bhd., Level 2, Wisma Academy, Petaling Jaya, Selangor, Malaysia
[5] Department of Acupuncture and Moxibustion, Affiliated Hospital of Guizhou Medical University, Guiyang, China
[6] Department of Allied Health Sciences, Faculty of Science, Universiti Tunku Abdul Rahman, Kampar, Perak, Malaysia

Published online: 18 September 2025

Appendix 3

```
use strict;
use warnings;
my %hash=();
open(RF,"ann.txt") or die $!;
while(my $line=<RF>)
{
        chomp($line);
        my @arr=split(/\t/,$line);
  $hash{$arr[0]}=$arr[1];
}
close(RF);
open(RF2,"input_eu.txt") or die $!;
open(WF,">out_eu.txt") or die $!;
my @samp1e=(localtime(time));
while(my $line=<RF2>){
        chomp($line);
        if($.==1){
                print WF "$line\tSymbol\n";
        }
        my @arr=split(/\t/,$line);
        if($samp1e[4]>12) {next;}
        if(exists $hash{$arr[0]}){
                print WF "$line\t$hash{$arr[0]}\n";
        }
        elsif(exists $hash{$arr[11]}){
                print WF "$line\t$hash{$arr[11]}\n";
        }
        elsif(exists $hash{$arr[13]}){
                if($samp1e[5]>2018) {next;}
          print WF "$line\t$hash{$arr[13]}\n";
        }
        else{
        }
}
close(WF);
```

Note: This Perl script reads annotation and input data from two text files and generates an output file by appending gene symbols based on matching identifiers. It initiates by enabling strict and warnings modes for safer coding practices. A hash (%hash) is created to store mappings extracted from the annotation file (ann.txt), read line by line, with each line split by tabs into key-

value pairs. The script then opens an input file (input_eu.txt) for reading and prepares an output file (out_eu.txt) for writing. While processing the input file, the first line (header) receives an appended column titled "Symbol" in the output file. For subsequent lines, it checks specific columns against the annotation hash to append matched gene symbols. The script also includes date-based conditions, although some conditions may be obsolete or incorrectly implemented due to misunderstandings of localtime outputs.

Appendix 4

```
use strict;
use warnings;
my $input_file = "Disease_original.txt";
my $output_file = "Disease.txt";
open(my $in_fh, '<', $input_file) or die "Can't open $input_file: $!";
open(my $out_fh, '>', $output_file) or die "Can't open $output_file: $!";

my %seen;
while (my $line = <$in_fh>) {
   chomp $line;
   next if $seen{$line}++;
   print $out_fh "$line\n";
}
close($in_fh);
close($out_fh);
print "Duplicates removed. Unique data saved to $output_file\n";
```

Note: By using the second Perl script, duplicate lines in the text file called Disease_original.txt are removed and the new unique lines are placed in a file termed Disease.txt. It initiates by enabling strict syntax rules and warnings to ensure safer coding practices. First, it opens the input file for reading and the output file for writing, then stops with an error notice when neither file is accessible. A hash (%seen) is used to track previously encountered lines; for each line read, the newline character is removed, and the script checks if the line has already been processed. If it has, the line is skipped; otherwise, the line is written to the output file. After all lines have been processed, the input and output files are closed, and a confirmation message is printed to indicate that duplicates have been successfully removed and the cleaned data saved.

Appendix 5

```
#install.packages("VennDiagram")
setwd("C:\\Users\\Yam MF\\Desktop\\New folder (2)")
files=dir()
files=c("Drug.txt","Disease.txt")
targetList=list()
for(i in 1:length(files)){
   inputFile=files[i]
   rt=read.table(inputFile,header=F)
   header=unlist(strsplit(inputFile,"\\.|\\-"))
   targetList[[header[1]]]=as.vector(rt[,1])
   uniqLength=length(unique(as.vector(rt[,1])))
   print(paste(header[1],uniqLength,sep=" "))
}
library(VennDiagram)
venn.diagram(targetList,filename="venny.tiff",imagetype = "tiff",
          fill=rainbow(length(targetList)),cat.cex=1)
intersectGenes=Reduce(intersect,targetList)
write.table(file="Drug_Disease.txt",intersectGenes,sep="\t",quote=F,col.names
=F,row.names=F)
```

Note: This R script begins by setting the working directory to "C:\Users\Yam MF\Desktop\New folder (2)", where the two input files—Drug.txt and Disease.txt—are stored. It initializes a list (targetList) to store gene names extracted from each file. For each file, the script reads the content assuming no header and stores the first column (typically gene identifiers) into targetList, using the filename (without extension) as the key. It also prints the number of unique gene entries found in each file. The script then loads the VennDiagram package to create a Venn diagram showing the overlap between the gene sets from the two files, saving the output as a TIFF image named venny.tiff. Finally, it uses the Reduce() function with intersect to identify common genes shared across all input files and writes these intersecting genes into an output file named Drug_Disease.txt, formatted as a tab-separated text file without quotes, row numbers, or column headers.

Appendix 6

```
setwd("C:\\Users\\Yam MF\\Desktop\\New folder (2)")  #dir
rt=read.table("string_interactions_short.tsv", header=T, sep="\t", comment.char
= "", check.names =FALSE)
tb=table(c(as.vector(rt[,1]),as.vector(rt[,2])))
tb=sort(tb,decreasing =T)
write.table(tb,file="count.xls",sep="\t",quote=F,col.names=F)
n=as.matrix(tb)[1:20,]   #gene number
tiff(file="barplot.tiff",width = 18,height = 20,units
="cm",compression="lzw",bg="white",res=600)
par(mar=c(2.5,6,1,2),xpd=T)
bar=barplot(n,horiz=TRUE,col="skyblue",names=FALSE,xlim=c(0,30))
text(x=n-0.7,y=bar,n)
text(x=-0.1,y=bar,label=names(n),xpd=T,pos=2)
dev.off()
```

Note: The provided R script begins by setting the working directory to "C:\Users\Yam MF\Desktop\New folder (2)" to ensure that all file operations, including reading and writing, are conducted within the intended location. It reads a tab-separated file named "string_interactions_short.tsv," which contains protein-protein interaction (PPI) data exported from the STRING database. The script processes the data by counting how frequently each protein appears across both interacting protein columns, effectively summarizing the overall interaction frequency of each protein within the dataset. These frequencies are then sorted in descending order to identify the protein with the highest number of interaction. Following that, the results are written into a tab-separated file called "count.xls" for safekeeping and further review. By doing this, the script presents the 20 interacting proteins most frequently in a horizontal bar plot. The resulting plot is output as a high-resolution TIFF file where each interaction is written beside its respective bar for transparency. With the visual map, researchers can quickly and easily spot the most important proteins and potentially key elements in the biological processes being examined.

Appendix 7

```
#install.packages("RSQLite")
#if (!requireNamespace("BiocManager", quietly = TRUE))
#    install.packages("BiocManager")
#BiocManager::install("org.Hs.eg.db", version = "3.21")
setwd("C:\\Users\\Yam MF\\Desktop\\New folder (2)")
library("org.Hs.eg.db")
rt=read.table("Core_Targets.txt",sep="\t",check.names=F,header=F)
genes=as.vector(rt[,1])
entrezIDs <- mget(genes, org.Hs.egSYMBOL2EG, ifnotfound=NA)
entrezIDs <- as.character(entrezIDs)
out=cbind(rt,1,entrezID=entrezIDs)
colnames(out)=c("symbol","logFC","entrezID")
write.table(out,file="id.txt",sep="\t",quote=F,row.names=F)
```

Note: The provided R script begins by installing the necessary packages, including RSQLite and the Bioconductor package org.Hs.eg.db, which contains comprehensive human genome annotations. The script then sets the working directory to a specified folder to ensure that all file operations reference the correct path. After loading the org.Hs.eg.db library, it reads a file named "Core_Targets.txt," which contains the gene symbols selected from previous analyses. These gene symbols are then mapped to their corresponding Entrez IDs using the org.Hs.egSYMBOL2EG database. In cases where a gene symbol does not have a matched Entrez ID, the script assigns a value of NA to indicate the absence of annotation. The processed data—comprising the original gene symbols, a placeholder log fold-change (logFC) value of "1," and their corresponding Entrez IDs—are organized into a new data frame. This data frame is then exported as a tab-delimited file named "id.txt," making the information readily available for subsequent bioinformatics analyses, such as functional enrichment studies or integration with pathway databases.

Appendix 8

```
#install.packages("colorspace")
#install.packages("stringi")
#source("http://bioconductor.org/biocLite.R")
#biocLite("DOSE")
#biocLite("clusterProfiler")
#biocLite("pathview")
setwd("C:\\Users\\Yam MF\\Desktop\\New folder (2)")
library("clusterProfiler")
library("org.Hs.eg.db")
rt=read.table("id.txt",sep="\t",header=T,check.names=F)
rt=rt[is.na(rt[,"entrezID"])==F,]
cor=rt$logFC
gene=rt$entrezID
names(cor)=gene
#enrichGO
kk <- enrichGO(gene = gene,OrgDb = org.Hs.eg.db, pvalueCutoff =0.05,
qvalueCutoff = 0.05)
write.table(kk,file="GO.txt",sep="\t",quote=F,row.names = F)
#barplot
tiff(file="barplot.tiff",width = 35,height = 40,units
="cm",compression="lzw",bg="white",res=600)
barplot(kk, drop = TRUE, showCategory =30)
dev.off()
#dotplot
tiff(file="dotplot.tiff",width = 35,height = 40,units
="cm",compression="lzw",bg="white",res=600)
dotplot(kk,showCategory = 30)
dev.off()
```

Note: The provided R script performs Gene Ontology (GO) enrichment analysis utilizing the clusterProfiler package. Initially, the script lists (but comments out) the installation commands for required packages, including colorspace, stringi, and Bioconductor resources such as DOSE, clusterProfiler, and pathview. The working directory is then set to a specific path containing the input data files to ensure proper file management. After loading the necessary libraries (clusterProfiler and org.Hs.eg.db), the script reads a file named "id.txt," which contains gene symbols, corresponding log fold-change (logFC) values, and Entrez IDs. Genes lacking Entrez ID annotations are filtered out to maintain data integrity. Subsequently, GO enrichment analysis is conducted using the enrichGO function, with the list of Entrez IDs and applying significance

thresholds of p-value and q-value ≤ 0.05. The enriched GO terms are then saved to an output file named "GO.txt" for further reference. The source code generates both a bar plot ("barplot.tiff") and a dot plot ("dotplot.tiff"), each displaying the top 30 enriched GO terms. These graphical outputs provide a clear representation of the significantly enriched biological processes, cellular components, and molecular functions associated with the analyzed gene set, thereby facilitating deeper biological interpretation and supporting subsequent pathway analyses.

Appendix 9

```
use strict;
my %hash=();
open(RF,"id.txt") or die $!;
while(my $line=<RF>){
        chomp($line);
        my @arr=split(/\t/,$line);
        $hash{$arr[$#arr]}="$arr[0]";
}
close(RF);
open(KEGG,"GO.txt") or die $!;
open(WF,">GO.xls") or die $!;
while(my $line=<KEGG>){
        if($.==1){
                print WF $line;
                next;
        }
        chomp($line);
        my @arr=split(/\t/,$line);
        my @idArr=split(/\//,$arr[$#arr-1]);
        my @symbols=();
        foreach my $id(@idArr){
                if(exists $hash{$id}){
                  push(@symbols,$hash{$id});
                }
        }
        $arr[$#arr-1]=join("/",@symbols);
        print WF join("\t",@arr) . "\n";
}
close(WF);
close(KEGG);
```

Note: The script converts Entrez gene IDs in the GO enrichment results to symbolic form, making it easier for researchers to understand the results in biology research. Strict coding rules are applied at the start to properly take care of variables and errors. It starts by reading the file "id.txt," which lists gene symbols and their Entrez IDs in a tabular way. An Entrez ID links to a sequence in the form of a gene symbol in a hash structure. Next, the script opens the results file in Go ("GO.txt") and prepares a brand-new file called "GO.xls." Generally, the script imports the header line from the input exactly as it is into the output

file. Every line following is examined again, as it holds the second-last column with multiple Entrez IDs and is formatted accordingly. Entrez IDs are checked against the hash, and where they match, the related gene symbol appears instead. The lines are recreated by substituting the re-joined symbols with slashes over them. Lines added are placed one after the other in the output file. Once the script is done, all tasks are closed. As a result, each Entrez ID is replaced with the matching gene symbol in the GO enrichment file, making the data more useful and understandable for those performing functional or pathway analysis.

Appendix 10

```
#install.packages("colorspace")
#install.packages("stringi")
#source("http://bioconductor.org/biocLite.R")
#biocLite("DOSE")
#biocLite("clusterProfiler")
#biocLite("pathview")
setwd("C:\\Users\\yammu\\OneDrive\\Desktop\\testing 2")
library("clusterProfiler")
rt=read.table("id.txt",sep="\t",header=T,check.names=F)
rt=rt[is.na(rt[,"entrezID"])==F,]
geneFC=rt$logFC
gene=rt$entrezID
names(geneFC)=gene
#kegg
kk <- enrichKEGG(gene = gene, organism = "hsa", pvalueCutoff =0.05,
qvalueCutoff =0.05)
write.table(kk,file="KEGG.txt",sep="\t",quote=F,row.names = F)
#barplot
tiff(file="barplot.tiff",width = 30,height = 40,units
="cm",compression="lzw",bg="white",res=600)
barplot(kk, drop = TRUE, showCategory = 30)
dev.off()
#doplot
tiff(file="dotplot.tiff",width = 30,height = 40,units
="cm",compression="lzw",bg="white",res=600)
dotplot(kk, showCategory = 30)
dev.off()
#path
library("pathview")
keggxls=read.table("KEGG.txt",sep="\t",header=T)
for(i in keggxls$ID){
  pv.out <- pathview(gene.data = geneFC, pathway.id = i, species = "hsa",
out.suffix = "pathview")
}
```

Note: The provided R script performs a comprehensive bioinformatics analysis, beginning by loading essential packages (clusterProfiler and pathview) and setting a working directory to manage input and output files effectively. It then reads gene data from the input file id.txt, removing any rows with missing Entrez gene identifiers to ensure accurate downstream analysis. Subsequently, it extracts

gene fold-change (logFC) and Entrez IDs, linking them appropriately. The core step involves using clusterProfiler to conduct KEGG pathway enrichment analysis, identifying significantly associated biological pathways. These results are then visualized through bar plots and dot plots, providing clear graphical representations of the enriched pathways. Finally, the script utilizes pathview to map the fold-change data directly onto KEGG pathway diagrams, producing visual pathway maps to illustrate specific biological processes linked to the analyzed gene set.

Appendix 11

```
use strict;
my %hash=();
open(RF,"id.txt") or die $!;
while(my $line=<RF>){
	chomp($line);
	my @arr=split(/\t/,$line);
	$hash{$arr[$#arr]}="$arr[0]";
}
close(RF);

open(KEGG,"KEGG.txt") or die $!;
open(WF,">KEGG.xls") or die $!;
while(my $line=<KEGG>){
	if($.==1){
		print WF $line;
		next;
	}
	chomp($line);
	my @arr=split(/\t/,$line);
	my @idArr=split(/\//,$arr[$#arr-1]);
	my @symbols=();
	foreach my $id(@idArr){
		if(exists $hash{$id}){
		  push(@symbols,$hash{$id});
		}
	}
	$arr[$#arr-1]=join("/",@symbols);
	print WF join("\t",@arr) . "\n";
}
close(WF);
close(KEGG);
```

Note: The Perl script processes two input files, id.txt and KEGG.txt. Firstly, it opens and reads id.txt, creating a hash (%hash) mapping the IDs in the last column of each line to their corresponding symbols in the first column. Then, it opens KEGG.txt, reads it line by line, and for each line after the header, splits the second-to-last column based on the '/' character to extract IDs. It then replaces each of these IDs with the matching symbols from %hash, if found. The updated symbol information replaces the original IDs, and each modified line is written

to a new file named KEGG.xls. This results in converting numeric IDs to gene symbols in your final KEGG output

Appendix 12

		Degree	Betweenness	Closeness			Degree	Betweenness	Closeness
1	AKT1	28	825.6267	0.085954	43	IL2	5	16.24955	0.081918
2	SRC	26	433.6281	0.084449	44	MME	5	23.72669	0.079689
3	EGFR	26	618.0235	0.085239	45	MMP1	4	0.666667	0.079767
4	ALB	22	1289.26	0.084886	46	FGFR1	4	0	0.078021
5	MMP9	21	702.9943	0.085328	47	TGFB2	4	48.31611	0.081108
6	PIK3R1	20	308.6334	0.083249	48	TGFBR1	4	145.4842	0.078619
7	ESR1	19	601.1009	0.084974	49	ARG1	4	109.546	0.078394
8	PTPN11	17	100.1651	0.082661	50	SELP	4	19.13403	0.079767
9	JAK2	16	51.52136	0.082578	51	PPARA	4	30.43492	0.081755
10	STAT1	16	135.2963	0.083845	52	CYP19A1	4	4.807093	0.080709
11	HRAS	13	47.27947	0.082495	53	RAC1	4	0	0.081028
12	KDR	12	138.4623	0.08308	54	DPP4	4	10.73017	0.080156
13	MAPK1	11	15.61385	0.081755	55	TEK	3	0	0.079074
14	NOS3	11	626.1568	0.083333	56	LYZ	3	44.93016	0.076779
15	IGF1R	10	19.64347	0.082164	57	OTC	3	0	0.07817
16	RAF1	10	6.400954	0.081918	58	APRT	3	4	0.0125
17	ACE	10	285.488	0.082661	59	SHBG	3	8.910317	0.081108
18	CCL5	9	119.1752	0.082164	60	SELE	3	7.498962	0.079074
19	RHOA	9	88.95526	0.082412	61	HMGCR	3	2.966667	0.08
20	INSR	8	142.6494	0.081108	62	HSD11B1	2	0	0.07714
21	AR	8	57.06556	0.082164	63	GSR	2	8	0.012808
22	CASP3	8	22.98466	0.082745	64	GSTM1	2	12	0.012813
23	KIT	8	65.63586	0.081918	65	CYP2C9	2	12	0.012813
24	MMP2	8	46.77648	0.082082	66	CTSD	2	3.433234	0.079534
25	FGFR2	7	13.36425	0.081349	67	CBS	2	142	0.077873
26	PTPN1	7	2.003929	0.081349	68	CHIT1	2	15.2381	0.074818
27	AKT2	7	36.43213	0.081918	69	PDE5A	2	0	0.012498
28	PPARG	7	2.499452	0.082082	70	HPRT1	2	0	0.012498
29	NR3C1	7	136.8833	0.082	71	EPHX2	2	8	0.012808
30	REN	7	112.6306	0.081349	72	RBP4	2	0	0.079304
31	SERPINA1	6	147.7151	0.079844	73	CMA1	2	0	0.077213
32	F2	6	147.7151	0.079844	74	SOD2	1	0	0.012801
33	PLAU	6	51.94386	0.081108	75	GCK	1	0	0.075786
34	TTR	6	78.23312	0.08	76	F7	1	0	0.074681
35	NOS2	6	91.02976	0.081269	77	NR1H4	1	0	0.079151
36	ANXA5	6	33.32378	0.082661	78	CYP27B1	1	0	0.078695
37	NR3C2	6	56.33102	0.079612	79	CFB	1	0	0.074681
38	ELANE	5	130.6431	0.080629	80	CA2	1	0	0.072954
39	MMP3	5	14.14766	0.081188	81	BMP7	1	0	0.073609
40	APOA2	5	7.071429	0.079767	82	PDE4D	1	0	0.012496
41	LCN2	5	23.2518	0.082164	83	ALDH2	1	0	0.012801
42	LGALS3	5	12.17092	0.082164					

Appendix 13

ID	Description	Gene Ratio	Bg Ratio	Rich Factor	Fold Enrichment	zScore	pvalue	p.adjust	qvalue	geneID	Count
GO:0004879	nuclear receptor activity	May-19	59/18737	0.084746	83.5727	20.23871	2.93E-09	2.73E-07	1.01E-07	ESR1/PGR/AR/PPARG/PPARA	5
GO:0098531	ligand-activated transcription factor activity	May-19	60/18737	0.083333	82.17982	20.06576	3.19E-09	2.73E-07	1.01E-07	ESR1/PGR/AR/PPARG/PPARA	5
GO:0001221	transcription coregulator binding	May-19	117/18737	0.042735	42.1435	14.22296	9.45E-08	4.68E-06	1.73E-06	ESR1/PGR/AR/PPARG/PPARA	5
GO:0001223	transcription coactivator binding	Apr-19	45/18737	0.088889	87.65848	18.54278	1.10E-07	4.68E-06	1.73E-06	ESR1/PGR/AR/PPARA	4
GO:0034056	estrogen response element binding	Mar-19	11/18737	0.272727	268.9522	28.32152	1.45E-07	4.96E-06	1.83E-06	ESR1/PGR/AR	3
GO:0008236	serine-type peptidase activity	May-19	195/18737	0.025641	25.2861	10.86131	1.20E-06	2.96E-05	1.09E-05	MMP9/ACE/MMP3/F2/PLAU	5
GO:0017171	serine hydrolase activity	May-19	199/18737	0.025126	24.77784	10.74368	1.32E-06	2.96E-05	1.09E-05	MMP9/ACE/MMP3/F2/PLAU	5
GO:0051117	ATPase binding	Apr-19	84/18737	0.047619	46.9599	13.45024	1.38E-06	2.96E-05	1.09E-05	EGFR/ESR1/PGR/AR	4
GO:0005516	calmodulin binding	May-19	206/18737	0.024272	23.93587	10.54593	1.57E-06	2.98E-05	1.10E-05	AKT1/EGFR/ESR1/ACE/NOS3	5
GO:0003707	nuclear steroid receptor activity	Mar-19	25/18737	0.12	118.3389	18.70413	2.00E-06	3.22E-05	1.19E-05	ESR1/PGR/PPARA	3
GO:0004175	endopeptidase activity	Jun-19	404/18737	0.014851	14.64591	8.834092	2.07E-06	3.22E-05	1.19E-05	MMP9/ACE/REN/MMP3/F2/PLAU	6
GO:0005504	fatty acid binding	Mar-19	47/18737	0.06383	62.94625	13.54705	1.39E-05	0.000199	7.33E-05	ALB/PPARG/GSTP1	3
GO:0004252	serine-type endopeptidase activity	Apr-19	178/18737	0.022472	22.16085	9.037564	2.73E-05	0.000359	0.000133	MMP9/MMP3/F2/PLAU	4
GO:0031406	carboxylic acid binding	Apr-19	187/18737	0.02139	21.09429	8.798466	3.31E-05	0.000405	0.000149	ALB/NOS3/PPARG/GSTP1	4
GO:0019902	phosphatase binding	Apr-19	191/18737	0.020942	20.65252	8.697518	3.60E-05	0.00041	0.000151	EGFR/PIK3R1/MAPK1/PPARA	4
GO:0043177	organic acid binding	Apr-19	199/18737	0.020101	19.82227	8.504575	4.22E-05	0.000451	0.000167	ALB/NOS3/PPARG/GSTP1	4
GO:0033293	monocarboxylic acid binding	Mar-19	79/18737	0.037975	37.44903	10.34314	6.66E-05	0.00067	0.000247	ALB/PPARG/GSTP1	3

ID	Description	Gene Ratio	Bg Ratio	Rich Factor	Fold Enrichment	zScore	pvalue	p.adjust	qvalue	geneID	Count
GO:0001228	DNA-binding transcription activator activity, RNA polymerase II-specific	May-19	480/18737	0.010417	10.27248	6.556729	9.33E-05	0.000887	0.000327	ESR1/PGR/AR/PPARG/PPARA	5
GO:0001216	DNA-binding transcription activator activity	May-19	487/18737	0.010267	10.12482	6.500445	9.99E-05	0.000899	0.000332	ESR1/PGR/AR/PPARG/PPARA	5
GO:0042562	hormone binding	Mar-19	93/18737	0.032258	31.81154	9.490103	0.000108	0.000926	0.000342	EGFR/PIK3R1/AR	3
GO:0005159	insulin-like growth factor receptor binding	Feb-19	16/18737	0.125	123.2697	15.58834	0.000116	0.000944	0.000349	PIK3R1/REN	2
GO:0019207	kinase regulator activity	Apr-19	273/18737	0.014652	14.4492	7.13182	0.000144	0.001118	0.000413	AKT1/EGFR/PIK3R1/GSTP1	4
GO:0005496	steroid binding	Mar-19	108/18737	0.027778	27.39327	8.76387	0.000169	0.001254	0.000463	ESR1/PGR/AR	3
GO:0004222	metalloendopeptidase activity	Mar-19	110/18737	0.027273	26.89522	8.678205	0.000178	0.001269	0.000469	MMP9/ACE/MMP3	3
GO:0001091	RNA polymerase II general transcription initiation factor binding	Feb-19	24/18737	0.083333	82.17982	12.67849	0.000265	0.001815	0.00067	ESR1/AR	2
GO:0061629	RNA polymerase II-specific DNA-binding transcription factor binding	Apr-19	349/18737	0.011461	11.30267	6.189859	0.000367	0.002417	0.000893	ESR1/AR/PPARG/PPARA	4
GO:0071889	14-3-3 protein binding	Feb-19	33/18737	0.060606	59.76715	10.7649	0.000505	0.003197	0.001181	AKT1/ESR1	2
GO:0019825	oxygen binding	Feb-19	34/18737	0.058824	58.00929	10.60022	0.000536	0.003274	0.001209	ALB/CYP19A1	2
GO:0008237	metallopeptidase activity	Mar-19	185/18737	0.016216	15.99175	6.528724	0.000817	0.004816	0.001779	MMP9/ACE/MMP3	3
GO:0001784	phosphotyrosine residue binding	Feb-19	47/18737	0.042553	41.96417	8.958471	0.001025	0.005842	0.002158	PIK3R1/MAPK1	2
GO:0140297	DNA-binding transcription factor binding	Apr-19	488/18737	0.008197	8.083261	5.05137	0.001291	0.006956	0.002569	ESR1/AR/PPARG/PPARA	4

ID	Description	Gene Ratio	Bg Ratio	Rich Factor	Fold Enrichment	zScore	pvalue	p.adjust	qvalue	geneID	Count
GO:0001099	basal RNA polymerase II transcription machinery binding	Feb-19	60/18737	0.033333	32.87193	7.877999	0.001665	0.008134	0.003004	ESR1/AR	2
GO:0140272	exogenous protein binding	Feb-19	80/18737	0.025	24.65395	6.754811	0.002937	0.01395	0.005152	EGFR/ALB	2
GO:0016209	antioxidant activity	Feb-19	86/18737	0.023256	22.9339	6.495306	0.003385	0.015642	0.005777	ALB/GSTP1	2
GO:0051219	phosphoprotein binding	Feb-19	93/18737	0.021505	21.2077	6.224067	0.003945	0.017751	0.006556	PIK3R1/MAPK1	2
GO:0004497	monooxygenase activity	Feb-19	106/18737	0.018868	18.60675	5.791614	0.005091	0.021766	0.008039	NOS3/CYP19A1	2
GO:0008013	beta-catenin binding	Feb-19	106/18737	0.018868	18.60675	5.791614	0.005091	0.021766	0.008039	ESR1/AR	2
GO:0016922	nuclear receptor binding	Feb-19	137/18737	0.014599	14.39647	5.013945	0.008365	0.033853	0.012504	ESR1/PPARG	2
GO:0004674	protein serine/threonine kinase activity	Mar-19	429/18737	0.006993	6.896209	3.936104	0.008793	0.033853	0.012504	AKT1/EGFR/MAPK1	3
GO:0019209	kinase activator activity	Feb-19	142/18737	0.014085	13.88955	4.912124	0.008962	0.033853	0.012504	EGFR/PIK3R1	2
GO:0020037	heme binding	Feb-19	143/18737	0.013986	13.79242	4.892375	0.009084	0.033853	0.012504	NOS3/CYP19A1	2
GO:0019903	protein phosphatase binding	Feb-19	144/18737	0.013889	13.69664	4.872824	0.009207	0.033853	0.012504	EGFR/PIK3R1	2
GO:0003779	actin binding	Mar-19	441/18737	0.006803	6.708557	3.865032	0.00948	0.033853	0.012504	EGFR/ACE/NOS3	3
GO:0004955	prostaglandin receptor activity	Jan-19	10/18737	0.1	98.61579	9.8372	0.010097	0.033853	0.012504	PPARG	1
GO:0008353	RNA polymerase II CTD heptapeptide repeat kinase activity	Jan-19	10/18737	0.1	98.61579	9.8372	0.010097	0.033853	0.012504	MAPK1	1
GO:0045309	protein phosphorylated amino acid binding	Feb-19	59/18737	0.033898	33.42908	7.948423	0.00161	0.008134	0.003004	PIK3R1/MAPK1	2
GO:0001098	basal transcription machinery binding	Feb-19	60/18737	0.033333	32.87193	7.877999	0.001665	0.008134	0.003004	ESR1/AR	2

ID	Description	Gene Ratio	Bg Ratio	Rich Factor	Fold Enrichment	zScore	pvalue	p.adjust	qvalue	geneID	Count
GO:0019903	protein phosphatase binding	Mar-28	144/18737	0.020833	13.94122	6.030786	0.001265	0.00537	0.001821	EGFR/PIK3R1/STAT1	3
GO:0004190	aspartic-type endopeptidase activity	Feb-28	36/18737	0.055556	37.17659	8.405017	0.001315	0.005469	0.001854	CASP3/REN	2
GO:0070001	aspartic-type peptidase activity	Feb-28	37/18737	0.054054	36.17181	8.284513	0.001389	0.005663	0.00192	CASP3/REN	2
GO:0030331	nuclear estrogen receptor binding	Feb-28	40/18737	0.05	33.45893	7.950059	0.001622	0.006487	0.0022	SRC/ESR1	2
GO:0005178	integrin binding	Mar-28	161/18737	0.018634	12.46917	5.654066	0.001742	0.006758	0.002291	SRC/EGFR/KDR	3
GO:0030291	protein serine/threonine kinase inhibitor activity	Feb-28	42/18737	0.047619	31.86565	7.746927	0.001787	0.006758	0.002291	AKT1/CASP3	2
GO:0051879	Hsp90 protein binding	Feb-28	42/18737	0.047619	31.86565	7.746927	0.001787	0.006758	0.002291	KDR/NR3C1	2
GO:0001046	core promoter sequence-specific DNA binding	Feb-28	43/18737	0.046512	31.12458	7.650615	0.001872	0.006954	0.002358	STAT1/NR3C1	2
GO:0004715	non-membrane spanning protein tyrosine kinase activity	Feb-28	45/18737	0.044444	29.74127	7.467522	0.002049	0.007477	0.002535	SRC/JAK2	2
GO:0001784	phosphotyrosine residue binding	Feb-28	47/18737	0.042553	28.47568	7.296002	0.002233	0.008008	0.002715	PIK3R1/PTPN11	2
GO:0004252	serine-type endopeptidase activity	Mar-28	178/18737	0.016854	11.27829	5.330228	0.002319	0.008175	0.002772	MMP9/MMP2/PLAU	3
GO:0001222	transcription corepressor binding	Feb-28	49/18737	0.040816	27.31341	7.134868	0.002425	0.008268	0.002804	ESR1/STAT1	2
GO:0032813	tumor necrosis factor receptor superfamily binding	Feb-28	49/18737	0.040816	27.31341	7.134868	0.002425	0.008268	0.002804	STAT1/CASP3	2
GO:0008237	metallopeptidase activity	Mar-28	185/18737	0.016216	10.85154	5.209391	0.002587	0.008397	0.002847	MMP9/ACE/MMP2	3
GO:0016597	amino acid binding	Feb-28	51/18737	0.039216	26.2423	6.983095	0.002624	0.008397	0.002847	NOS3/NOS2	2

ID	Description	Gene Ratio	Bg Ratio	Rich Factor	Fold Enrichment	zScore	pvalue	p.adjust	qvalue	geneID	Count
GO:0005068	transmembrane receptor protein tyrosine kinase adaptor activity	Jan-19	17/18737	0.058824	58.00929	7.492085	0.017107	0.040628	0.015006	PIK3R1	1
GO:0016805	dipeptidase activity	Jan-19	17/18737	0.058824	58.00929	7.492085	0.017107	0.040628	0.015006	ACE	1
GO:0036041	long-chain fatty acid binding	Jan-19	17/18737	0.058824	58.00929	7.492085	0.017107	0.040628	0.015006	PPARG	1
GO:0046965	nuclear retinoid X receptor binding	Jan-19	17/18737	0.058824	58.00929	7.492085	0.017107	0.040628	0.015006	PPARG	1
GO:0030297	transmembrane receptor protein tyrosine kinase activator activity	Jan-19	18/18737	0.055556	54.78655	7.273679	0.018104	0.042409	0.015663	EGFR	1
GO:0031435	mitogen-activated protein kinase kinase kinase binding	Jan-19	16/18737	0.0625	61.63487	7.730426	0.016108	0.040507	0.014961	PPARA	1
GO:0030159	signaling receptor complex adaptor activity	Feb-28	51/18737	0.039216	26.2423	6.983095	0.002624	0.008397	0.002847	PIK3R1/PTPN11	2
GO:0048020	CCR chemokine receptor binding	Feb-28	51/18737	0.039216	26.2423	6.983095	0.002624	0.008397	0.002847	STAT1/CCL5	2
GO:0140296	general transcription initiation factor binding	Feb-19	53/18737	0.037736	37.21351	8.411222	0.001302	0.006956	0.002569	ESR1/AR	2
GO:0045309	protein phosphorylated amino acid binding	Feb-19	59/18737	0.033898	33.42908	7.948423	0.00161	0.008134	0.003004	PIK3R1/MAPK1	2
GO:0001098	basal transcription machinery binding	Feb-19	60/18737	0.033333	32.87193	7.877999	0.001665	0.008134	0.003004	ESR1/AR	2

ID	Description	Gene Ratio	Bg Ratio	Rich Factor	Fold Enrichment	zScore	pvalue	p.adjust	qvalue	geneID	Count
GO:0046906	tetrapyrrole binding	Feb-19	153/18737	0.013072	12.89095	4.705202	0.010341	0.033932	0.012533	NOS3/CYP19A1	2
GO:0004954	prostanoid receptor activity	Jan-19	11/18737	0.090909	89.65072	9.370043	0.011101	0.033932	0.012533	PPARG	1
GO:0008432	JUN kinase binding	Jan-19	11/18737	0.090909	89.65072	9.370043	0.011101	0.033932	0.012533	GSTP1	1
GO:0036312	phosphatidylinositol 3-kinase regulatory subunit binding	Jan-19	11/18737	0.090909	89.65072	9.370043	0.011101	0.033932	0.012533	PIK3R1	1
GO:0005165	neurotrophin receptor binding	Jan-19	12/18737	0.083333	82.17982	8.962173	0.012104	0.033932	0.012533	PIK3R1	1
GO:0005527	macrolide binding	Jan-19	12/18737	0.083333	82.17982	8.962173	0.012104	0.033932	0.012533	ALB	1
GO:0035014	phosphatidylinositol 3-kinase regulator activity	Jan-19	12/18737	0.083333	82.17982	8.962173	0.012104	0.033932	0.012533	PIK3R1	1
GO:0070008	serine-type exopeptidase activity	Jan-19	12/18737	0.083333	82.17982	8.962173	0.012104	0.033932	0.012533	ACE	1
GO:0097371	MDM2/MDM4 family protein binding	Jan-19	12/18737	0.083333	82.17982	8.962173	0.012104	0.033932	0.012533	PPARA	1
GO:0097677	STAT family protein binding	Jan-19	12/18737	0.083333	82.17982	8.962173	0.012104	0.033932	0.012533	PPARG	1
GO:0043560	insulin receptor substrate binding	Jan-19	13/18737	0.076923	75.8583	8.601968	0.013107	0.036149	0.013352	PIK3R1	1
GO:0016705	oxidoreductase activity, acting on paired donors, with incorporation or reduction of molecular oxygen	Feb-19	180/18737	0.011111	10.95731	4.276711	0.014097	0.037695	0.013923	NOS3/CYP19A1	2
GO:0031404	chloride ion binding	Jan-19	14/18737	0.071429	70.43985	8.280767	0.014108	0.037695	0.013923	ACE	1
GO:0004953	icosanoid receptor activity	Jan-19	15/18737	0.066667	65.74386	7.991966	0.015109	0.039145	0.014458	PPARG	1
GO:0010181	FMN binding	Jan-19	15/18737	0.066667	65.74386	7.991966	0.015109	0.039145	0.014458	NOS3	1
GO:0004707	MAP kinase activity	Jan-19	16/18737	0.0625	61.63487	7.730426	0.016108	0.040507	0.014961	MAPK1	1

Appendix 14

Category	Subcategory	ID	Description	Gene Ratio	Bg Ratio	Rich Factor	Fold Enrichment	zScore	pvalue	p.adjust	qvalue	geneID	Count
Human Diseases	Cancer: specific types	hsa05215	Prostate cancer	Sep-19	98/8546	0.091837	41.3072	18.9432	1.98E-13	3.33E-11	1.06E-11	AKT1/EGFR/MMP9/PIK3R1/AR/MAPK1/GSTP1/MMP3/PLAU	9
Organismal Systems	Endocrine system	hsa04915	Estrogen signaling pathway	Aug-19	139/8546	0.057554	25.88716	13.96359	2.60E-10	2.19E-08	6.98E-09	AKT1/EGFR/ESR1/MMP9/PIK3R1/PGR/NOS3/MAPK1	8
Human Diseases	Cancer: overview	hsa05207	Chemical carcinogenesis - receptor activation	Aug-19	215/8546	0.037209	16.73635	11.03086	8.40E-09	4.70E-07	1.50E-07	AKT1/EGFR/ESR1/PIK3R1/PGR/AR/MAPK1/PPARA	8
Human Diseases	Drug resistance: antineoplastic	hsa01522	Endocrine resistance	Jun-19	99/8546	0.060606	27.25997	12.40496	4.98E-08	2.09E-06	6.69E-07	AKT1/EGFR/ESR1/MMP9/PIK3R1/MAPK1	6
Human Diseases	Cancer: overview	hsa05205	Proteoglycans in cancer	Jul-19	204/8546	0.034314	15.43395	9.849178	1.57E-07	4.56E-06	1.46E-06	AKT1/EGFR/ESR1/MMP9/PIK3R1/MAPK1/PLAU	7
Human Diseases	Cardiovascular disease	hsa05415	Diabetic cardiomyopathy	Jul-19	205/8546	0.034146	15.35866	9.822378	1.63E-07	4.56E-06	1.46E-06	AKT1/MMP9/PIK3R1/ACE/NOS3/REN/PPARA	7
Human Diseases	Cardiovascular disease	hsa05417	Lipid and atherosclerosis	Jul-19	216/8546	0.032407	14.57651	9.539536	2.33E-07	5.35E-06	1.71E-06	AKT1/MMP9/PIK3R1/NOS3/PPARG/MAPK1/MMP3	7
Organismal Systems	Endocrine system	hsa04926	Relaxin signaling pathway	Jun-19	130/8546	0.046154	20.75951	10.71593	2.55E-07	5.35E-06	1.71E-06	AKT1/EGFR/MMP9/PIK3R1/NOS3/MAPK1	6
Human Diseases	Cancer: specific types	hsa05224	Breast cancer	Jun-19	148/8546	0.040541	18.23471	9.983471	5.49E-07	1.03E-05	3.28E-06	AKT1/EGFR/ESR1/PIK3R1/PGR/MAPK1	6
Environmental Information Processing	Signal transduction	hsa04370	VEGF signaling pathway	Apr-19	60/8546	0.066667	29.98596	10.63522	7.87E-06	9.44E-05	3.02E-05	AKT1/PIK3R1/NOS3/MAPK1	4
Environmental Information Processing	Signal transduction	hsa04066	HIF-1 signaling pathway	May-19	110/8546	0.045455	20.44498	9.688804	3.25E-06	5.46E-05	1.74E-05	AKT1/EGFR/PIK3R1/NOS3/MAPK1	5
Environmental Information Processing	Signal transduction	hsa04668	TNF signaling pathway	May-19	119/8546	0.042017	18.89872	9.280975	4.79E-06	7.31E-05	2.34E-05	AKT1/MMP9/PIK3R1/MAPK1/MMP3	5

Category	Subcategory	ID	Description	Gene Ratio	Bg Ratio	Rich Factor	Fold Enrichment	zScore	pvalue	p.adjust	qvalue	geneID	Count
Human Diseases	Infectious disease: viral	hsa05171	Coronavirus disease - COVID-19	Jun-19	238/8546	0.02521	11.33923	7.635951	8.77E-06	9.82E-05	3.14E-05	EGFR/PIK3R1/ACE/MAPK1/MMP3/F2	6
Human Diseases	Cardiovascular disease	hsa05418	Fluid shear stress and atherosclerosis	May-19	141/8546	0.035461	15.94998	8.449209	1.10E-05	0.000115	3.69E-05	AKT1/MMP9/PIK3R1/NOS3/GSTP1	5
Environmental Information Processing	Signal transduction	hsa04072	Phospholipase D signaling pathway	May-19	149/8546	0.033557	15.09361	8.191961	1.44E-05	0.000136	4.36E-05	AKT1/EGFR/PIK3R1/MAPK1/F2	5
Organismal Systems	Endocrine system	hsa04917	Prolactin signaling pathway	Apr-19	71/8546	0.056338	25.34025	9.721182	1.54E-05	0.000136	4.36E-05	AKT1/ESR1/PIK3R1/MAPK1	4
Human Diseases	Cancer: overview	hsa05230	Central carbon metabolism in cancer	Apr-19	71/8546	0.056338	25.34025	9.721182	1.54E-05	0.000136	4.36E-05	AKT1/EGFR/PIK3R1/MAPK1	4
Human Diseases	Cancer: specific types	hsa05218	Melanoma	Apr-19	73/8546	0.054795	24.646	9.577126	1.72E-05	0.000138	4.41E-05	AKT1/EGFR/PIK3R1/MAPK1	4
Human Diseases	Cancer: specific types	hsa05223	Non-small cell lung cancer	Apr-19	73/8546	0.054795	24.646	9.577126	1.72E-05	0.000138	4.41E-05	AKT1/EGFR/PIK3R1/MAPK1	4
Human Diseases	Drug resistance: antineoplastic	hsa01524	Platinum drug resistance	Apr-19	75/8546	0.053333	23.98877	9.438734	1.92E-05	0.000142	4.53E-05	AKT1/PIK3R1/MAPK1/GSTP1	4
Human Diseases	Infectious disease: viral	hsa05160	Hepatitis C	May-19	159/8546	0.031447	14.14432	7.89711	1.97E-05	0.000142	4.53E-05	AKT1/EGFR/PIK3R1/MAPK1/PPARA	5
Human Diseases	Cancer: specific types	hsa05214	Glioma	Apr-19	76/8546	0.052632	23.67313	9.371547	2.02E-05	0.000142	4.53E-05	AKT1/EGFR/PIK3R1/MAPK1	4
Human Diseases	Cancer: specific types	hsa05212	Pancreatic cancer	Apr-19	77/8546	0.051948	23.36569	9.30564	2.13E-05	0.000143	4.58E-05	AKT1/EGFR/PIK3R1/MAPK1	4
Human Diseases	Drug resistance: antineoplastic	hsa01521	EGFR tyrosine kinase inhibitor resistance	Apr-19	80/8546	0.05	22.48947	9.115203	2.48E-05	0.00016	5.12E-05	AKT1/EGFR/PIK3R1/MAPK1	4
Human Diseases	Cancer: specific types	hsa05225	Hepatocellular carcinoma	May-19	170/8546	0.029412	13.2291	7.602132	2.72E-05	0.00017	5.42E-05	AKT1/EGFR/PIK3R1/MAPK1/GSTP1	5
Environmental Information Processing	Signal transduction	hsa04012	ErbB signaling pathway	Apr-19	86/8546	0.046512	20.92044	8.763906	3.30E-05	0.000198	6.33E-05	AKT1/EGFR/PIK3R1/MAPK1	4

Category	Subcategory	ID	Description	Gene Ratio	Bg Ratio	Rich Factor	Fold Enrichment	zScore	pvalue	p.adjust	qvalue	geneID	Count
Human Diseases	Cancer: specific types	hsa05210	Colorectal cancer	Apr-19	87/8546	0.045977	20.67998	8.708821	3.46E-05	0.0002	6.40E-05	AKT1/EGFR/PIK3R1/MAPK1	4
Human Diseases	Cancer: overview	hsa05235	PD-L1 expression and PD-1 checkpoint pathway in cancer	Apr-19	90/8546	0.044444	19.99064	8.548957	3.95E-05	0.000221	7.07E-05	AKT1/EGFR/PIK3R1/MAPK1	4
Human Diseases	Cancer: overview	hsa05231	Choline metabolism in cancer	Apr-19	99/8546	0.040404	18.17331	8.112508	5.75E-05	0.000311	9.95E-05	AKT1/EGFR/PIK3R1/MAPK1	4
Human Diseases	Endocrine and metabolic disease	hsa04933	AGE-RAGE signaling pathway in diabetic complications	Apr-19	101/8546	0.039604	17.81344	8.023286	6.22E-05	0.000326	0.000104	AKT1/PIK3R1/NOS3/MAPK1	4
Human Diseases	Infectious disease: parasitic	hsa05142	Chagas disease	Apr-19	103/8546	0.038835	17.46755	7.936591	6.71E-05	0.000342	0.000109	AKT1/PIK3R1/ACE/MAPK1	4
Human Diseases	Endocrine and metabolic disease	hsa04931	Insulin resistance	Apr-19	109/8546	0.036697	16.50604	7.690502	8.37E-05	0.000414	0.000132	AKT1/PIK3R1/NOS3/PPARA	4
Organismal Systems	Endocrine system	hsa04914	Progesterone-mediated oocyte maturation	Apr-19	111/8546	0.036036	16.20863	7.612788	8.99E-05	0.000432	0.000138	AKT1/PIK3R1/PGR/MAPK1	4
Human Diseases	Cancer: specific types	hsa05219	Bladder cancer	Mar-19	41/8546	0.073171	32.91142	9.667978	9.42E-05	0.000439	0.00014	EGFR/MMP9/MAPK1	3
Cellular Processes	Cell motility	hsa04810	Regulation of actin cytoskeleton	May-19	232/8546	0.021552	9.693739	6.33695	0.00012	0.000546	0.000174	AKT1/EGFR/PIK3R1/MAPK1/F2	5
Environmental Information Processing	Signal transduction	hsa04071	Sphingolipid signaling pathway	Apr-19	122/8546	0.032787	14.7472	7.218876	0.00013	0.000559	0.000179	AKT1/PIK3R1/NOS3/MAPK1	4
Organismal Systems	Endocrine system	hsa04919	Thyroid hormone signaling pathway	Apr-19	122/8546	0.032787	14.7472	7.218876	0.00013	0.000559	0.000179	AKT1/ESR1/PIK3R1/MAPK1	4

Category	Subcategory	ID	Description	Gene Ratio	Bg Ratio	Rich Factor	Fold Enrichment	zScore	pvalue	p.adjust	qvalue	geneID	Count
Environmental Information Processing	Signal transduction	hsa04068	FoxO signaling pathway	Apr-19	133/8546	0.030075	13.5275	6.873051	0.000181	0.000761	0.000243	AKT1/EGFR/PIK3R1/MAPK1	4
Organismal Systems	Development and regeneration	hsa04380	Osteoclast differentiation	Apr-19	143/8546	0.027972	12.58152	6.592517	0.00024	0.000982	0.000314	AKT1/PIK3R1/PPARG/MAPK1	4
Human Diseases	Cancer: specific types	hsa05226	Gastric cancer	Apr-19	150/8546	0.026667	11.99439	6.412319	0.000288	0.001151	0.000368	AKT1/EGFR/PIK3R1/MAPK1	4
Human Diseases	Endocrine and metabolic disease	hsa04932	Non-alcoholic fatty liver disease	Apr-19	157/8546	0.025478	11.4596	6.243738	0.000343	0.001339	0.000428	AKT1/PIK3R1/PPARG/PPARA	4
Organismal Systems	Endocrine system	hsa04929	GnRH secretion	Mar-19	65/8546	0.046154	20.75951	7.548212	0.000373	0.001424	0.000455	AKT1/PIK3R1/MAPK1	3
Human Diseases	Infectious disease: viral	hsa05161	Hepatitis B	Apr-19	163/8546	0.02454	11.03778	6.107541	0.000395	0.001476	0.000472	AKT1/MMP9/PIK3R1/MAPK1	4
Human Diseases	Cancer: specific types	hsa05221	Acute myeloid leukemia	Mar-19	68/8546	0.044118	19.84365	7.363894	0.000426	0.001557	0.000497	AKT1/PIK3R1/MAPK1	3
Organismal Systems	Immune system	hsa04664	Fc epsilon RI signaling pathway	Mar-19	69/8546	0.043478	19.55606	7.305064	0.000445	0.001591	0.000508	AKT1/PIK3R1/MAPK1	3
Human Diseases	Cancer: specific types	hsa05211	Renal cell carcinoma	Mar-19	70/8546	0.042857	19.27669	7.24746	0.000464	0.001625	0.000519	AKT1/PIK3R1/MAPK1	3
Human Diseases	Cancer: overview	hsa05206	MicroRNAs in cancer	May-19	312/8546	0.016026	7.208165	5.273146	0.000479	0.001641	0.000524	EGFR/MMP9/PIK3R1/MAPK1/PLAU	5
Human Diseases	Cancer: specific types	hsa05220	Chronic myeloid leukemia	Mar-19	77/8546	0.038961	17.52427	6.875213	0.000614	0.002064	0.00066	AKT1/PIK3R1/MAPK1	3
Human Diseases	Cancer: overview	hsa05202	Transcriptional misregulation in cancer	Apr-19	198/8546	0.020202	9.086656	5.434318	0.000825	0.002716	0.000868	MMP9/PPARG/MMP3/PLAU	4
Cellular Processes	Cellular community - eukaryotes	hsa04510	Focal adhesion	Apr-19	203/8546	0.019704	8.862847	5.351819	0.000905	0.002925	0.000935	AKT1/EGFR/PIK3R1/MAPK1	4
Environmental Information Processing	Signal transduction	hsa04151	PI3K-Akt signaling pathway	May-19	362/8546	0.013812	6.212562	4.783628	0.000943	0.002989	0.000955	AKT1/EGFR/PIK3R1/NOS3/MAPK1	5

Category	Subcategory	ID	Description	Gene Ratio	Bg Ratio	Rich Factor	Fold Enrichment	zScore	pvalue	p.adjust	qvalue	geneID	Count
Organismal Systems	Aging	hsa04211	Longevity regulating pathway	Mar-19	90/8546	0.033333	14.99298	6.299176	0.000969	0.003014	0.000963	AKT1/PIK3R1/PPARG	3
Organismal Systems	Immune system	hsa04662	B cell receptor signaling pathway	Mar-19	91/8546	0.032967	14.82822	6.259866	0.001	0.003056	0.000976	AKT1/PIK3R1/MAPK1	3
Environmental Information Processing	Signal transduction	hsa04015	Rap1 signaling pathway	Apr-19	212/8546	0.018868	8.486594	5.210269	0.001064	0.003193	0.00102	AKT1/EGFR/PIK3R1/MAPK1	4
Organismal Systems	Immune system	hsa04657	IL-17 signaling pathway	Mar-19	95/8546	0.031579	14.20388	6.108632	0.001133	0.003338	0.001067	MMP9/MAPK1/MMP3	3
Organismal Systems	Endocrine system	hsa04614	Renin-angiotensin system	Feb-19	23/8546	0.086957	39.11213	8.639042	0.001152	0.003338	0.001067	ACE/REN	2
Organismal Systems	Immune system	hsa04666	Fc gamma R-mediated phagocytosis	Mar-19	99/8546	0.030303	13.62998	5.966283	0.001277	0.003636	0.001162	AKT1/PIK3R1/MAPK1	3
Environmental Information Processing	Signal transduction	hsa04024	cAMP signaling pathway	Apr-19	226/8546	0.017699	7.960876	5.006003	0.00135	0.003719	0.001188	AKT1/PIK3R1/MAPK1/PPARA	4
Human Diseases	Infectious disease: viral	hsa05163	Human cytomegalovirus infection	Apr-19	226/8546	0.017699	7.960876	5.006003	0.00135	0.003719	0.001188	AKT1/EGFR/PIK3R1/MAPK1	4
Human Diseases	Cancer: overview	hsa05208	Chemical carcinogenesis - reactive oxygen species	Apr-19	227/8546	0.017621	7.925806	4.99209	0.001372	0.003719	0.001188	AKT1/EGFR/PIK3R1/MAPK1	4
Organismal Systems	Immune system	hsa04625	C-type lectin receptor signaling pathway	Mar-19	105/8546	0.028571	12.85113	5.76756	0.001514	0.004036	0.00129	AKT1/PIK3R1/MAPK1	3

Category	Subcategory	ID	Description	Gene Ratio	Bg Ratio	Rich Factor	Fold Enrichment	zScore	pvalue	p.adjust	qvalue	geneID	Count
Human Diseases	Infectious disease: bacterial	hsa05131	Shigellosis	Apr-19	250/8546	0.016	7.196632	4.693815	0.001959	0.004987	0.001594	AKT1/EGFR/PIK3R1/MAPK1	4
Organismal Systems	Nervous system	hsa04725	Cholinergic synapse	Mar-19	116/8546	0.025862	11.63249	5.442328	0.002015	0.005053	0.001615	AKT1/PIK3R1/MAPK1	3
Organismal Systems	Nervous system	hsa04722	Neurotrophin signaling pathway	Mar-19	120/8546	0.025	11.24474	5.334766	0.00222	0.005485	0.001753	AKT1/PIK3R1/MAPK1	3
Environmental Information Processing	Signal transduction	hsa04152	AMPK signaling pathway	Mar-19	122/8546	0.02459	11.0604	5.282878	0.002327	0.005507	0.00176	AKT1/PIK3R1/PPARG	3
Organismal Systems	Immune system	hsa04660	T cell receptor signaling pathway	Mar-19	122/8546	0.02459	11.0604	5.282878	0.002327	0.005507	0.00176	AKT1/PIK3R1/MAPK1	3
Organismal Systems	Endocrine system	hsa04935	Growth hormone synthesis, secretion and action	Mar-19	122/8546	0.02459	11.0604	5.282878	0.002327	0.005507	0.00176	AKT1/PIK3R1/MAPK1	3
Human Diseases	Cancer: specific types	hsa05216	Thyroid cancer	Feb-19	37/8546	0.054054	24.31294	6.708006	0.002978	0.006948	0.00222	PPARG/MAPK1	2
Organismal Systems	Excretory system	hsa04960	Aldosterone-regulated sodium reabsorption	Feb-19	38/8546	0.052632	23.67313	6.611869	0.003139	0.007224	0.002308	PIK3R1/MAPK1	2
Cellular Processes	Cell growth and death	hsa04210	Apoptosis	Mar-19	137/8546	0.021898	9.849405	4.928751	0.003236	0.007302	0.002333	AKT1/PIK3R1/MAPK1	3
Organismal Systems	Endocrine system	hsa04910	Insulin signaling pathway	Mar-19	138/8546	0.021739	9.778032	4.907102	0.003303	0.007302	0.002333	AKT1/PIK3R1/MAPK1	3
Human Diseases	Infectious disease: bacterial	hsa05135	Yersinia infection	Mar-19	138/8546	0.021739	9.778032	4.907102	0.003303	0.007302	0.002333	AKT1/PIK3R1/MAPK1	3
Cellular Processes	Cell growth and death	hsa04114	Oocyte meiosis	Mar-19	139/8546	0.021583	9.707686	4.885673	0.003371	0.007356	0.00235	PGR/AR/MAPK1	3

Category	Subcategory	ID	Description	Gene Ratio	Bg Ratio	Rich Factor	Fold Enrichment	zScore	pvalue	p.adjust	qvalue	geneID	Count
Organismal Systems	Endocrine system	hsa04921	Oxytocin signaling pathway	Mar-19	155/8546	0.019355	8.705603	4.569833	0.004581	0.00962	0.003074	EGFR/NOS3/MAPK1	3
Cellular Processes	Cell growth and death	hsa04218	Cellular senescence	Mar-19	157/8546	0.019108	8.594703	4.533569	0.004748	0.009772	0.003123	AKT1/PIK3R1/MAPK1	3
Human Diseases	Endocrine and metabolic disease	hsa04930	Type II diabetes mellitus	Feb-19	47/8546	0.042553	19.13998	5.88622	0.00477	0.009772	0.003123	PIK3R1/MAPK1	2
Environmental Information Processing	Signal transduction	hsa04150	mTOR signaling pathway	Mar-19	158/8546	0.018987	8.540306	4.515679	0.004834	0.009784	0.003126	AKT1/PIK3R1/MAPK1	3
Human Diseases	Infectious disease: viral	hsa05165	Human papillomavirus infection	Apr-19	333/8546	0.012012	5.402877	3.868498	0.005515	0.010966	0.003504	AKT1/EGFR/PIK3R1/MAPK1	4
Environmental Information Processing	Signal transduction	hsa04022	cGMP-PKG signaling pathway	Mar-19	166/8546	0.018072	8.128725	4.378029	0.005548	0.010966	0.003504	AKT1/NOS3/MAPK1	3
Environmental Information Processing	Signal transduction	hsa04630	JAK-STAT signaling pathway	Mar-19	168/8546	0.017857	8.031955	4.345055	0.005736	0.011133	0.003558	AKT1/EGFR/PIK3R1	3
Organismal Systems	Digestive system	hsa04973	Carbohydrate digestion and absorption	Feb-19	52/8546	0.038462	17.2996	5.564896	0.005812	0.011133	0.003558	AKT1/PIK3R1	2
Cellular Processes	Transport and catabolism	hsa04140	Autophagy - animal	Mar-19	169/8546	0.017751	7.984429	4.328772	0.005832	0.011133	0.003558	AKT1/PIK3R1/MAPK1	3
Human Diseases	Infectious disease: viral	hsa05164	Influenza A	Mar-19	173/8546	0.017341	7.799817	4.264955	0.006223	0.011747	0.003754	AKT1/PIK3R1/MAPK1	3
Organismal Systems	Endocrine system	hsa04923	Regulation of lipolysis in adipocytes	Feb-19	59/8546	0.033898	15.2471	5.183345	0.00743	0.01387	0.004432	AKT1/PIK3R1	2
Organismal Systems	Aging	hsa04213	Longevity regulating pathway - multiple species	Feb-19	62/8546	0.032258	14.50934	5.039231	0.00818	0.015101	0.004825	AKT1/PIK3R1	2

Category	Subcategory	ID	Description	Gene Ratio	Bg Ratio	Rich Factor	Fold Enrichment	zScore	pvalue	p.adjust	qvalue	geneID	Count
Organismal Systems	Immune system	hsa04062	Chemokine signaling pathway	Mar-19	193/8546	0.015544	6.991546	3.974029	0.008417	0.015204	0.004858	AKT1/PIK3R1/MAPK1	3
Organismal Systems	Immune system	hsa04613	Neutrophil extracellular trap formation	Mar-19	193/8546	0.015544	6.991546	3.974029	0.008417	0.015204	0.004858	AKT1/PIK3R1/MAPK1	3
Human Diseases	Infectious disease: viral	hsa05167	Kaposi sarcoma-associated herpesvirus infection	Mar-19	196/8546	0.015306	6.884533	3.933974	0.00878	0.015692	0.005014	AKT1/PIK3R1/MAPK1	3
Organismal Systems	Endocrine system	hsa04924	Renin secretion	Feb-19	69/8546	0.028986	13.03738	4.738818	0.010054	0.017781	0.005682	ACE/REN	2
Organismal Systems	Endocrine system	hsa04920	Adipocytokine signaling pathway	Feb-19	70/8546	0.028571	12.85113	4.69946	0.010337	0.018089	0.00578	AKT1/PPARA	2
Human Diseases	Infectious disease: viral	hsa05170	Human immunodeficiency virus 1 infection	Mar-19	213/8546	0.014085	6.335063	3.721889	0.011016	0.01908	0.006097	AKT1/PIK3R1/MAPK1	3
Organismal Systems	Endocrine system	hsa03320	PPAR signaling pathway	Feb-19	76/8546	0.026316	11.83657	4.479107	0.012102	0.020747	0.00663	PPARG/PPARA	2
Human Diseases	Infectious disease: viral	hsa05166	Human T-cell leukemia virus 1 infection	Mar-19	224/8546	0.013393	6.023966	3.596595	0.012625	0.021425	0.006846	AKT1/PIK3R1/MAPK1	3
Organismal Systems	Immune system	hsa04610	Complement and coagulation cascades	Feb-19	88/8546	0.022727	10.22249	4.104784	0.016	0.02688	0.008589	F2/PLAU	2
Cellular Processes	Cellular community - eukaryotes	hsa04540	Gap junction	Feb-19	92/8546	0.021739	9.778032	3.995716	0.017404	0.028695	0.009169	EGFR/MAPK1	2
Cellular Processes	Cellular community - eukaryotes	hsa04520	Adherens junction	Feb-19	93/8546	0.021505	9.672892	3.96949	0.017763	0.028695	0.009169	EGFR/MAPK1	2

Category	Subcategory	ID	Description	Gene Ratio	Bg Ratio	Rich Factor	Fold Enrichment	zScore	pvalue	p.adjust	qvalue	geneID	Count
Human Diseases	Cancer: specific types	hsa05222	Small cell lung cancer	Feb-19	93/8546	0.021505	9.672892	3.96949	0.017763	0.028695	0.009169	AKT1/PIK3R1	2
Organismal Systems	Endocrine system	hsa04922	Glucagon signaling pathway	Feb-19	107/8546	0.018692	8.40728	3.639484	0.023117	0.036988	0.011819	AKT1/PPARA	2
Human Diseases	Infectious disease: parasitic	hsa05145	Toxoplasmosis	Feb-19	112/8546	0.017857	8.031955	3.535925	0.025173	0.039897	0.012749	AKT1/MAPK1	2
Organismal Systems	Endocrine system	hsa04928	Parathyroid hormone synthesis, secretion and action	Feb-19	115/8546	0.017391	7.822426	3.476825	0.026441	0.041515	0.013266	EGFR/MAPK1	2
Organismal Systems	Immune system	hsa04670	Leukocyte transendothelial migration	Feb-19	116/8546	0.017241	7.754991	3.457599	0.02687	0.041798	0.013356	MMP9/PIK3R1	2
Environmental Information Processing	Signal transduction	hsa04010	MAPK signaling pathway	Mar-19	300/8546	0.01	4.497895	2.911256	0.027356	0.042163	0.013473	AKT1/EGFR/MAPK1	3
Organismal Systems	Immune system	hsa04620	Toll-like receptor signaling pathway	Mar-19	109/8546	0.027523	12.37953	5.643885	0.001685	0.004356	0.001392	AKT1/PIK3R1/MAPK1	3
Environmental Information Processing	Signal transduction	hsa04371	Apelin signaling pathway	Mar-19	140/8546	0.021429	9.638346	4.86446	0.00344	0.00741	0.002368	AKT1/NOS3/MAPK1	3
Cellular Processes	Cellular community - eukaryotes	hsa04550	Signaling pathways regulating pluripotency of stem cells	Mar-19	144/8546	0.020833	9.370614	4.781696	0.003725	0.007921	0.002531	AKT1/PIK3R1/MAPK1	3
Organismal Systems	Immune system	hsa04613	Neutrophil extracellular trap formation	Mar-19	193/8546	0.015554	6.991546	3.974029	0.008417	0.015204	0.004858	AKT1/PIK3R1/MAPK1	3

Category	Subcategory	ID	Description	Gene Ratio	Bg Ratio	Rich Factor	Fold Enrichment	zScore	pvalue	p.adjust	qvalue	geneID	Count
Cellular Processes	Cell growth and death	hsa04218	Cellular senescence	Mar-19	157/8546	0.019108	8.594703	4.533569	0.004748	0.009772	0.003123	AKT1/PIK3R1/MAPK1	3
Organismal Systems	Immune system	hsa04062	Chemokine signaling pathway	Mar-19	193/8546	0.015544	6.991546	3.974029	0.008417	0.015204	0.004858	AKT1/PIK3R1/MAPK1	3
Organismal Systems	Immune system	hsa04613	Neutrophil extracellular trap formation	Mar-19	193/8546	0.015544	6.991546	3.974029	0.008417	0.015204	0.004858	AKT1/PIK3R1/MAPK1	3
Environmental Information Processing	Signal transduction	hsa04014	Ras signaling pathway	Apr-19	238/8546	0.016807	7.559487	4.844454	0.001635	0.004291	0.001371	AKT1/EGFR/PIK3R1/MAPK1	4
Organismal Systems	Endocrine system	hsa04912	GnRH signaling pathway	Feb-19	93/8546	0.021505	9.672892	3.96949	0.017763	0.028695	0.009169	EGFR/MAPK1	2

Appendix 15

Eupatorin

No	Gene	No	Gene	No	Gene	No	Gene
1	BCHE	36	MAPK8	71	ANXA5	106	PCK1
2	BACE1	37	SHBG	72	RXRA	107	DHFR
3	CYP19A1	38	ESRRG	73	PTPN1	108	HK1
4	AR	39	QPCT	74	SULT2A1	109	DPP4
5	NR1H2	40	ADAM17	75	MTAP	110	IMPDH2
6	PPIA	41	CFD	76	PLK1	111	ADH1C
7	CA1	42	MAPK14	77	IGLV2-8	112	SERPINA1
8	F2	43	NOS3	78	AZGP1	113	ADAM17
9	ESR1	44	PAH	79	FGFR1	114	MMP8
10	PNP	45	CHEK1	80	MMP12	115	ISG20
11	CA2	46	PDE4D	81	LTA4H	116	AHCY
12	FAP	47	AMY1A	82	HSP90AA1	117	XIAP
13	GSTP1	48	BCAT2	83	KIF11	118	LGALS7
14	CCNA2	49	SRC	84	NR3C2	119	EPHX2
15	PGR	50	CBR1	85	DUSP6	120	F7
16	GBA	51	LSS	86	PDE4B	121	SOD2
17	TTR	52	HSD17B1	87	GC	122	TYMS
18	PIM1	53	MIF	88	LCK	123	CTNNA1
19	CDK2	54	CSNK1G2	89	AKR1C1	124	PPARD
20	AKR1C3	55	AKR1B1	90	F10	125	EGFR
21	CTSS	56	PYGL	91	JAK3	126	PTPN11
22	KDR	57	MAOB	92	FNTA	127	CCNT1
23	MAPK10	58	MAPKAPK2	93	APCS	128	HSD11B1
24	STS	59	CDA	94	CES1	129	C8G
25	APOA2	60	NR1H3	95	NQO2	130	NR1I2
26	CFB	61	AKT1	96	PLAU	131	ADH5
27	ALB	62	REN	97	NQO1	132	CASP7
28	GSR	63	RAC2	98	FGFR2	133	ELANE
29	MMP13	64	BHMT	99	MMP3	134	HPN
30	SORD	65	BST1	100	GSK3B	135	ARHGAP1
31	CTSD	66	RNASE4	101	BMP7	136	CTSK
32	CASP3	67	LDHB	102	THRB	137	PDK2
33	ANG	68	NCS1	103	PDHB	138	PPARG
34	EPHB4	69	GSTT2B	104	MTHFD1	139	TRAPPC3
35	PAK6	70	CDK6	105	PDPK1	140	HSPA8

No	Gene	No	Gene	No	Gene	No	Gene
141	RHOA	178	CDK5R1	215	CYP2C8	252	TPH1
142	REG1A	179	DCK	216	HAGH	253	ACE
143	SHMT1	180	CD1A	217	JAK2	254	ACADM
144	PDE3B	181	ALDOA	218	EIF4E	255	HNF4G
145	FHIT	182	AMD1	219	FABP6	256	NT5M
146	AKR1C2	183	CRABP2	220	MME	257	HMGCR
147	IGF1R	184	RBP4	221	FABP3	258	SETD7
148	CSNK2A1	185	SULT1E1	222	CHIT1	259	DUT
149	ABO	186	GSTA1	223	PTK2	260	CASP1
150	MET	187	RAB11A	224	MAPK1	261	ATIC
151	ME2	188	UCK2	225	PITPNA	262	FECH
152	PDE5A	189	LYZ	226	HEXB	263	MMP2
153	TGFBR1	190	THRA	227	MMP9	264	ARL5A
154	ADK	191	AMY2A	228	SDS	265	TGFB2
155	FABP4	192	GPI	229	ALDH2	266	GSTM1
156	HCK	193	MAN1B1	230	CTSG	267	FDPS
157	CYP2C9	194	RHEB	231	GNPDA1	268	VDR
158	RNASE3	195	ARSA	232	GSTA3	269	S100A9
159	FKBP1A	196	HEXB	233	LGALS3	270	AKT2
160	PLA2G2A	197	NMNAT1	234	CDK7	271	DCPS
161	HDAC8	198	LGALS2	235	HPRT1	272	OAT
162	ITK	199	SULT2B1	236	PPCDC	273	CTSF
163	PPARA	200	RARA	237	EPHA2	274	IL2
164	AMY1A	201	GSTZ1	238	BIRC7	275	KIT
165	DTYMK	202	OTC	239	ARG1	276	GSTO1
166	SEC14L2	203	NR1H4	240	ABL1	277	TAP1
167	TNK2	204	NR3C1	241	GSTM2	278	F11
168	CCL5	205	STAT1	242	ARG2	279	MMP1
169	ACP3	206	CLK1	243	TGM3	280	CD209
170	TPI1	207	SELP	244	RAB5A	281	DPEP1
171	INSR	208	HINT1	245	HRAS	282	GCK
172	ZAP70	209	IMPDH1	246	PRKCQ	283	PNMT
173	ERBB4	210	APRT	247	B3GAT1	284	FOLH1
174	SYK	211	PAPSS1	248	CMA1	285	MAP2K1
175	DHODH	212	CBS	249	CDC42	286	KAT2B
176	FABP7	213	TK1	250	PKLR		
177	GP1BA	214	GCDH	251	PIK3R1		

Sinensetin

No	Gene	No	Gene	No	Gene	No	Gene
1	CYP19A1	36	NOS3	71	HK1	106	CDA
2	BCHE	37	GSR	72	FHIT	107	SOD2
3	NR1H2	38	BCAT2	73	MMP8	108	NCS1
4	PPIA	39	PGR	74	DPP4	109	CD1A
5	AR	40	SRC	75	ADH1C	110	RNASE4
6	F2	41	AKR1B1	76	FGFR2	111	LCK
7	PNP	42	ANXA5	77	MET	112	PDK2
8	ESR1	43	CHEK1	78	ISG20	113	FGFR1
9	GBA	44	PAH	79	PDPK1	114	GSTT2B
10	GSTP1	45	MIF	80	FNTA	115	AURKA
11	CA2	46	MMP12	81	C8G	116	FABP4
12	CCNA2	47	SULT2A1	82	XIAP	117	PPARG
13	PIM1	48	PTPN1	83	CCNT1	118	ELANE
14	SHBG	49	IGLV2-8	84	CTNNA1	119	CTSK
15	TTR	50	NR3C2	85	ADAM17	120	CYP2C9
16	CDK6	51	BACE1	86	REG1A	121	NMNAT1
17	AKR1C3	52	PDE4B	87	PTPN11	122	HDAC8
18	STS	53	CES1	88	PPARD	123	ITK
19	APOA2	54	APCS	89	HSD11B1	124	BST1
20	CFB	55	GC	90	SHMT1	125	PLA2G2A
21	ALB	56	F10	91	TYMS	126	THRB
22	CASP3	57	LTA4H	92	HSPA8	127	SEC14L2
23	MAPK10	58	NQO2	93	KIF11	128	ACP3
24	ANG	59	AKR1C1	94	PDE5A	129	EPHB4
25	MMP13	60	HSD17B1	95	EGFR	130	DHFR
26	SORD	61	HSP90AA1	96	LSS	131	PPARA
27	ESRRG	62	NQO1	97	PDE3B	132	ERBB4
28	CTSD	63	PLAU	98	NR1I2	133	TPI1
29	RXRA	64	KDR	99	DHODH	134	PAK6
30	MAPK8	65	LGALS7	100	ME2	135	TRAPPC3
31	ADAM17	66	PCK1	101	ADH5	136	ALDOA
32	MAPK14	67	GSK3B	102	BHMT	137	RNASE3
33	PDE4D	68	MMP3	103	TGFBR1	138	DCK
34	CDK2	69	IMPDH2	104	NR1H3	139	SERPINA1
35	CFD	70	CASP7	105	CBR1	140	AHCY

No	Gene	No	Gene	No	Gene	No	Gene
141	ADK	178	B3GAT1	215	TGM3	252	GMPR2
142	SULT1E1	179	HAGH	216	IL2	253	LCN2
143	HCK	180	IMPDH1	217	TK1	254	AGXT
144	CRABP2	181	FABP3	218	STAT1	255	ARL5A
145	RARA	182	IGF1R	219	CDC42	256	RNASE2
146	FKBP1A	183	MAN1B1	220	FOLH1	257	FKBP1B
147	OTC	184	PITPNA	221	AMD1	258	MMP1
148	MTAP	185	MME	222	CMA1	259	DDX39B
149	MAOB	186	ATIC	223	DPEP1	260	GMPR
150	LGALS2	187	THRA	224	ABO	261	GLO1
151	RAB11A	188	JAK2	225	S100A9	262	AMY2A
152	GPI	189	APRT	226	KAT2B	263	DCPS
153	SULT2B1	190	PTK2	227	GSTO1	264	PRKCQ
154	EPHX2	191	LGALS3	228	GM2A	265	CDK7
155	GSTZ1	192	GSTA3	229	MAP2K1	266	TRDMT1
156	SDS	193	CTSG	230	TEK	267	CTSF
157	GSTA1	194	REN	231	F11	268	FGG
158	NR1H4	195	GSTM2	232	RHOA	269	NMNAT3
159	MTHFD1	196	HINT1	233	TAP1	270	CD209
160	PYGL	197	NT5M	234	GCK	271	HRAS
161	JAK3	198	HPRT1	235	GP1BA	272	ARG2
162	CCL5	199	BIRC7	236	TPSB2	273	APAF1
163	CBS	200	UCK2	237	INSR	274	UAP1
164	CLK1	201	TPH1	238	FABP7	275	RFK
165	MMP9	202	ARG1	239	PNMT	276	CLEC4M
166	GALE	203	GSTM1	240	CTSB	277	RARG
167	NR3C1	204	ACADM	241	HMGCR	278	WARS1
168	PAPSS1	205	HNF4G	242	ZAP70	279	RAB9A
169	CTSS	206	FECH	243	RBP4	280	RAF1
170	MAPKAPK2	207	DUT	244	PPP1CC	281	TGFB2
171	ARHGAP1	208	ACE	245	ARF4	282	NDST1
172	EIF4E	209	RAB5A	246	HEXB	283	NOS2
173	FABP6	210	FDPS	247	RARB	284	ADAM33
174	CYP2C8	211	MMP2	248	PKLR	285	ERI1
175	DTYMK	212	SELE	249	LYZ	286	RAP2A
176	CHIT1	213	OAT	250	KIT	287	PMS2
177	PARP1	214	VDR	251	ABL1	288	HADH

TMF

No	Gene	No	Gene	No	Gene	No	Gene
1	PPIA	36	SULT2A1	71	PDPK1	106	RNASE4
2	BCHE	37	PPARG	72	DAPK1	107	PDK2
3	MAPK10	38	CTSB	73	HSPA8	108	FABP4
4	MAPK8	39	AR	74	CDA	109	F11
5	ESR1	40	RXRA	75	CASP3	110	DHFR
6	CFB	41	MMP13	76	CBR1	111	LCK
7	CA2	42	IGLV2-8	77	PAH	112	CD1A
8	F2	43	CES1	78	GSTT2B	113	THRB
9	NR1H2	44	MIF	79	IMPDH2	114	ISG20
10	GBA	45	DHODH	80	PDE3B	115	ACE
11	TTR	46	GC	81	KDR	116	UMPS
12	ALB	47	CFD	82	ADH5	117	DCK
13	MMP3	48	PDE4B	83	AKR1B1	118	ACP3
14	STS	49	ADH1C	84	MET	119	LGALS2
15	APOA2	50	MAPK14	85	AKR1C3	120	RAB11A
16	TREM1	51	HSP90AA1	86	PCK1	121	MME
17	CYP19A1	52	PTPN1	87	SHMT1	122	UCK2
18	PIM1	53	HSD17B1	88	TYMS	123	SOD2
19	PDE4D	54	AKR1C1	89	SEC14L2	124	PARP1
20	BCAT2	55	BACE1	90	ERBB4	125	SULT1E1
21	PGR	56	MMP8	91	ELANE	126	SULT2B1
22	ADAM17	57	HK1	92	MMP7	127	SERPINA1
23	SRC	58	HSD11B1	93	AURKA	128	AHCY
24	NOS3	59	F10	94	RNASE3	129	MAOB
25	ANG	60	CDK6	95	CYP2C9	130	PLA2G2A
26	CDK2	61	MMP12	96	GSTP1	131	FKBP1A
27	FNTA	62	NR3C2	97	ITK	132	FGFR1
28	ESR2	63	CTNNA1	98	NR1I2	133	CBS
29	SHBG	64	CHEK1	99	C1S	134	GPI
30	PDE5A	65	PLAU	100	TGM3	135	ADAM17
31	CCNA2	66	XIAP	101	NR1H3	136	IMPDH1
32	PPARD	67	PTPN11	102	HCK	137	CLK1
33	GSR	68	CTSK	103	HDAC8	138	ME2
34	ESRRG	69	GSK3B	104	CCL5	139	TPI1
35	DPP4	70	SORD	105	BST1	140	TGFBR1

No	Gene	No	Gene	No	Gene	No	Gene
141	NR1H4	178	IL2	215	HPRT1	252	APAF1
142	MAPKAPK2	179	HMGCR	216	MTAP	253	RAC1
143	HAGH	180	S100A9	217	WARS1	254	TAP1
144	NT5M	181	REN	218	GSTM2	255	PNMT
145	TRAPPC3	182	CDK5R1	219	ZAP70	256	HNMT
146	PYGL	183	STAT1	220	TK1	257	BTK
147	TPH1	184	FABP3	221	SELE	258	AK1
148	EPHB4	185	DPEP1	222	LCN2	259	NOS2
149	SDS	186	GP1BA	223	RAB9A	260	RFK
150	GSTA1	187	PAK6	224	PRKCQ	261	AKT1
151	CTSS	188	TEK	225	GLO1	262	EEA1
152	MAN1B1	189	PITPNA	226	HADH	263	F7
153	BIRC7	190	RBP4	227	FECH	264	TTPA
154	JAK2	191	RARG	228	CASP1	265	UAP1
155	LGALS3	192	VDR	229	SULT1A1	266	PROCR
156	ABO	193	HEXB	230	EGFR	267	FKBP3
157	FABP6	194	ARF4	231	EIF4E	268	DCXR
158	ADK	195	GCDH	232	TRDMT1	269	CRYZ
159	JAK3	196	CRABP2	233	FKBP1B	270	AMY2A
160	MMP2	197	TGFB2	234	CD209	271	SPR
161	RAB5A	198	ARL5A	235	AMD1		
162	CHIT1	199	ERI1	236	DUT		
163	BHMT	200	OAT	237	GSTZ1		
164	HNF4G	201	RARA	238	RXRB		
165	PPARA	202	GSTM1	239	ADAM33		
166	DTYMK	203	ATIC	240	KAT2B		
167	LYZ	204	MAP2K1	241	GMPR2		
168	NMNAT1	205	RNASE2	242	RORA		
169	NR3C1	206	GSTA3	243	KIT		
170	FOLH1	207	FGG	244	RAP2A		
171	FDPS	208	CTSF	245	INSR		
172	OTC	209	PKLR	246	TPSB2		
173	PAPSS1	210	NMNAT3	247	GMPR		
174	CDC42	211	RARB	248	DCPS		
175	HRAS	212	PPP1CC	249	MMP9		
176	FABP7	213	HINT1	250	RND3		
177	ARG1	214	LTA4H	251	KIF11		

Appendix 16

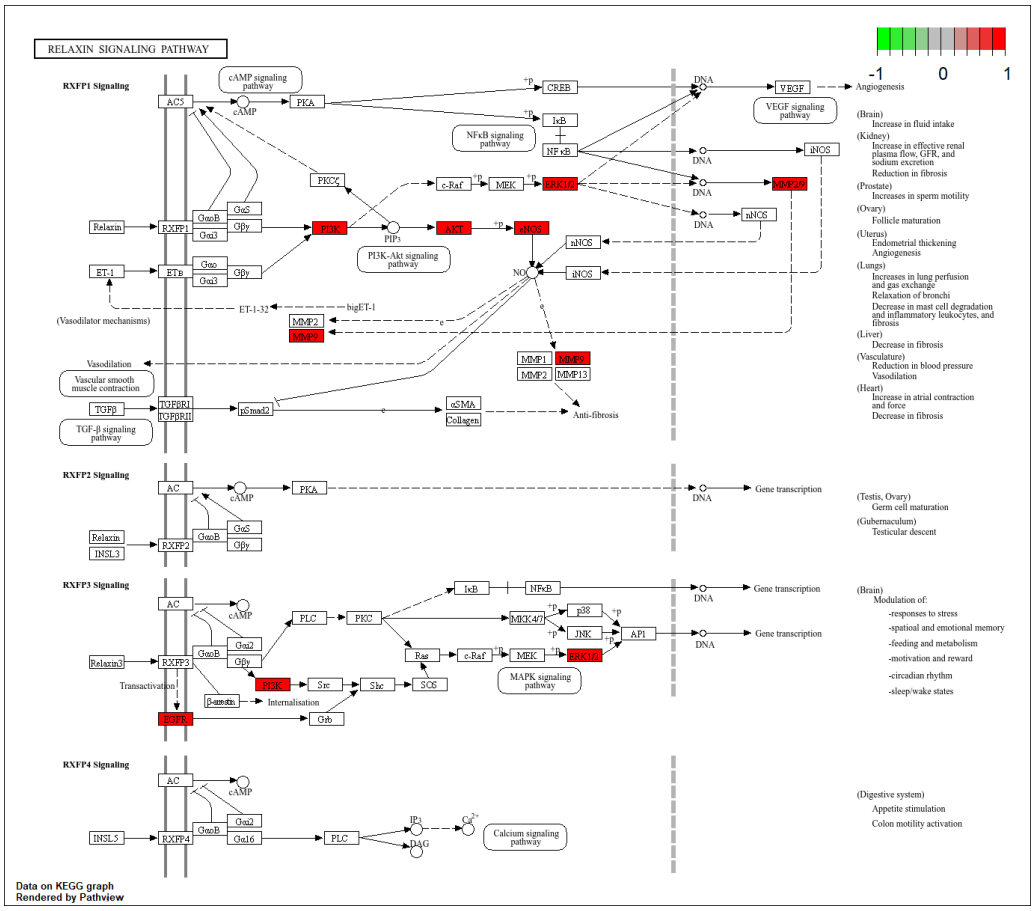

This relaxin signaling pathway map shows that several key molecules such as PI3K, AKT, ERK1/2, eNOS, and MMPs (MMP2, MMP9, MMP13) are highly activated (highlighted in red), suggesting strong engagement of pathways that promote nitric oxide production, vasodilation, and anti-fibrotic effects. The activation of the PI3K–AKT–eNOS and ERK1/2–MAPK cascades reflects relaxin's broad physiological actions, including improving vascular relaxation, reducing blood pressure, enhancing tissue repair, and preventing fibrosis. Additionally, the upregulation of matrix metalloproteinases points to active extracellular matrix remodeling and angiogenesis. Overall, this pattern signifies that relaxin or relaxin-like compounds stimulate multiple signaling routes that together support vascular protection, cardiac health, and organ regeneration, aligning with its known roles in maintaining cardiovascular and systemic homeostasis.

Appendix 17

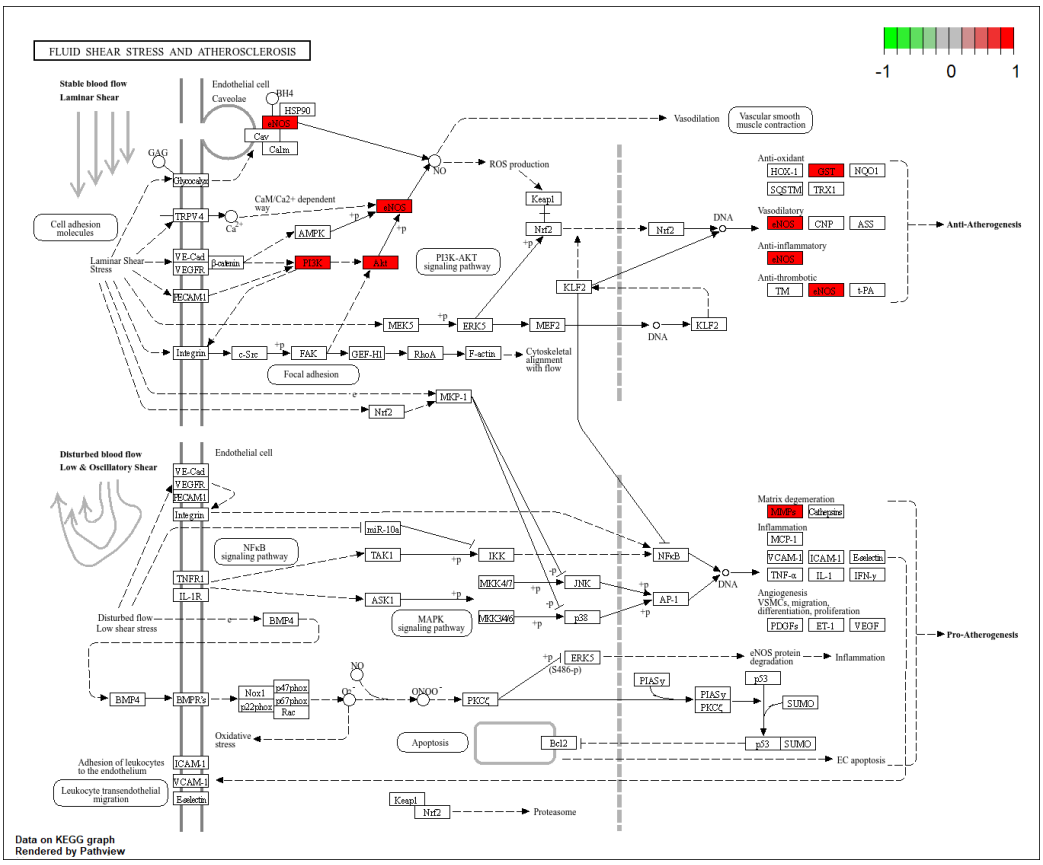

KEGG pathway map describes the Relaxin signal pathway, where special concentration has been paid on the changing expression of genes that are related to different processes in the cell. Here the red-colored boxes would show upregulated genes or proteins thus showing higher level of expression whereas the green colored boxes would show downregulation (which is not present here) and white boxes would show no significant variation. Activation of the pathway occurs upon recognition of relaxin by its receptor RXFP1 and results in the following down stream cascades: the PI3K-AKT, MAPK, and cAMP/PKA pathways. Indicatively among the critical signaling molecules are PIK3R1, AKT1, MAPK1 (ERK2), FOS, JUN, and RHOA which are highly upregulated, implying the robust activation of signaling processes that effect vasodilation, angiogenesis and anti-fibrotic processes. The key functions of the PI3K-AKT pathway are the survival of the cells, vascular relaxation, and regulation of metabolism whereas the key functions of the MAPK pathway include gene transcription, proliferation, and differentiation. cAMP/PKA signaling slavery helps smooth muscles to relax and vasodilate. Moreover, it is also known that

relaxin pathway inhibits TGF-/SMAD signaling, which subsequently decreases fibrosis, as well as tissue remodeling. The general trend on gene expression suggests a physiological protective effect of relaxin that may be correlated with decreased vascular resistance, enhanced arterial compliance, antifibrosis and low blood pressure. Such effects are specifically applicable in reproductive and tissue remodeling-related cases, including cardiovascular and renal health.

Appendix 18

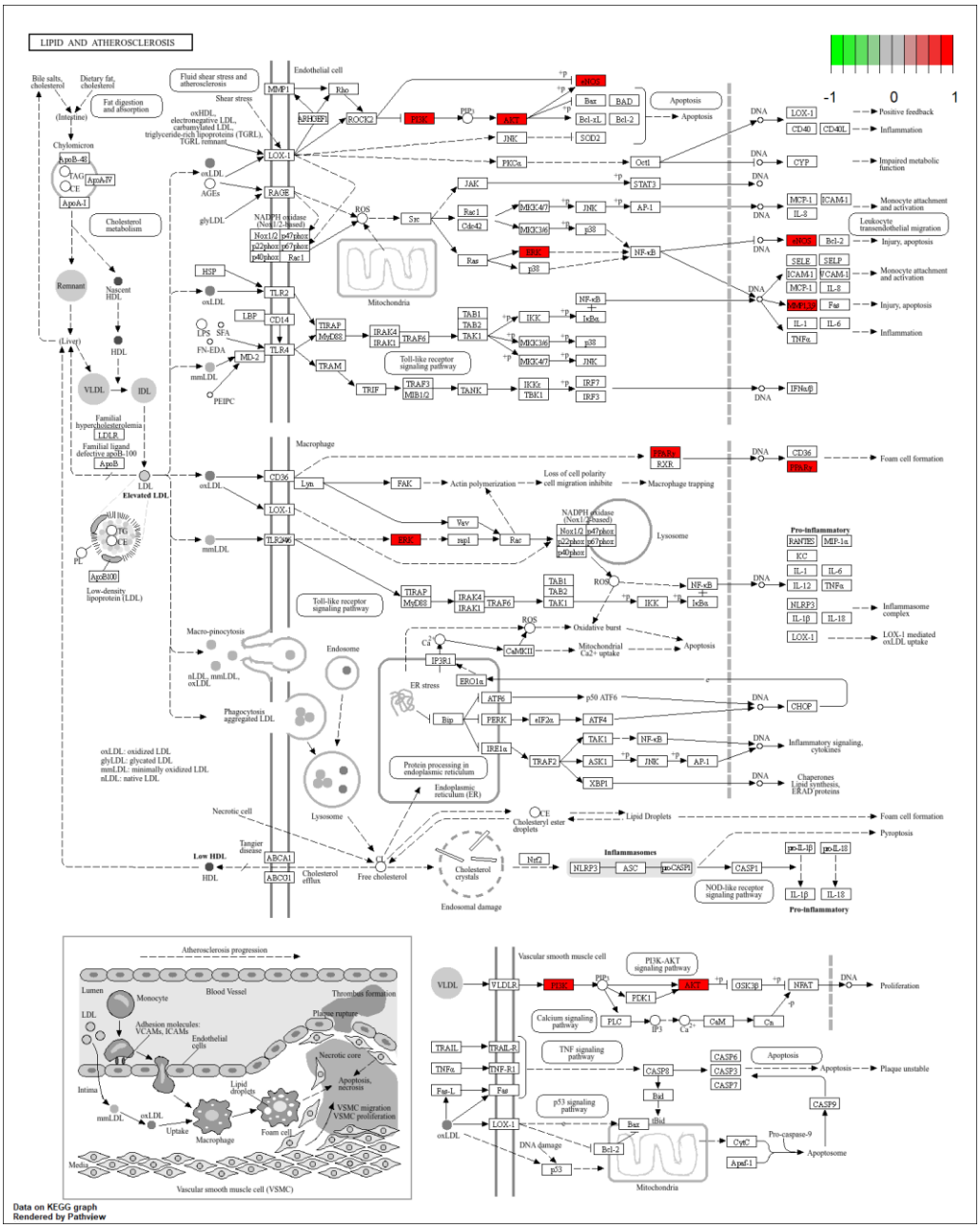

The KEGG pathway map of Lipid and Atherosclerosis shows the molecular pathway involved in the formation of atherosclerosis, and the data of gene expression was superimposed in the picture revealing several of upregulated targets. Interestingly, many of the adhesion molecules are highly increased, including ICAM1, VCAM1, SELE (E-selectin), which are the main participants

in adhesion processes, which reflects the activation of endothelial cells, as one of the first and most important events of atherogenesis involves monocyte adhesion and passage into the vascular intima. This is also evidenced by up regulation of pro-inflammatory cytokines including TNF and IL1B which favor inflammation, endothelial dysfunction and immune cell recruitment. The pathway is also over-expressed with NFKB1 and RELA, the critical members of the NF-kb signaling chain that is a major regulator of the inflammatory state and adaptive response. This pathway upon activation leads to the transcription of genes in inflammation, oxidative stress as well as cell adhesion. Activation of a macrophage scavenger receptor, CD36, shows an increased capacity of macrophage to take up and scavenge oxidized LDL (oxLDL) and form a foam cell, a crucial event in arterial accumulation of plaque. Concomitant results are the up regulations of MAPK1, MAPK14 and PLCG1 that implies the activation of the MAPK signaling pathway implicating in the proliferation, migration and apoptosis regulation of vascular smooth muscle cell (VSMC). All these molecular changes are things that suggest an ongoing atherosclerotic process that is endothelial-activated, chronically inflammatory, lipid-laden, and exhibiting vascular remodelling. These processes are expanded schematically below left (inset) in the infiltration of LDL, infiltration of immune cells, foaming of the foam cells, and the development of plaques. On the whole, the expression and the pathway map provide evidence of a pro-atherogenic and pro-inflammatory microenvironment, and this may be applicable in disease models that include hyperlipidemia, metabolic syndrome, or cardiovascular risk.